Indian Institute of Technology Guwahati
Department of Physics

Field theory in time dependent background: Superradiance and Sonoluminescence

A thesis submitted by:
Rajesh Karmakar

to

Indian Institute of Technology Guwahati
in partial fulfillment of the requirements
for the award of the degree of
Doctor of Philosophy in Physics

Supervisor: **Dr. Debaparasad Maity**

March 2024

Statement

.

The work contained in the thesis entitled "**Field theory in time dependent background: Superradiance and Sonoluminescence**" has been carried out at the Department of Physics, Indian Institute of Technology Guwahati, India by me, under the supervision of Dr. Debaprasad Maity. The material of this thesis is original and has not been submitted elsewhere for any other degree or diploma. Works presented in the thesis are all my own unless referenced in contrary to the text.

Rajesh Karmakar
PhD student
Department of Physics
Indian Institute of Technology Guwahati
Guwahati, Assam, India-781039
Date:

Disclaimer

.

The bibliography included in this thesis is, by no means, complete; rather contains the ones which are consulted thoroughly by me. I apologize for inadvertently missing out on some of the research papers, review articles, and other scientific documents pertaining to this thesis which also should have been cited. For illustration purposes, some of the figures in this thesis are taken from other sources and properly cited.

Certificate

.

It is certified that the work contained in the thesis entitled "**Field theory in time dependent background: Superradiance and Sonoluminescence**" by Rajesh Karmakar (roll number-166121105), a Ph.D. student of the Department of Physics, IIT Guwahati, was carried out under my supervision. The material of this thesis is original and has not been submitted elsewhere for any other degree or diploma.

.....
(Signature of the supervisor)

Dr. Debaprasad Maity
Associate Professor,
Indian Institute of Technology Guwahati,
Guwahati-781039, Assam, India
Date:

Acknowledgement

I want to express my sincere gratitude to my supervisor, Dr. Debaprasad Maity, for his unwavering belief in me on interesting and challenging research problems. Since the beginning of this journey, he has consistently guided me through ups and downs with his research expertise and experience in various aspects of life. He has always pushed me to work proactively. Through his mentorship, I gained insight into the importance of paying attention to the finer details often overlooked and dedicating maximum effort to them, so as to be able to generate new research problems to work with.

I am grateful to my doctoral committee members, Dr. Sayan Chakraborti, Dr. Sovon Chakraborty and Dr. Bibhas Ranjan Majhi for their support and suggestions in various contexts. They have always fostered a friendly environment for various discussions. I always feel fortunate to have them in a close association.

The weekly journal club organized by the department's gravity and high energy physics group has consistently served as a driving force for me, enabling me to nurture new research papers appearing on arXiv and engage with members from various fields of study.

I express my deep appreciation for Subhradip Ghosh and Perumal Alagarsamy, who have served as the heads of the Department of Physics at our institute throughout my tenure, consecutively. They have helped me to smoothly resolve various administrative issues. However, I would like to mention that I have maintained a special rapport with Subhradip Ghosh, engaging in numerous discussions on prevalent political and academic matters within our country. I am also grateful to the department staff for effectively managing various technical issues within our department.

I must thank my former and present group members Pankaj Saha, Mousumi Mitra, Riajul Haque, Sourav Pal, Gargi Sen, Banashree Baishya, Ayan Chakraborty, Subhasis Maiti, Rajesh Mandal, Sovon sau and Jitumani Kalita for useful and charming discussion now and then. Besides that, all of them have been good company for various activities. Specially Gargi has been my constant companion for tea/coffee and other things. Her childish whimsical nature has made my stay at IIT Guwahati enjoyable. I have also had enjoyable times with my batchmates, Rakesh Sarkar, Dipti Kanika Mahato, Sayan Lahiri and Manavendra Singh Gangwar, who have always stayed beside me.

I am grateful to my senior friends, Krishnanjan Da, Basabendu Da, Srimoy Da, Aritra Da, Sunando Da, Subhajit Da, Asmita Di and juniors, Surojit, Mandira and Arghyajit. I can not express how much I miss endless chats with them on endless topics. As time progressed, I met some other excellent companions, Swarup, Rony, Soumen, Avishek, Samit, and Sanket, who have made every day lively with versatile topics of discussion ranging from politics to ghost stories. I also want to acknowledge the musical group of Manas Hostel, where I resided during my stay at IIT Guwahati. We have performed together many times, notably, securing the first position in the inter hostel band competition, Manthan, was a special moment for me. I must thank Anjishnu Biswas, and Chandrima Dey for accompanying and encouraging me, often forcefully, to perform on various occasions, for that matter the cultural group, *Tero Parbon*, where I have performed several times.

I am indebted to my old friends, Himadri Roy, Pritam Palit, Supriyo Naskar, Shirsendu Nanda and Mainak Chakraborty, whom I met during graduation and post graduation. They are still in my contact and have always been very supportive. Coming from a very remote village, I should add to this regard, Presidency University (my undergrad.), which has played a major role in shaping my outlook and developing my consciousness on social, economic and political affairs. Importantly, this institution has driven me to pursue my interest in physics further. I can not forget the course of mathematical physics by Tarasankar Nag, statistical mechanics by Muktish Acharyya, and electrodynamics by Arabinda Nayek. I should also mention Asmita Mukherjee and Urjit Yajnik, under whom I have been guided in my post graduation at IIT Bombay. My interest in theoretical physics got a boost in association with them.

My parents, sister and extended family members have always played a crucial role in the background of this journey with their unconditional love and affection.

During this PhD tenure, I have met so many people and have so many interesting stories with them to tell, however, near the end of this journey, I feel that my story is very much unique like others.

March 2024

Rajesh Karmakar
IIT Gauwahati

Abstract

The dissipative nature of time dependent systems is well known to have an intriguing feature of superradiance like phenomena when interacting with radiation either classically or quantum mechanically. In this thesis we have considered two particular dynamical systems arising in two different realms namely, oscillating black holes (BH) in the sky and oscillating bubbles in the laboratory. In the first part of the thesis, we studied the classical scattering of massless fields from oscillating BHs and calculated the absorption cross-section. In the second part of the thesis, we have considered a laboratory system of an oscillating gas bubble, where we have proposed a framework and studied the phenomena of quantum mechanical particle production mapping the system into an analog geometric background.

The first system of the oscillating BH emerges in the merging event of binary BHs. This merging of two back holes comprises three distinct stages: inspiral, merger and ringdown. The recent detection of gravitational waves by LIGO-Virgo has been shown to describe these three phases with great detail which should be extremely useful to gain deep insight into the nature of spacetime. One of the motivations of this thesis would be to further study the properties of the oscillating BHs by exploring the scattering processes of different fundamental fields. Particularly, as a first case study we have attempted to study the last phase of the merger which is the ringdown phase. We have analysed the absorption cross section of the BHs in its ringdown phase for two fundamental fields: scalar and electromagnetic field. The absorption cross section turns out to be oscillating in time reflecting the time dependent nature of the ringing BHs. Interestingly, in the appropriate parameter range (discussed in detail in the thesis) the cross section turns negative during the course of its evolution, and such change suggests that the ringing BHs is superradiant within the time scale of its oscillation. The time dependent superradiant cross section naturally encodes the information of the decay time scale of the gravitational wave perturbation of the BH under consideration, which is related to the quasinormal modes of gravitational waves bearing the signature of the ringdown phase.

To observe this signature, we have proposed two possible scenarios in the context of scalar and electromagnetic field scattering. In the first case, we assumed the scalar field to be axion-like and exploited its natural interaction with the electromagnetic field via the well known Chern-Simons coupling and with the Fermion via dipole like coupling. Due to superradiant scattering of the ringing BHs, the scattered axion acquires enhanced amplitude with non-trivial time dependence, and that induces a time varying rotation of the plane of polarization of the photon and dipole moment of a nucleon. In the second scenario, we have directly analyzed the scattering of the electromagnetic field from the ringing BHs and computed the time dependent absorption cross-section which is superradiant in nature. The observable so calculated associated with the electromagnetic field can possibly be detected directly by different electromagnetic wave detectors. Taking into account the frequency range and precision time scale of such detectors we have put constraints on the BH mass for which superradiance could be observed.

In the second case, we have studied a special laboratory system where an air bubble submerged in the water is perturbed by an external sound wave, and the bubble

undergoes rapid oscillation. Experimentally it is found that during the course of its oscillation, the bubble emits a periodic flash of light within the ranges from visible to far ultraviolet wavelength. This phenomenon is popularly known as sonoluminescence. Over the years the mechanism of such light emission has been formulated in the framework of both classical and quantum mechanics with limited success, and various potential drawbacks. Particularly, we should point out that all the proposed quantum mechanical models predict divergent photon flux. In this thesis, we have attempted to explain this phenomenon by proposing a model in the framework of quantum field theory in curved spacetime. We modelled the oscillating bubble as a time dependent analog geometric background. This background geometry is described by an acoustic metric. We have introduced a conformal breaking coupling of the quantum field such as photon with the Ricci curvature scalar of this effective acoustic metric. With this set up we utilize the well known technique of quantum particle production in time dependent background and computed physical quantity namely the particle number spectrum which has been experimentally observed. We argue that the sonoluminescence is indeed a non-perturbative phenomena, and it is the parametric resonance in the oscillating background which is responsible for the photon production without any ultraviolet divergences. To this end, we should point out that due to extreme stiffness in the systems of differential equations, we could compute the spectrum up to an order of magnitude lower frequency compared to the experimentally observed values. However, the trend of the spectrum with frequency implies that the present formalism has the potential to match the experimentally measured data, which we have fitted with our results by extrapolation.

The universal nature of particle production in time dependent background has motivated us to propose a similar formalism for neutrino production from the oscillating air bubble in sonoluminescence phenomena. We have minimally coupled the massive fermion field to the same effective time dependent background as introduced in the case of photon production. With this coupling, we have quantified the produced number spectrum and power spectrum. The maximum mass of the fermion for which we have obtained production happens to be $\sim 10^{-6}$ eV. This has motivated us to identify the fermion as a neutrino. Therefore, the oscillating bubble in the water gives rise to an intriguing event of neutrino production in Laboratory settings.

List of Publications in chronological order

1. **Ringing black holes are superradiant: The case of ultralight scalar fields**,
   Rajesh Karmakar, Debaprasad Maity
   Phys. Rev. D **105**, no.10, 104045 (2022)
   arXiv:2109.10940

2. **Superradiant scattering of electromagnetic fields from ringing black holes**,
   Rajesh Karmakar, Debaprasad Maity
   arXiv:2310.01548

3. **Sonoluminescence: Photon production in time dependent analog system**,
   Rajesh Karmakar, Debaprasad Maity
   Phys. Rev. D **109**, no.10, 105016 (2024)
   arXiv:2311.03305,

4. **Sononeutrinoescence: Neutrinos from Ringing Bubble of Sonoluminescence**
   Rajesh Karmakar, Debaprasad Maity
   Eur. Phys. J. Plus **139**, no.8, 674 (2024)
   arXiv: 2401.02405

Talks and Poster presentations at workshops and conferences

1. 10th International Conference on Gravitation and Cosmology: New Horizons and Singularities in Gravity (ICGC 2023)

   Poster title- Superradiant scattering of the electromagnetic field from ringing black holes.

2. 32nd meeting of Indian Association for General Relativity and Gravitation (IAGRG32): Offline conference at IISER Kolkata, India, Dec 19-21, 2022

   Title of the Talk and the Poster- Ringing Black Holes Are Superradiant

3. 27th International Conference of International Academy of Physical Sciences On Advances in Relativity and Cosmology (PARC-2021), Oct 26-28, 2021

   Title of the Talk- Ringing Black Holes Are Superradiant

4. AAPPS-DACG Workshop 2021 on Astrophysics, Cosmology and Gravitation: Online Workshop with the headquarters at APCTP, 6th Oct 2021

   Title of the Talk- Absorption Cross Sections Of Ringing Black Holes: Superradiance

Contents

List of Figures

List of Tables

"...We lost the skyline, We stepped right off the map
Drifted into black space, And let the clocks
relapse..."

Steven Wilson 'The Sky Moves Sideways'

1.1 Dynamical physical systems: classical and quantum phenomena

Our universe is full of dynamical events [1, 2]. A static system may be interesting in its own right. However, it is the dynamical behaviour which captures the most fundamental natures of a system. Objects far away from us naturally may not show anything interesting but can reveal their characteristics through some probable means such as the emission of radiation if they happen to be in a dynamical condition, at least, for some duration. This radiation may be in the form of gravitational waves from the quadrupole oscillation of massive compact objects [1], electromagnetic flux from supernova explosions [3] or Sonoluminescence [5] due to oscillating gas bubbles in water. We particularly mentioned the above systems, for those are the focus of our present study. The fundamental features shared by all these systems are their inherent dissipative and oscillatory nature. Importantly, dissipative systems play a very significant role in testifying underlying theories of physics and their predictions. We will be particularly focussing on dynamical events that arise in two contexts: astrophysical systems and fluid systems. We will start with astrophysical systems first.

1.2 Astrophysical system: ringing black hole

Einstein's formulation of gravity in terms of the general theory of relativity (GTR) has been very crucial in our understanding of the universe [6, 7]. In the context of strong gravity, this formulation has been proven to be highly effective, whereas the Newtonian approach encounters difficulties [7]. GTR has systematically linked the geometry of spacetime with the presence of matter through Einstein's field equation, which can be obtained from the following Einstein-Hilbert action, including a matter lagrangian, $\mathcal{L}_m$, as,

$$\mathcal{S} = \int \sqrt{-g}\, d^4x \left[\frac{R}{16\pi G} + \mathcal{L}_m\right]. \tag{1.1}$$

Where G is Newton's gravitational constant, R is the Ricci scalar curvature of the metric $g_{\mu\nu}$, and the determinant of the metric is denoted as $g \equiv det[g_{\mu\nu}]$. Applying the variational principle, one could be able to derive the famous Einstein equation [7],

$$R_{\mu\nu} - \frac{1}{2}Rg_{\mu\nu} = 8\pi G T_{\mu\nu}, \tag{1.2}$$

where $R_{\mu\nu}$ is the Ricci tensor of the background metric and $T_{\mu\nu}$ describes the energy momentum tensor of the matter existing in the space time. However, in the absence of matter, the above equation takes the following obvious form

$$R_{\mu\nu} - \frac{1}{2}Rg_{\mu\nu} = 0, \tag{1.3}$$

which is known as the vacuum Einstein equation. The most general solution of the above equation is the Kerr solution, which describes an axis symmetric, spinning BH space time. In 1963, Kerr developed [8] this solution. In Boyer-Lindquist coordinates, the Kerr BH spacetime metric is expressed as follows:

$$ds^2 = -\left(1-\frac{2Mr}{\rho^2}\right)dt^2 - \frac{4aMr\sin^2\theta}{\rho^2}dtd\phi + \frac{\rho^2}{\Delta}dr^2 + \rho^2 d\theta^2 + \left(r^2+a^2+\frac{2Mra^2\sin^2\theta}{\rho^2}\right)\sin^2\theta d\varphi^2. \tag{1.4}$$

Where $\rho^2 = r^2 + a^2\cos^2\theta$ and $\Delta = r^2 - 2Mr + a^2$. M and a are the mass and angular momentum of the BH respectively. This space-time allows two horizons, $r_\pm = M \pm \sqrt{M^2 - a^2}$, where r_+ is the outer event horizon. However, in the investigation of perturbations in the BH spacetime, our primary focus will be on the static spherically symmetric solution of the vacuum Einstein equation, derived by Schwarzschild in 1916. This solution is described by the following metric, known as the Schwarzschild metric,

$$ds^2 = -f(r)dt^2 + f(r)^{-1}dr^2 + r^2 d\theta^2 + r^2\sin^2\theta d\varphi^2 \tag{1.5}$$

where, $f(r) = 1 - 2GM/r$ and interestingly, M initially appears as a parameter, which we can be interpreted as the Newtonian mass. As it turns out, Schwarzschild's metric provides for a unique spherically symmetric solution of the vacuum Einstein's equation,

which is known as a statement of Birkhoff's theorem [9]. Curvature invariant for this space time turns out as $R_{\mu\nu\alpha\beta}R^{\mu\nu\alpha\beta} = 48G^2M^2/r^2$. Hence, the above metric essentially describes the space time outside a spherically symmetric source characterized by the parameter M. Henceforth, we will consider the unit system with Newton's gravitational constant $G = 1$. In the following analysis, we will discuss the ringing black hole by developing perturbation on the Schwarzschild black hole.

1.2.1 Quadrupole perturbation to Black hole: ring down phase in radiation gauge

Black holes (BHs) can interact through various channels with the surrounding environment, which, due to Einstein's formulation, enter into the picture through the energy-momentum tensor. The analysis of BH perturbation, in general, is very old but still very relevant and become diversified throughout the years. The importance of this study stems from the fact that the properties of the BHs, such as the information of mass, charge and angular momentum, get imprinted in the emitted radiation known as gravitational waves (GW). In this section, we will particularly discuss the generation of gravitational waves due to the perturbation in Schwarzschild space time and derive the space time structure of this perturbed Schwarzschild background during the period of this GWs emission.

As discussed before, Schwarzschild BH space time being the vacuum solution of the Einstein equation, we will start with the vacuum Einstein equation, (1.3), and apply a small perturbation with

$$g_{\mu\nu} \to g^0_{\mu\nu} + h_{\mu\nu}, \tag{1.6}$$

where, the condition $|h_{\mu\nu}|/|g^0_{\mu\nu}| << 1$ should be satisfied. As a result, (1.3) will take the following form [10],

$$R^0_{\mu\nu} + \delta R_{\mu\nu} = 0, \tag{1.7}$$

with $\delta R_{\mu\nu}$ signifying the linearized perturbation, upto first order in $h_{\mu\nu}$. Whereas, $R^0_{\mu\nu}$ represents the unperturbed components, and this can be put to zero. Hence the above equation finally becomes

$$\delta R_{\mu\nu} = 0. \tag{1.8}$$

As the unperturbed Schwarzschild space time is spherically symmetric, the general form of the perturbation, $h_{\mu\nu}$, can be built in the basis, constructed out of spherical harmonics. Moreover, depending on the nature of the components of $h_{\mu\nu}$ as to how they change under parity transformation, $(\theta, \phi) \to (\pi - \theta, \pi + \phi)$, can be separated into parity-even and parity-odd parts. The general form of the perturbation following this decomposition has been constructed a long time back by Regge-Wheeler [11] and Zerrili [12] (having issues of typos, one may look at [13]) and can be given as [14],

$$(h_{lm})_{\mu\nu} = (h^{(\mathrm{e})}_{lm})_{\mu\nu} + (h^{(\mathrm{o})}_{lm})_{\mu\nu}. \tag{1.9}$$

The index (o) and (e) in the exponents signify the odd and even parity part of the perturbation respectively. Suppressing the space-time index, μ, ν, and using boldface to

represent these tensorial quantities, we express the above decomposition as

$$\mathbf{h}_{lm} = \mathbf{h}^{(\mathrm{e})}_{lm} + \mathbf{h}^{(\mathrm{o})}_{lm}, \tag{1.10}$$

where,

$$\mathbf{h}^{(\mathrm{o})}_{lm} = \frac{\mathrm{i}}{r}\sqrt{2l(l+1)}\Big[\mathrm{i}h^{(0)}_{lm}(t,r)\mathbf{c}^{(0)}_{lm} + h^{(1)}_{lm}(t,r)\mathbf{c}^{(1)}_{lm} - \frac{1}{2r}\sqrt{(l-1)(l+2)}h^{(2)}_{lm}(t,r)\mathbf{d}_{lm}\Big], \tag{1.11}$$

and

$$\begin{aligned}\mathbf{h}^{(\mathrm{e})}_{lm} = &\left(1-\frac{2M}{r}\right)H^{(0)}_{lm}(t,r)\mathbf{a}^{(0)}_{lm} - \sqrt{2}\mathrm{i}H^{(1)}_{lm}(t,r)\mathbf{a}^{(1)}_{lm} + \left(1-\frac{2M}{r}\right)^{-1}H^{(2)}_{lm}(t,r)\mathbf{a}^{(2)}_{lm}\\ &- \frac{1}{r}\sqrt{2l(l+1)}\Big(\mathrm{i}h^{(0)(\mathrm{e})}_{lm}(t,r)\mathbf{b}^{(0)}_{lm} + \mathrm{i}h^{(1)(\mathrm{e})}_{lm}(t,r)\mathbf{b}^{(1)}_{lm}\Big)\\ &+ \sqrt{\{l(l+1)(l-1)(l+2)/2\}}G_{lm}(t,r)\mathbf{f}_{lm} + \sqrt{2}\{K_{lm}(t,r) - \frac{1}{2}G_{lm}(t,r)\}\mathbf{g}_{lm}.\end{aligned} \tag{1.12}$$

Where, $\mathbf{a}^{(0)}_{lm}, \mathbf{a}^{(1)}_{lm}$ and $\mathbf{a}^{(2)}_{lm}$ represent the scalar basis, with the respective components of perturbation, $H^{(0)}_{lm}(t,r), H^{(1)}_{lm}(t,r)$ and $H^{(2)}_{lm}(t,r)$, which transform as scalar. $\mathbf{b}^{(0)}_{lm}, \mathbf{b}^{(1)}_{lm}, \mathbf{c}^{(0)}_{lm}$ and $\mathbf{c}^{(1)}_{lm}$ represent the vector basis, with the respective components of perturbation, $h^{(0)(\mathrm{e})}_{lm}(t,r), h^{(1)(\mathrm{e})}_{lm}(t,r), h^{(0)}_{lm}(t,r)$ and $h^{(1)}_{lm}(t,r)$, which transform as vector. Whereas $\mathbf{d}_{lm}, \mathbf{f}_{lm}$ and $\mathbf{g}_{lm}$ represent the 2nd rank tensor basis, with the respective components of perturbation, $h^{(2)}_{lm}(t,r), G_{lm}(t,r)$ and $K_{lm}(t,r) - \frac{1}{2}G_{lm}(t,r)$, which transform as tensor of rank-2. The explicit form of these bases is given in Appendix (A). $\mathbf{h}_{lm}$ being a symmetric metric tensor, it primarily contains 10 independent components (among them three belong to odd parity components and seven belong to the even parity components).

Quasinormal mode (QNMs) of GWs: In their pioneering work, Regge-Wheeler [11] and Zerrili [12] derived the perturbation equations governing the components of (1.11) and (1.12). They found that all the perturbation equation ultimately boil down to a single differential equation, which resembles to a form of Schrödinger like equation.

$$\frac{d^2Z_i}{dr_*^2} + (\omega^2 - V_i)Z_i = 0. \tag{1.13}$$

Where the Tortoise coordinate is denoted as $dr_* = dr/f(r)$, and upon integrating one gets $r_* = r + 2M\ln(r/2M-1)$. Whereas, the Z_i with $i \equiv \{(\mathrm{e}),(\mathrm{o})\}$ represent a spatial function arising in even and odd parity respectively, while the temporal part for both of the perturbation is governed by $e^{-\mathrm{i}\omega t}$. The potential corresponding to the odd parity perturbation, $V_{(\mathrm{o})}$ is referred to as Regge-Wheeler potential, which for quadrupole mode ($l=2$), assumes the following form [11],

$$V_{(\mathrm{o})} = f(r)\left(\frac{l(l+1)}{r^2} - \frac{6M}{r^3}\right). \tag{1.14}$$

Where, $f(r) = 1 - 2M/r$ with M signifying the BH mass. The potential corresponding to the even parity perturbation, $V_{(e)}$ is referred to as Zerrili potential, which for quadrupole mode takes the following form [12],

$$V_{(e)} = f(r)\frac{2\lambda^2(\lambda+1)r^3 + 6\lambda^2 M r^2 + 18\lambda M^2 r + 18m^3}{r^3(\lambda r + 3M)^2}, \tag{1.15}$$

where $\lambda = (l-1)(l+2)/2$. It is important to note that azimuthal mode, m does not appear in the potential. Moreover, both the even and odd parity potentials have the following limiting form

$$V_i \to \begin{cases} f(r), & r \to r_h, \\ \frac{1}{r^2}, & r \to \infty. \end{cases} \tag{1.16}$$

Similarly, it is straightforward to deduce the limiting form of Z_i (1.13). A particular set of the asymptotic solution, which constitutes the quasinormal mode (QNM) boundary condition, can be given as,

$$Z_i \to \begin{cases} e^{-\mathrm{i}\omega r_*}, & r \to r_h, \\ e^{\mathrm{i}\omega r_*}, & r \to \infty, \end{cases} \tag{1.17}$$

with the temporal part of the perturbation $e^{-\mathrm{i}\omega t}$, these solutions demonstrate an ingoing mode near the horizon of BH and an outgoing mode near spatial infinity. There are various methods to find out the solution of Z_i, which satisfies the above set of QNM boundary conditions. A long time back, S. Chandrasekhar [15, 16] implemented the shooting method to find out the solution and discovered that the QNM boundary condition is satisfied for a set of complex values of the frequency ω. These frequencies are popularly known as QNM frequency, such as for $l = 2$, $\omega = (0.74734 - \mathrm{i}\ 0.17792)(r_h)^{-1}$. Where $r_h = 2M$ is the radius of the event horizon of Schwarzschild BH. Moreover the perturbation potentials, V_i being independent of the azimuthal mode, m, QNMs also turn out to be independent of m.

The gauge choice given in Regge-Wheeler is suitable for analysing the stability of the BH. However, it does not provide for the expected asymptotic behaviour of the perturbation, which should decrease as $1/r^n$ $(n \geq 1)$ in $r \to \infty$. The reason is attributed to the bad choice of the coordinate system (one may look at [17] for detail). Therefore, later studies [14, 17] have attempted to achieve the correct asymptotic behaviour of the perturbation by modifying the gauge choice of Regge-Wheeler. This modified gauge choice is known as a *radiation gauge*. The invariance of the curvature of the perturbed space time under different choice of coordinate system leaves a redundancy in the perturbation variables. Hence, this freedom could be exploited. Under infinitesimal diffeomorphism transformation, $x_\mu \to x_\mu + \zeta_\mu$, the perturbation $(h^{lm})_{\mu\nu}$ modifies to

$$(\tilde{h}^{lm})_{\mu\nu} = (h^{lm})_{\mu\nu} - (\nabla_\mu \zeta_\nu^{lm} + \nabla_\nu \zeta_\mu^{lm}). \tag{1.18}$$

With ζ_μ acting as an infinitesimal displacement four vector, we can fix four of the components of perturbation. The covariant derivatives are computed with respect to the background metric.

Gauge fixing of the odd parity components: We will be specifically following the procedure detailed in [14] while dealing with the radiation gauge, and for the odd parity components of the perturbation it is given as,

$$\zeta^{(o)}_{lm} = \frac{\mathrm{i}}{r}\Lambda_{lm}(t,r)(0,0,\mathbf{L}Y_{lm}(\Omega)), \tag{1.19}$$

(four components of ζ are understood from the parenthesis) where, $\mathbf{L} = -\mathrm{i}\{\hat{e}_\phi\partial_\theta - \hat{e}_\theta(1/sin\theta)\partial_\phi\}$, $\hat{e}_\theta$ and $\hat{e}_\phi$ are the unit vectors along θ and ϕ respectively. Consequently, by adjusting $\Lambda_{lm}(t,r)$, one of the components (1.18) of the transformed perturbation (full expression is given in Appendix.A) could be fixed. We list here the expressions of the odd parity perturbation components under gauge transformation,

$$\begin{aligned}
\tilde{h}^{(0)}_{lm}(t,r) &= h^{(0)}_{lm}(t,r) - \frac{\partial\Lambda_{lm}}{\partial t},\\
\tilde{h}^{(1)}_{lm}(t,r) &= h^{(1)}_{lm}(t,r) - r^2\frac{\partial}{\partial r}\left(\frac{\Lambda_{lm}}{r^2}\right),\\
\tilde{h}^{(2)}_{lm}(t,r) &= h^{(2)}_{lm}(t,r) + 2\Lambda_{lm}(t,r).
\end{aligned} \tag{1.20}$$

In the radiation gauge, we will set $\tilde{h}^{(0)}_{lm}(t,r)$ to be zero, which can be obtained by fixing the gauge Λ_{lm} in the following way,

$$\tilde{h}^{(0)}_{lm}(t,r) = 0 \implies h^{(0)}_{lm}(t,r) - \frac{\partial\Lambda_{lm}}{\partial t} = 0 \implies \Lambda_{lm} = -\frac{1}{\mathrm{i}\omega}h^{(0)}_{lm}(t,r). \tag{1.21}$$

Where, the quantities with *tilde* represent the components of the perturbation in the radiation gauge, while the same without *tilde* signify the components which have been obtained by Regge-Wheeler gauge. We have listed in Appendix.A the functional form of the gauge fixed perturbation components obtained by Regge-Wheeler [11]. It is important to note that the temporal part, $e^{-\mathrm{i}\omega t}$ of the perturbation remains the same in this new gauge. We utilize this temporal part of the components as per the need. Remember that we are only concerned with the asymptotic radial behaviour of the perturbation as previously discussed. Once the gauge fixing function, Λ_{lm} is fixed, we will be able to obtain other odd parity components as,

$$\tilde{h}^{(1)}_{lm}(t,r) = \frac{2\lambda}{\omega^2 r^2}\left(1-\frac{2M}{r}\right)h^{(1)}_{lm}(t,r), \quad \tilde{h}^{(2)}_{lm}(t,r) = -\frac{2}{\mathrm{i}\omega}h^{(0)}_{lm}(t,r), \tag{1.22}$$

where $\lambda = (l-1)(l+2)/2$. We have also utilized the Einstein equations governing the perturbation [13, 14] that connect $h^{(0)}_{lm}(t,r)$ and $h^{(1)}_{lm}(t,r)$ to obtain $\tilde{h}^{(1)}_{lm}(t,r)$.

We will be mainly considering quadrupolar perturbation to the BH. Hence, we present

here the matrix form of the gauge fixed odd parity perturbation for $l = 2$ and $m = 0$,

$$h^{(\mathrm{o})}_{\mu\nu} \equiv \begin{pmatrix} 0 & 0 & 0 & 0 \\ 0 & 0 & 0 & \tilde{h}^{(0)}_{20}(t,r) s_\theta \partial_\theta Y_{20} \\ 0 & 0 & 0 & \frac{1}{2}\tilde{h}^{(2)}_{20}(t,r)\mathcal{C}_{20}(\theta) \\ 0 & \tilde{h}^{(0)}_{20}(t,r) s_\theta \partial_\theta Y_{20} & \frac{1}{2}\tilde{h}^{(2)}_{20}(t,r)\mathcal{C}_{20}(\theta) & 0 \end{pmatrix}, \tag{1.23}$$

where, $\mathcal{C}_{20}(\theta) = (c_\theta \partial_\theta Y_{20} - s_\theta \partial^2_\theta Y_{20})$. whereas, $s_\theta = \sin\theta$ and $c_\theta = \cos\theta$.

Gauge fixing of the even parity components: To address the even parity component of the perturbation, we choose the following gauge transformation,

$$\zeta^{(\mathrm{e})}_{lm} = \mathcal{M}_0(t,r) Y_{lm}(\Omega)\hat{e}_t + \mathcal{M}_1(t,r) Y_{lm}(\Omega)\hat{e}_r + \mathcal{M}_2(0, \boldsymbol{\nabla} Y_{lm}), \tag{1.24}$$

with, $\boldsymbol{\nabla} = \hat{e}_\theta \partial_\theta + \hat{e}_\phi (1/\sin\theta)\partial_\phi$. Using this transformation, three even parity components can be fixed by selecting $\mathcal{M}_0$, $\mathcal{M}_1$, and $\mathcal{M}_2$ in a manner closely resembling the approach taken in the odd parity scenario. We list here the even parity components of the perturbation under gauge transformation (one may look at Appendix.A for the expression of the transformed components),

$$\begin{aligned}
\tilde{H}^{(0)}_{lm}(t,r) &= H^{(0)}_{lm}(t,r) - 2\Big(1 - \frac{2M}{r}\Big)^{-1}\Big(\frac{\partial \mathcal{M}_0}{\partial t} - \frac{M}{r^3}(r-2M)\mathcal{M}_1\Big), \\
\tilde{H}^{(1)}_{lm}(t,r) &= H^{(1)}_{lm}(t,r) - \Big(\frac{\partial \mathcal{M}_1}{\partial t} + \frac{\partial \mathcal{M}_0}{\partial r} - \frac{2M}{r(r-2M)}\mathcal{M}_0\Big), \\
\tilde{H}^{(2)}_{lm}(t,r) &= H^{(2)}_{lm}(t,r) - 2\Big(1 - \frac{2M}{r}\Big)\Big(\frac{\partial \mathcal{M}_1}{\partial r} + \frac{M}{r(r-2M)}\mathcal{M}_1\Big), \\
\tilde{h}^{(0)(\mathrm{e})}_{lm}(t,r) &= h^{(0)(e)}_{lm}(t,r) - \Big(\frac{\partial \mathcal{M}_2}{\partial t} + \mathcal{M}_0\Big), \\
\tilde{h}^{(1)(e)}_{lm} &= h^{(1)(e)}_{lm} - \Big(\frac{\partial \mathcal{M}_2}{\partial r} - \frac{2}{r}\mathcal{M}_2 + \mathcal{M}_1\Big), \\
\tilde{K}_{lm} &= K_{lm}(t,r) - \frac{2}{r^2}(r-2M)\mathcal{M}_1, \\
\tilde{G}_{lm}(t,r) &= G_{lm}(t,r) - \frac{2}{r^2}\mathcal{M}_2.
\end{aligned} \tag{1.25}$$

We have found that for the following choice,

$$\mathcal{M}_1(t,r) = \frac{1}{2} r \Big(1 - \frac{2M}{r}\Big)^{-1}\Big[\mathrm{i}\omega - \frac{3M}{\lambda r^2}\Big] Z_{(\mathrm{e})}(t,r), \tag{1.26}$$

one of the even parity perturbation components becomes,

$$\tilde{K}_{lm}(t,r) = K_{lm}(t,r) - \frac{2}{r^2}(r-2M)\mathcal{M}_1. \tag{1.27}$$

This component goes as $1/r$ in $r \to \infty$, leaving out the plane wave part $e^{-i\omega(t-r_*)}$ (as $Z \sim e^{i\omega r_*}$). Once $\mathcal{M}_1(t,r)$ is chosen, $\mathcal{M}_0$ and $\mathcal{M}_2$ can be obtained by fixing the other components in the following manner. From the Einstein equation, governing the perturbation, one can find that having no source term implies, $H^{(0)}_{lm} = H^{(2)}_{lm} = H_{lm}$ (here we have introduced a new function H_{lm} for the equality) [13, 14], and accordingly, we also fix $\tilde{H}^{(0)}_{lm} = \tilde{H}^{(2)}_{lm} = \tilde{H}_{lm}$, which implies(1.25),

$$\mathcal{M}_0 = -\frac{1}{i\omega}\Big\{\Big(1-\frac{2M}{r}\Big)^2\frac{\partial\mathcal{M}_1}{\partial r} + \Big(1-\frac{2M}{r}\Big)\frac{2M}{r^2}\mathcal{M}_1\Big\}, \tag{1.28}$$

(remember time dependence of the perturbation assumed to be $e^{-i\omega t}$) which fixes $\mathcal{M}_0$ in terms of $\mathcal{M}_1$. Making $\tilde{h}^{(0)(e)}_{lm} = 0$ would lead (A.4) to $\mathcal{M}_2 = \frac{1}{i\omega}\mathcal{M}_0$. Therefore substituting $\mathcal{M}_0$ in terms of $\mathcal{M}_2$ in (1.28) one can fix $\mathcal{M}_2$ as,

$$\mathcal{M}_2 = \frac{1}{i\omega}\Big[-\frac{1}{i\omega}\Big\{\Big(1-\frac{2M}{r}\Big)^2\frac{\partial\mathcal{M}_1}{\partial r} + \Big(1-\frac{2M}{r}\Big)\frac{2M}{r^2}\mathcal{M}_1\Big\}\Big]. \tag{1.29}$$

To summarize, we have fixed $\mathcal{M}_1$ (1.26) in terms of the background solution, so that K_{lm} behaves as $\mathcal{O}(1/r)$ asymptotically, and we have fixed the other two gauge parameters, $\mathcal{M}_0, \mathcal{M}_2$, in terms of $\mathcal{M}_1$. Again considering the quadrupolar modes of the perturbation, we present here the matrix form of the gauge fixed even parity components for $l = 2$ and $m = 0$,

$$h^{(e)}_{\mu\nu} = \begin{pmatrix} \tilde{H}_{20}(t,r)(1-\frac{2M}{r})Y_{20} & \tilde{H}^{(1)}_{20}(t,r)Y_{20} & 0 & 0 \\ \tilde{H}^{(1)}_{20}(t,r)Y_{20} & \tilde{H}_{20}(t,r)(1-\frac{2M}{r})^{-1}Y^0_2 & \tilde{h}^{(1)(e)}_{20}\partial_\theta Y_{20} & 0 \\ 0 & \tilde{h}^{(1)(e)}_{20}\partial_\theta Y_{2^0} & r^2\mathcal{D}_{20} & 0 \\ 0 & 0 & 0 & r^2\sin^2\theta\tilde{\mathcal{D}}_{20} \end{pmatrix}, \tag{1.30}$$

where, $\mathcal{D}_{20} = \tilde{K}_{20}(t,r)Y_{20} + \tilde{G}_{20}(t,r)\partial^2_\theta Y_{20}$ and $\tilde{\mathcal{D}}_{20} = \tilde{K}(t,r)Y_{20} + \cot\theta\tilde{G}(t,r)\partial_\theta Y_{20}$. Keeping in mind that the terms containing $\partial_\phi Y_{20}(=0)$ have been omitted. One can check the trace of the perturbation behaves as

$$h^\mu_\mu \sim [\tilde{K}_{20} - (\lambda+1)\tilde{G}_{20}] \sim \mathcal{O}\Big(\frac{1}{r^3}\Big), \quad r \to \infty. \tag{1.31}$$

After achieving the appropriate asymptotic behaviour of the perturbation components, we simply add the matrix of gauge-fixed perturbation components of both odd and even parity. The near horizon values of the ringing fields will be parameterized by ($|\tilde{Z}_{(o)}(r \to 2M)| = \mathcal{O}_h, |\tilde{Z}_{(e)}(r \to 2M)| = \mathcal{E}_h$). Implementing the shooting method [15, 16, 18] with the QNMs boundary conditions, one will be able to solve the Regge-Wheeler equations(1.13) to find out the quasinormal mode eigenfunctions. With these eigenfunctions, one can reconstruct the full solution of ringing Schwarzschild BH background, which depicts a Schwarzschild BH subjected to quadrupolar perturbation. The oscillation of this space time, governed by the quasinormal mode, is a consequence of the ringdown phase. We henceforth refer to this BH as ringing BH.

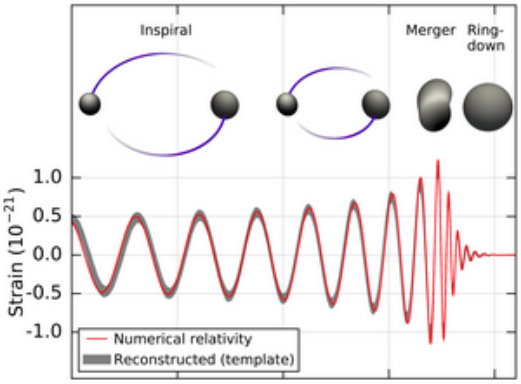

FIGURE 1.1: This figure has been taken from the LIGO-Virgo's published paper [1]. Estimated strain of the gravitational wave signal observed in the GW150914 event. As reported by LIGO-Virgo collaboration [1], the numerical relativity result, represented by the red solid line, matches 99.9% with the result, represented by the grey line, obtained from the received signal.

1.2.2 Direct detection of gravitational wave

In 2015 [1], the LIGO-Virgo collaboration achieved a groundbreaking milestone by successfully detecting the gravitational wave signature for the first time. This remarkable feat has paved the way for the emergence of a new field called gravitational wave astronomy. Subsequently, new observatories, such as KAGRA also joined in this endeavour and together, LVK (LIGO-Virgo-KAGRA) have made several detections [1, 19–32] (90 events have been detected so far [33]). These observations not only confirm the prediction of GTR in the strong field gravity regime, but they have correctly reproduced theoretically (numerical relativity) simulated phases in the merging of compact objects that consist of inspiral- merger-ringdown Fig.1.1. The consecutive observations by LVK have reported the gravitational signals coming from BH-BH, BH-NS (Neutron star) and NS-NS merger. In 2017, simultaneous observation [24] of the GW signal by LVK and EM signal by Fermi GRB have set forth the source for both of the signals as an NS-NS merger. Which in a way provides a complementary signature of the same event. In a similar setting, the question arises as to what else could be observed that may bear the signature of this merging event. Although most of the astrophysical BHs are spinning, the first step one may take for simplification is to consider a Schwarzschld BH as the end state of a binary BH merging event. During the ringdown phase, the structure of the BH can be constructed through gravitational perturbation as discussed in the preceding subsection. Once this information about the background space time is known, the next question is to define a suitable observable quantity, which can be measured. To start with, the absorption cross section of the BH, which is going through the ringdown phase, could be one such physical quantity. Therefore it will be interesting to look at the existing study on the absorption cross section of BHs.

1.2.3 Absorption cross section of static and stationary black holes

In the present case, the BH being the scatterer, the absorption cross-section is defined as the energy absorbed by the BH horizon, divided by the energy density of the wave incident at asymptotic spatial infinity. For a generic BH space time which allows killing vector, ξ^μ, one will have the following covariant conservation equation [7],

$$\nabla_\mu P^\mu = 0, \quad P^\mu = \mathscr{T}^\mu{}_\nu \xi^\nu, \tag{1.32}$$

where P^μ is the conserved quantity associated with the Killing vector ξ^μ. Whereas, $\mathscr{T}^\mu{}_\nu$ is the energy momentum tensor of the scattering field. The next step is to find out the Killing vectors for a given space time. We will discuss about the definition of absorption cross section for static Schwarzschild BH, however, it can be suitably generalized to stationary BH. The Schwarzschild metric is given in (1.5), which allows time like killing vector, $\xi_0 = \delta^\mu_0 \partial_\mu$. The conserved quantity associated with this particular Killing vector turns out as,

$$\mathcal{F} = \int d^3x \sqrt{-g_0} P^0, \tag{1.33}$$

where, g_0 denoted the determinant of Schwarzschild metric (1.5). Taking the time derivative on both sides of the above equation we get

$$\partial_t \mathcal{F} = \int d^3x \partial_t \left(\sqrt{-g_0} P^0\right) = -\int d^3x \partial_i \left(\sqrt{-g_0} P^i\right). \tag{1.34}$$

By choosing a r-constant hypersurface and applying the divergence theorem in the above equation one will arrive at

$$\partial_t \mathcal{F} = -\int r^2 d\Omega P^r \Big|_{r_h}^{\infty} = -\int r^2 d\Omega \mathscr{T}^r{}_t \xi^t \Big|_{r_h}^{\infty} = -\left[\int r^2 d\Omega \mathscr{T}^r{}_t \Big|_{r\to\infty} - \int r^2 d\Omega \mathscr{T}^r{}_t \Big|_{r_h}\right]. \tag{1.35}$$

Where, $d\Omega \equiv \sin\theta d\theta d\phi$. We can see that two terms in the last equality of the above equation are equal by the fact that $\partial_t \mathcal{F} = 0$, as mentioned previously. Therefore, one may infer that the energy being absorbed by the BH horizon per unit time could be equated with, $\partial_t \mathcal{F}_{r\to\infty}$. Now, the definition of the absorption cross section [34] is the amount of energy being absorbed by the BH horizon divided by the incident energy density. We define the incident energy density as, $\partial_t \mathcal{G} = \mathscr{T}^z{}_t$, which sometimes called as energy density current [35]. Utilizing this technology we obtain the absorption cross section in terms of the stress-energy tensor of the fields as,

$$\sigma \equiv \frac{\partial_t \mathcal{F}}{\partial_t \mathcal{G}}\Big|_{r\to\infty} = \frac{\int r^2 d\Omega \mathscr{T}^r{}_t}{\mathscr{T}^z{}_t}\Big|_{r\to\infty}. \tag{1.36}$$

Important to note that for an incident plane wave, the energy density per unit time, $\mathscr{T}^z{}_t$ is independent of the spatial coordinate, which will be discussed in the following section for different matter fields.

1.2.3.a Absorption cross section of the static Schwarzschild black hole for scalar field

In this section, we shall elaborately discuss the procedure to evaluate the absorption cross section of static Schwarzschild for the scalar field. We leave out the extension of this procedure to the electromagnetic field case for the later chapters. Nevertheless, for minimal interaction with the BH space time, the governing equation of the scalar field is given by

$$\frac{1}{\sqrt{-g}}\partial_\mu(\sqrt{-g}g^{\mu\nu}\partial_\nu\phi) = 0. \tag{1.37}$$

As the background space time is spherically symmetric, we decompose the scalar field with the help of spherical harmonics, $Y_{lm}(\theta,\varphi)$ as,

$$\phi(t,\mathbf{r}) = \sum \mathcal{N}^{\phi}_{lm}\xi^{lm}(t,r)Y_{lm}(\theta,\varphi), \tag{1.38}$$

where N^{ϕ}_{lm} is the normalization constant for the scalar field, ϕ. Expanding the above scalar field equation, the mode function satisfies,

$$\partial_t^2\xi^{lm}(t,r) + f(r)\frac{1}{r^2}\partial_r\{r^2f(r)\partial_r\xi^{lm}(t,r)\} - f(r)\frac{l(l+1)}{r^2}\xi^{lm}(t,r) = 0. \tag{1.39}$$

Utilizing the static nature of the background space time we can identify the frequency (k) modes of the scalar fields as,

$$\xi^{lm}(t,r) = \int dk e^{-\mathrm{ikt}}\xi^{lm}(\mathrm{k},r). \tag{1.40}$$

The remaining task is to find out the solution of $\xi^{klm}(r)$, which satisfies the following equation,

$$f(r)\frac{1}{r^2}\partial_r\{r^2f(r)\partial_r\xi^{lm}(\mathrm{k},r)\} + \left[\mathrm{k}^2 - f(r)\frac{l(l+1)}{r^2}\right]\xi^{lm}(\mathrm{k},r) = 0. \tag{1.41}$$

At this point, we should mention that this equation could be solved analytically for limiting cases of frequency, k [34]. However, to find out the absorption cross section for all the frequency ranges, the above equation should be solved numerically. Definition of absorption cross section requires that the modes have to be ingoing near the horizon (r_h) of the BH. Hence the relevant asymptotic form of modes, which are straightforward to derive from the above equation, can be expressed as the,

$$\xi^{lm}(\mathrm{k},r) \to \begin{cases} \mathcal{T}_{\mathrm{kl}}e^{-\mathrm{ikr}_*}, & r \to r_h, \\ \mathcal{I}_{\mathrm{kl}}e^{-\mathrm{ikr}_*} + \mathcal{R}_{\mathrm{kl}}e^{\mathrm{ikr}_*}, & r \to \infty, \end{cases} \tag{1.42}$$

where $\mathcal{T}_{\mathrm{kl}}, \mathcal{I}_{\mathrm{kl}}$ and $\mathcal{R}_{\mathrm{kl}}$ are the transmission, incidence and reflection coefficients respectively. With the ingoing initial condition, one needs to evolve the field modes, $\xi^{klm}(r)$, governed by (1.41) up to $r \to \infty$ (which, for practical purpose, is considered to be far away from

the BH horizon). Once this solution is obtained near infinity for different modes, one will immediately be able to evaluate the numerator of (1.36), from the stress energy tensor of the scalar field,

$$\mathscr{T}_{\mu\nu} = \frac{1}{2}(\partial_\mu\phi^*\partial_\nu\phi + \partial_\mu\phi\partial_\nu\phi^*) - \frac{1}{2}g_{\mu\nu}\partial^\alpha\phi^*\partial_\alpha\phi. \tag{1.43}$$

The energy flux rate integrated over a spherical surface at spatial infinity gives us,

$$\int d\Omega r^2 \mathscr{T}_{tr} = \frac{1}{2}\int dk \sum_{lm} |\mathcal{N}^{\phi}_{\mathrm{k}lm}|^2 \left[\partial_t\xi^{lm^*}(\mathrm{k},r)\partial_r\xi^{lm}(\mathrm{k},r) + \partial_t\xi^{lm}(\mathrm{k},r)\partial_r\xi^{lm^*}(\mathrm{k},r)\right]. \tag{1.44}$$

Hence, the mode wise energy flux rate can be expressed as

$$\partial_t\mathcal{F}^{kl} = \frac{1}{2}\sum_{lm} |\mathcal{N}^{\phi}_{\mathrm{k}lm}|^2 \left[\partial_t\xi^{lm^*}(\mathrm{k},r)\partial_r\xi^{lm}(\mathrm{k},r) + \partial_t\xi^{lm}(\mathrm{k},r)\partial_r\xi^{lm^*}(\mathrm{k},r)\right]. \tag{1.45}$$

Furthermore, in the spatial infinity, the numerical solution of the scalar field could be matched with the asymptotic analytical form of the modes given in (1.42), so that we will obtain the following simplified expression,

$$\partial_t\mathcal{F}^{\mathrm{k}l} = \sum_{lm} |\mathcal{N}^{\phi}_{\mathrm{k}lm}|^2 \mathrm{k}^2\mathcal{I}^2_{\mathrm{k}l}\left(1 - \frac{\mathcal{R}^2_{\mathrm{k}l}}{\mathcal{I}^2_{\mathrm{k}l}}\right). \tag{1.46}$$

It is important to note that the azimuthal index does not appear in the energy flux rate. This will be clear in a moment. We are now left with the evaluation of the normalization factor and the incident energy density (the denominator of (1.36)). An incident plane wave of unit amplitude propagating along the z-direction can be expressed as,

$$\phi(t,\mathbf{x}) = e^{-\mathrm{i}\mathrm{k}(t+z)}, \tag{1.47}$$

which evaluates the incident energy density as,

$$\partial_t\mathcal{G} = \mathscr{T}^z{}_t = \frac{1}{2}(\partial_t\phi^*\partial_z\phi + \partial_t\phi\partial_z\phi^*) = \mathrm{k}^2. \tag{1.48}$$

Now the strategy to evaluate the normalization factor is to express the plane in spherical coordinates and match the expression with the incident part of the asymptotic form of the scalar field at spatial infinity. Rayleigh expansion of a plane wave propagating along the z-direction given by [34, 36],

$$e^{-\mathrm{i}\mathrm{k}(t+z_*)} \sim \sum \frac{e^{-\mathrm{i}\mathrm{k}(t+r_*)}}{2\mathrm{i}\mathrm{k}r}\sqrt{4\pi(2l+1)}Y^0_l(\Omega) + \text{Outgoing}. \tag{1.49}$$

Comparing the right hand side with the asymptotic form of the scalar field at spatial infinity provides for the normalization factor,

$$\mathcal{N}_{\mathrm{k}lm} = \frac{\sqrt{4\pi(2l+1)}}{2\mathrm{i}\mathrm{k}\mathcal{I}_{\mathrm{k}l}}\delta^0_m. \tag{1.50}$$

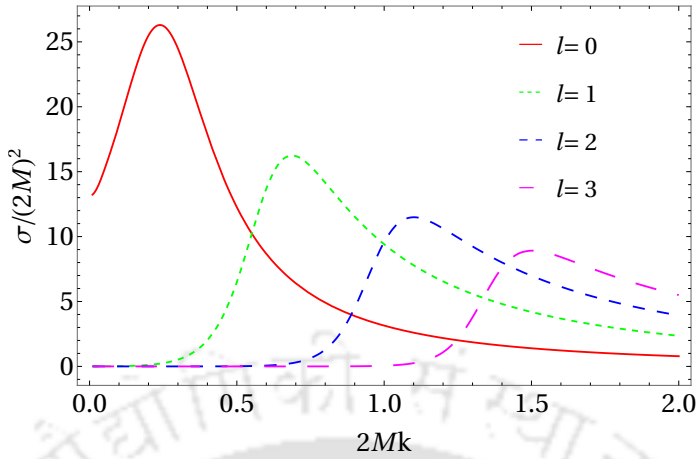

FIGURE 1.2: Partial absorption cross section of Schwarzschild BH has been plotted for different orbital modes, l with frequency.

Utilizing this normalization factor, finally, the absorption cross section can be expressed as,

$$\sigma^{kl} \equiv \frac{\partial_t \mathcal{F}^{\mathrm{kl}}}{\partial_t \mathcal{G}} = \sum_l \frac{\pi(2l+1)}{\mathrm{k}^2}\left(1 - \frac{\mathcal{R}^2_{\mathrm{kl}}}{\mathcal{I}^2_{\mathrm{kl}}}\right). \tag{1.51}$$

Absorption cross section corresponding to individual modes, often dubbed as partial absorption cross section, has been plotted with the frequency in Fig.1.2. In the low frequency limit, the absorption cross section is dominated by the $l = 0$ mode and the corresponding value resembles the area of the BH. This is a universal feature of static spherically symmetric BHs as identified by [37]. However, for high frequency the absorption cross section is dominated by the higher l modes.

1.2.3.b Negative absorption cross section of Kerr-Newman Black Hole: Superradiance

In this subsection, we will consider a little more general case of a rotating and charged BH, which is well described by the Kerr-Newman solution [38]. In the Boyer-Lindquist coordinate, this metric is given as,

$$ds^2 = -\left(1-\frac{2Mr}{\rho^2}\right)dt^2 - \frac{4aMr\sin^2\theta}{\rho^2}dtd\phi + \frac{\rho^2}{\Delta}dr^2 + \rho^2 d\theta^2 + \left(r^2+a^2+\frac{2Mra^2\sin^2\theta}{\rho^2}\right)\sin^2\theta d\varphi^2, \tag{1.52}$$

where $\rho^2 = r^2 + a^2\cos^2\theta$ and $\Delta = r^2 - 2Mr + a^2 + Q^2$. Whereas, Q, M and a are the charge, mass and angular momentum of the BH. This space time allows two horizons, $r_\pm = M \pm \sqrt{M^2 - a^2 - Q^2}$, where r_+ is the event horizon. On this background, we consider the action of a minimally coupled massless complex Scalar Field, which is governed by the following equation of motion,

$$(\nabla_\mu - \mathrm{i}qA_\mu)(\nabla^\mu - \mathrm{i}qA^\mu)\phi = 0. \tag{1.53}$$

Where ∇_μ represents the metric covariant derivative, and q denotes the charge being carried by the field. The background electromagnetic field will be considered as,

$$A_\mu = \left(-\frac{Qr}{\rho^2}, 0, 0, \frac{aQr\sin^2\theta}{\rho^2}\right). \tag{1.54}$$

The stationary and axis symmetric nature of the background space time prompts us to decompose the scalar field as,

$$\phi(t, r, \theta, \phi) = \sum_{lm} e^{-\mathrm{i}\mathrm{k}t} e^{\mathrm{i}m\phi} R_{lm}(\mathrm{k}, r) S_{lm}(\theta), \tag{1.55}$$

where l and m are the orbital angular mode and the azimuthal mode of the scalar field respectively. Substituting the expansion in the field equation we get two separate equations, for $S_{lm}(\theta)$ and $R_{lm}(r)$, the equation governing $R(r)$ is

$$\Delta \frac{d}{dr}\left(\Delta \frac{dR_{\mathrm{k}lm}(r)}{dr}\right) + U(r) R_{lm}(\mathrm{k}, r) = 0, \tag{1.56}$$

with the effective potential, $U(r)$, turns out as

$$U(r) = [\mathrm{k}(r^2 + a^2) - am - qQr]^2 + \Delta\left(2am\mathrm{k} - \mathcal{C}_{lm}\right). \tag{1.57}$$

Where $\mathcal{C}_{lm}$ is the separation constant, and it can be determined from the equation corresponding to $S(\theta)$, which is given as,

$$\frac{1}{\sin\theta}\frac{d}{d\theta}\left(\sin\theta \frac{d}{d\theta} S_{lm}(\theta)\right) + \left\{\mathcal{C}_{lm} - a^2\mathrm{k}^2\sin^2\theta - \frac{m^2}{\sin^2\theta}\right\} S_{lm}(\theta) = 0. \tag{1.58}$$

The physical solution of the above equation is well studied in the literature[39, 40], and corresponds to spheroidal-eigenfunction which resembles the usual Legendre's function in the limit, a or $\mathrm{k} \to 0$. The radial equation (1.56) can simply be solved in the near horizon and near infinity limit by parametrizing the variable in the following way[41],

$$\frac{d\tilde{r}}{dr} = \frac{r^2 + a^2}{\Delta}, \quad R_{lm}(\mathrm{k}, r) = \frac{\xi_{lm}(\mathrm{k}, r)}{\sqrt{r^2 + a^2}}, \tag{1.59}$$

where tortoise coordinate for Kerr-Newmann BH is given by

$$\tilde{r} = r + \frac{2M}{r_+ - r_-}\left(r_+ \ln\left|\frac{r - r_+}{2M}\right| - r_- \ln\left|\frac{r - r_-}{2M}\right|\right). \tag{1.60}$$

With this setup the radial equation (1.56) can be transformed into a equation in terms of $\tilde{r}$ as,

$$\frac{d^2\xi_{lm}(\mathrm{k}, r)}{d\tilde{r}^2} + V(r)\xi_{lm}(\mathrm{k}, r) = 0, \tag{1.61}$$

where,

$$V(r) = \left(\mathrm{k} - \frac{am}{r^2+a^2} - \frac{qQr}{r^2+a^2}\right)^2 - \frac{\Delta}{(r^2+a^2)^2}\left\{\mathcal{C}_{lm} - 2am\omega + \sqrt{r^2+a^2}\frac{d}{dr}\left\{\frac{r\Delta}{(r^2+a^2)^{\frac{3}{2}}}\right\}\right\}. \tag{1.62}$$

The asymptotic form of the above potential turns out as,

$$V(r) = \begin{cases} \left(\mathrm{k} - \frac{am}{r^2+a^2} - \frac{qQr}{r^2+a^2}\right)^2, & r \to r_+, \\ \mathrm{k}^2, & r \to \infty. \end{cases} \tag{1.63}$$

Given the above form of the potential, now, it is straightforward to derive the asymptotic form of the scalar field, and can be expressed as,

$$\xi_{lm}(\mathrm{k}, r) = \begin{cases} \mathcal{T}^{\mathrm{k}}_{lm} e^{-\mathrm{i}(\mathrm{k}-m\Omega-q\Phi)\tilde{r}}, & r \to r_+, \\ \mathcal{I}^{\mathrm{k}}_{lm} e^{-\mathrm{i}\mathrm{k}\tilde{r}} + \mathcal{R}^{\mathrm{k}}_{lm} e^{\mathrm{i}\mathrm{k}\tilde{r}}, & r \to \infty, \end{cases} \tag{1.64}$$

where, $\Omega = \frac{a}{r^2+a^2}$ is the angular velocity of the BH and $\Phi = \frac{Qr}{r^2+a^2}$ is the electrostatic potential. In accordance with the definition of absorption cross section we have considered the boundary condition, which states that the scalar wave is purely ingoing near the horizon and superposition of ingoing and outgoing near special infinity. Without doing the actual calculation, the amplification of the reflected signal can be understood with the help of the Wronskian of (1.61), which turns out to be

$$\begin{aligned} W[\xi_{lm}(\mathrm{k}, r), \xi^*_{lm}(\mathrm{k}, r)] &= \xi_{lm}(\mathrm{k}, r)\partial_{\tilde{r}}\xi^*_{lm}(\mathrm{k}, r) - \xi^*_{lm}(\mathrm{k}, r)\partial_{\tilde{r}}\xi_{lm}(\mathrm{k}, r), \\ &= \begin{cases} 2\mathrm{i}(\mathrm{k} - m\Omega - q\Phi)|\mathcal{T}^{\mathrm{k}}_{lm}|^2, & r \to r_+, \\ 2\mathrm{i}\mathrm{k}(|\mathcal{I}^{\mathrm{k}}_{lm}|^2 - |\mathcal{R}^{\mathrm{k}}_{lm}|^2), & r \to \infty. \end{cases} \end{aligned} \tag{1.65}$$

Then the conservation of the Wronskian implies

$$(|\mathcal{I}^{\mathrm{k}}_{lm}|^2 - |\mathcal{R}^{\mathrm{k}}_{lm}|^2) \sim sign(\mathrm{k} - m\Omega - q\Phi). \tag{1.66}$$

This suggests that the incoming wave will be scattered with enhanced amplitude as long as the frequency of the scalar field satisfies the condition, $\mathrm{k} < m\Omega + q\Phi$. This phenomenon is popularly known as superradiance. The amplification of the reflected wave will automatically make the absorption cross section negative; we refer the reader to [42] for rigorous analysis.

Importantly, there is a more fundamental viewpoint [43] to conceive the notion of superradiance in the case of rotating and charged BH, following the laws of BH thermodynamics. The first law of BH thermodynamics is stated as

$$dM = \frac{\kappa}{8\pi} dA + \Omega dJ + \Phi dQ. \tag{1.67}$$

where A and κ are respectively the area and the surface gravity of the BH. Substituting the variation of the angular momentum of the BH, $dJ/dM = m/\omega$ and the variation in the electrostatic potential $d\Phi/dM = q/\omega$, we can rewrite the above equation as

$$dM\left(1 - \frac{m\Omega + q\Phi}{\mathrm{k}}\right) = \frac{\kappa}{8\pi}dA. \tag{1.68}$$

if the energy of the wave packet $\mathrm{k} < m\Omega + q\Phi$, the change in the mass of the BH dM will be negative implying mass loss of the BH.

1.2.3.c Other cases where Superradiance phenomena is reported to happen

Energy extraction from a moving BH: The negative absorption cross section of moving Schwarzschild BHs as reported in [35], is fundamentally different compared to what we discussed just above. In this context, using isotropic coordinates, the metric of Schwarzschild BH is written as

$$ds^2 = -\frac{1-A}{1+A}dt^2 + (1+A)^4(dx^2 + dy^2 + dz^2), \tag{1.69}$$

where, $A \equiv M/(2\rho)$ with $\rho^2 = x^2 + y^2 + z^2$ and M denoting the BH mass. The above structure of the Schwarzschild metric could be obtained with the transformation $r = \rho(1+A)$. To obtain the moving BH, one can apply a boost along the direction-z in the following manner,

$$\tilde{t} = \gamma(t + vz), \quad \tilde{z} = \gamma(z + vt), \quad \tilde{y} = y, \tilde{z} = z. \tag{1.70}$$

With this setup, one can analyse the behaviour of the null geodesics associated with the moving BH space time. In the high frequency limit, massless scalar waves or photons propagate along the null geodesics [7]. One can evaluate the absorption cross section in the high frequency range by studying the geodesic capture cross section, σ [44]. In [35] authors have obtained the value of σ in the high frequency limit as,

$$\sigma \sim \left[27 - a_1 v - a_2 \frac{v(1+v)}{1-v}\right]\pi M^2, \tag{1.71}$$

where $a_1 = 28.8$ and $a_2 = 29.1$ are some fitting constants. With $v = 0.90$, the absorption cross section has been shown to reach a large negative value, $\sigma \sim -496.8\pi M^2$. With this result, authors have argued about the possibility of extracting energy from a moving BH. One can speculate as to whether the existence of an ergoregion is always a necessary criterion to extract energy from BH.

Superradiance in non-GR case: A rotating body inside a cavity resonator is one of the earliest models put forward by Zeldovich [45, 46] to investigate the amplification of scattered waves. Qualitatively (one may look at [47] for rigorous discussion) the line of argument is the following. For a dissipative medium in a vacuum, the governing equation of a scalar field can be written as

$$\Box\phi + \alpha\frac{\partial\phi}{\partial t} = 0, \tag{1.72}$$

where, the term with the α symbolizes the damping with α as the damping factor. This term breaks the Lorentz invariance, a characteristic feature of a dissipative system. In a coordinate system, where the rotating body seems to be moving along x direction, where $x = r\varphi$, this damping term looks like

$$\alpha\frac{\partial\phi}{\partial t} \to \alpha\gamma\left(\frac{\partial\phi}{\partial t} - v\frac{\partial\phi}{\partial x}\right), \tag{1.73}$$

with the Lorentz factor $\gamma = \sqrt{1-v^2}$, with v as the boost factor. Considering the Fourier modes of the scalar field as $\phi(t,\mathbf{r}) \sim \xi(r)e^{-\mathrm{ikt}}e^{\mathrm{im}\varphi}$, the damping term effectively becomes $\alpha\mathrm{k} \to \alpha(\mathrm{k} - m\Omega)$, where $\Omega = vr$. So, as long as $k < m\Omega$, the effective damping term happens to be negative, which implies that the scalar field fluctuation rather than being absorbed gets amplified.

Therefore, the above discussion suggests that the premise of superradiance is very broad [48] and relevant conditions are also debatable [49, 50]. However, one common characteristic that we can identify is the dissipative nature of the systems. Motivated by this aspect, we have taken up the investigation of the scattering of fields in the background of a Shwarzschild BH, which is going through the ringdown phase. Moreover, if superradiant enhancement can be obtained for BHs in the ringdown phase, this could address two issues simultaneously: *whether there are other instances where BHs can exhibit superradiant scattering and the alternative avenue for further exploration of gravitational waves from merging event.*

1.3 Fluid system: Oscillating air bubble in water

In the remaining section of the Introduction chapter, we will delve into another time-dependent system that emerges in a fluid medium. The crucial aspect of this study is that any predictions made can experimentally be tested within a laboratory framework. As previously noted in this chapter, dynamical systems hold significant potential for energy conversion or amplification. Driven by this prospect, dynamical fluid systems have been extensively studied for a long time [51–57]. One such physical system is an air bubble in a water medium driven by acoustic perturbation [5]. Experiments have revealed that the acoustic energy applied at a macroscopic length scale could be concentrated on a microscopic scale by the quasiperiodic oscillation of the bubble. In each period of the oscillation as the bubble comes to its minimum radius there will be flashes of light. This mysterious phenomena, which had been long known as sonoluminescence, remains an unsolved problem despite many efforts.

1.3.1 Brief description of the sonoluminescence event

Although Sonoluminescence was known for a long time [58], it was difficult to drive the bubble under stable oscillation and obtain repeated flashes of light. Felipe Gaitan [59], in 1989, first successfully performed the experiment for a single bubble and found repeated emission of light from the pulsating bubble under the sound field. A schematic sketch of a

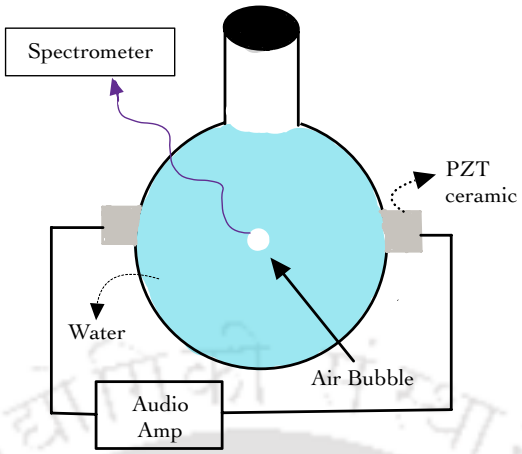

Figure 1.3: A typical setup to perform the experiment of Sonoluminescence has been given here. The above schematic figure is inspired from [5, 64]

typical experimental setup is given in Fig.1.3. A flask containing the fluid is subjected to the sound wave via the piezoelectric (PZT) ceramic attached to the flask. It is also found that some amount of inert gas is necessary for sonoluminescence to happen. The pressure amplitude of the fluid due to the sound wave is controlled by an audio amplifier. When this pressure amplitude becomes larger than the ambient pressure ($\sim 1\ atm$) inside the jar, the fluid gains high acoustic drive and cavitation forms. To drive the bubble formed in such a manner, into resonance with the sound field, one needs to tune the frequency of the sound wave. Experiments have found that this resonant frequency depends on several factors such as the temperature in the fluid, inert gas content, etc. Typical values of this frequency lie in the range of $20 - 40$kHz. During each period, the bubble expands from its ambient radius of $R_{\text{eq}} = 4.5\mu m$ to the maximum $R_{max} = 45\mu m$, given the sound wave frequency ~ 27kHz. After which the bubble wall collapses to its minimum radius $R_{min} \sim 0.5\mu m$ rapidly (typical collapse speed is found out to be 4 times the speed of sound) and a flash of light comes out. The emitted radiation displays [59–61] a broadband spectrum, which starts from the visible range and extends up to the ultraviolet range. The intensity peaks at far ultraviolet near $\sim 200nm$, which is attributed to the ultraviolet cutoff of water. This limit obstructs the experiment, and beyond that, the nature of the spectrum is thus unknown. A typical spectrum, as shown in Fig. 1.4, (the spectrum is obtained by extracting the data from the plot given in [61]), can be fit to a black body spectrum. From this one can infer the corresponding temperature, which usually turns out to be in the order of several thousand Kelvin. For example, Sonoluminescence occurring at a temperature of 22°C conforms to the black body spectrum for a temperature of 25000 K. Depending on the temperature of the fluid, it can reach up to 40000K-50000K. In each flash, 10^6 numbers of photons are emitted. It appears to the naked eye as a diffuse glow due to a very short pulse width of the spectrum and a short time period of bubble oscillation. Experiments [60, 61] have reported this pulse width falls in the range of picoseconds. Total emitted power for a single flash measured to be in the range of $30 - 100$mW.

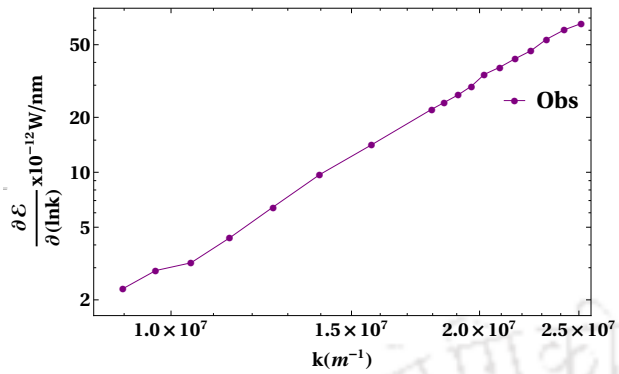

((a)) This figure is generated with the data represented by black points in the figure of the right panel excluding the error bars. This plot exhibits the Power spectrum with frequency k, which ranges from the visible to far ultraviolet range. We will utilize this plot to match our models in the later chapters.

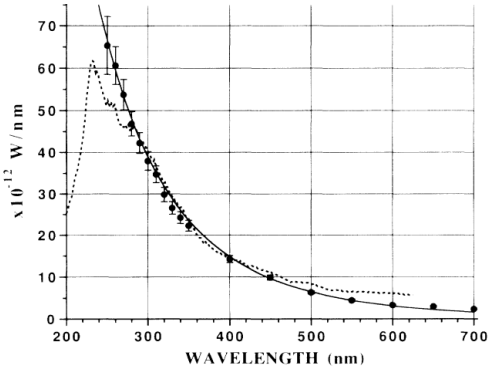

((b)) This figure is obtained from [4], which depicts the power spectrum as measured in the experiment. Two dotted lines were obtained via two different types of calibration. The black solid line, which fits very well with the experimental data corresponds to the black body spectrum of temperature 25000 K.

FIGURE 1.4: (a) describes the frequency spectrum of the emitted photon in sonoluminescence. The bold points are the measured data extracted from the plot given in [4], which we have presented in the right panel (b).

1.3.2 Dynamics of the bubble motion

The dynamics of the oscillating air bubble in water is well described by the Rayleigh-Plesset (RP) equation. In the following discussion, we will be presenting the derivation of the RP equation through the method of energy balance between the interior and exterior medium of the bubble. In the context of incompressible fluid flow, the velocity of the medium is governed by the following inverse square law type formula [62, 63],

$$\frac{u(t,r)}{U(t,r)} = \frac{R^2(t)}{r^2}, \tag{1.74}$$

where, the coordinate r represents the measure of distance from the centre of the bubble. $u(t,r)$ denotes the velocity at $r > R$, i.e. for the exterior region of the bubble of radius $R(t)$, while $U(t,r)$ represents the velocity at the surface of the bubble. Substituting the velocity at the surface, $U \sim \dot{R}(t)$ (note that the dot represent the time derivative) in the above equation, one directly arrives at

$$u(t,r) = \frac{R^2(t)}{r^2}\dot{R}(t). \tag{1.75}$$

As the sound wave perturbs the air bubble within the fluid, one can compare the kinetic energy of the fluid outside the bubble with the work done by the net pressure acting on the bubble's surface. Therefore, quantitatively one can write

$$\frac{1}{2}\rho \int_{r=\infty}^{R} 4\pi r^2 u^2 dr = \int_{r=\infty}^{R} [P(R,t) - P_{\text{eq}} - P_a(t)] 4\pi R^2 dR, \tag{1.76}$$

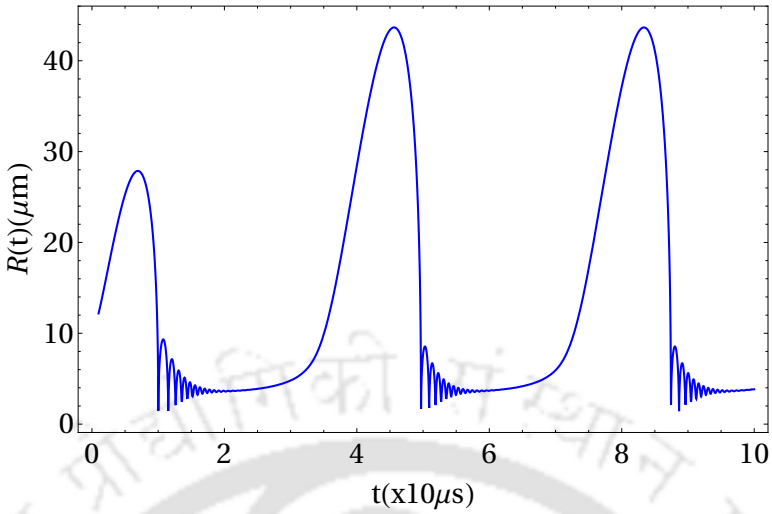

FIGURE 1.5: Evolution of the radius of the bubble is plotted with time. Apart from some initial fluctuation, repeated oscillation can be identified at ~ 50 μs and 90 μs. In the later chapters, we will be mainly focussing on a particular period, ~ 20 μs to 60 μs.

where the left-hand side represents the kinetic energy of the fluid with ρ denoting the density of the fluid. Whereas the right-hand side represents the work done with, $P_{\rm eq}$, the ambient pressure in the fluid at equilibrium, $P_a(t)$, the acoustic drive pressure arising from the sound wave perturbation. The bubble wall being a fluid-gas interface, the pressure on the interior surface of the wall, $P(R,t)$ can be further expressed in terms of the gas pressure, $P_g(R,t)$, as [4, 64],

$$P(R,t) = P_g(R,t) - 4\frac{\eta\dot{R}}{R} - 2\frac{\sigma}{R}, \tag{1.77}$$

where η is the shear viscosity of the fluid and σ denotes the surface tension of the fluid. Now, substituting the above expression in (1.76) and integrating both sides with respect to $R(t)$, we arrive at,

$$R\ddot{R} + \frac{3}{2}\dot{R}^2 = \frac{1}{\rho}\left[P_g(R,t) - P_{\rm eq} + P_a(t) - 4\frac{\eta\dot{R}}{R} - 2\frac{\sigma}{R}\right]. \tag{1.78}$$

Furthermore, the gas pressure inside the bubble can be expressed as, van der Waals hard core radius, $a = 0.5$ μm [4],

$$P_g(R) = \frac{P_{\rm eq}R_{\rm eq}^{3\gamma}}{(R^3 - a^3)^\gamma}, \tag{1.79}$$

where, γ is the adiabatic index of the fluid inside. Air being the medium inside the bubble $\gamma = 1/4$. Including the effect of damping due to the sound wave emission from the bubble itself, finally the governing equation (1.78) of the bubble radius can be recast into the following form [4, 64],

$$- R\ddot{R}\left(1-\frac{2\dot{R}}{c_s}\right)-\frac{3}{2}\dot{R}^2\left(1-\frac{4}{3}\frac{\dot{R}}{c_s}\right)+\frac{1}{\rho}\left[\frac{P_{\rm eq}R_{\rm eq}^3\gamma}{(R^3-a^3)^\gamma}-\frac{4\eta\dot{R}}{R}-\frac{2\sigma}{R}\right]$$
$$+\frac{1}{\rho c_s}\left[\frac{-3\gamma R^3 P_{\rm eq}R_{\rm eq}^{3\gamma}}{(R^3-a^3)^{\gamma+1}}\dot{R}+\frac{2\sigma}{R}\dot{R}-\frac{4\eta}{R}(R\ddot{R}-\dot{R}^2)\right]+\frac{P_{\rm eq}R_{\rm eq}^{3\gamma}\cos\omega t}{\rho(R^3-a^3)^\gamma}-\frac{R}{\rho c_s}P_a\omega\sin\omega t-\frac{P_0}{\rho}=0. \tag{1.80}$$

where we have used the acoustic drive pressure as $P_a(t) = P_a\cos\omega t$. c_s represents the sound speed in the fluid. Now, considering the fluid as the water, (as experiments have found the water medium to be the most suitable component for stable sonluminescemce) we will discuss about the value of the parameters', which one will require to solve the above equation. It is important to note that we will fix these parameters as has been used in the experiment by Putterman [5] for discussions in the later chapters. Shear viscosity, $\eta = 0.003$ Kg/(m − sec), surface tension, $\sigma = 0.03$ Kg/sec^2, the density of the water $\rho \sim 1000$ Kg/m^3, pressure-amplitude of the sound field, $P_a = 1.35$ atm, while the ambient pressure is usually taken as $P_{eq} = 1$ atm. In water the speed of sound, $c_s = 1481$ m/sec. The frequency of the sound wave is $\omega = 2\pi(26.5)$ kHz,

With these parameters, one will be able to solve the radial dynamics of the bubble by suitable fixing the initial conditions $R(t=0) = R_{\rm eq} = 4.5\mu m$ (ambient radius of the bubble) and $\dot{R}(t=0) = 0$. However, the very nature of the graph is independent of these initial conditions. We have plotted the solution in Fig.1.5 describing the quasiperiodic oscillation of the radius of the bubble. This above hydrodynamical explanation of the bubble dynamics has been found to be well matched with the experiment. As already described earlier, it is the repeated flash of light in accordance with the bubble oscillation which has not been well understood yet. In the following, we will briefly describe the existing theoretical analysis which primarily can be categorized in to two main domains: hydrodynamical processes and quantum vacuum radiation. Hydrodynamical models, which rely on the Bremsstrahlung process, and those based on quantum vacuum radiation, center around the dynamical Casimir effect.

1.3.3 Sonoluminescence as a Bremsstrahlung process and its drawbacks

There have been numerous efforts to explain the light emission mechanism of Sonoluminescence. Among them, Bremsstrahlung radiation from an imploding gas bubble is a well studied and well motivated [64, 65] candidate for Sonoluminescence. As described in the previous section, due to the acoustic drive pressure the gas-filled bubble undergoes repeated oscillation. Due to such rapid contraction, it is assumed that a shock wave may form in the medium inside the bubble (see Fig.1.6) when the bubble shrinks to half of its maximum expanded radius. The speed of the bubble wall at this moment becomes four to five times the speed of sound. This accelerating shock font leads to the heating of the inside gas medium, consequently, a dense ionized region is formed with large number of free electrons. Accelerated free electrons so produced lead to the emission of thermal photons. In this framework, ambiguities arise due to the requirement for the Bremsstrahlung process to

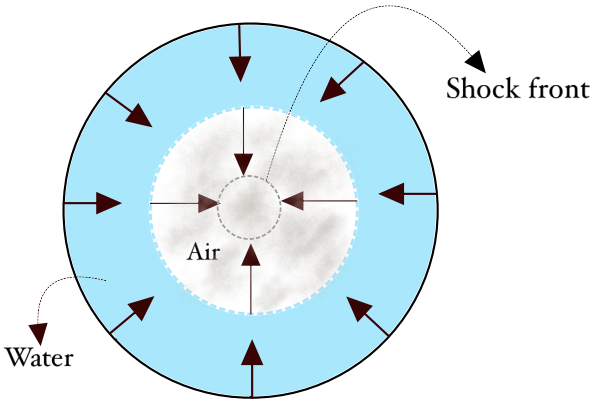

FIGURE 1.6: This schematic figure, drawn with the help of the diagram given in [5] and [66], demonstrates the shock formation due to the rapid contraction of the air bubble in the water.

have a linearly focussed shockwave, even in the micrometer length scale. However, in the contraction phase, the bubble surface shrinks nonlinearly to its minimum radius.Therefore, later studies [67] has analysed the development of the shock front, and found that the convergence of the shock wave ceases upon approaching the van der Waals volume of the fluid. Another concern, argued also by the authors [5] who initially introduced this formalism, is that the cut-off wavelength of the thermal Bremsstrahlung spectrum is determined by the Planck constant. This cut-off scale does not account for the ultraviolet cut-off imposed by the water in Sonoluminescence.

1.3.4 Issues with the models based on Dynamical Casimir effect to explain sonoluminescence

Schwinger's proposal: It has been predicted long ago by Hendrick Casimir [68] that the presence of conducting boundaries in a vacuum can modify the zero point energy of the existing fields. The associated effect is popularly known as the Casimir effect. This effect has been experimentally observed[69, 70]. J. Schwinger, later implemented this idea for a time dependent spherical boundary to explain sonoluminescence. In his simplified treatment, the excess energy due to having a spherical vacuum cavity in an infinite dielectric medium has been put forward as the responsible factor for light emission [71–77]. This excess energy with an approximation of the instantaneous collapse of the bubble is given as,

$$\mathcal{E} = \frac{4}{3}\pi R^3 \int^K \frac{4\pi k^2 dk}{(2\pi)^3}\frac{1}{2}k\left(1-\frac{1}{\sqrt{\epsilon}}\right) = \frac{1}{12\pi}R^3K^4\left(1-\frac{1}{\sqrt{\epsilon}}\right), \tag{1.81}$$

where ϵ is the dielectric constant of the medium outside the cavity and R is the radius of the spherical cavity. In the above expression an ad-hoc cut off momemtum $k = K$, of the

wave number is introduced. Although later studies [78] have provided a probable argument for this cut off, suggesting that the dielectric constant goes to unity as one approaches the ultraviolet region. Nevertheless, one can obtain the average number of photons emitted per flash, from the above expression,

$$N = \frac{4}{3}\pi R^3 \int^K \frac{4\pi k^2 dk}{(2\pi)^3}\frac{1}{2}\left(\sqrt{\epsilon}-1\right) = \frac{1}{9\pi}(RK)^3(\sqrt{\epsilon}-1). \tag{1.82}$$

To see how much this expression provides, Schwinger proceeds by substituting the values of the parameters derived from experimental measurements of Sonoluminescence. The value of $R = 4\times10^{-3}$cm is chosen for the maximum radius of the bubble. In accordance with the propagation of visible light in a water medium, the value of the dielectric constant, $\epsilon = 16/9$ is used. Then considering, $N = 3\times10^6$ number of photons emitted per flash, the cutoff wavenumber turned out as $K = 1.7\times10^5\text{cm}^{-1}$. Interestingly this value of K belongs to the ultraviolet range as observed in the experiment.

Time dependent refractive index: Following the same approach of quantum vacuum production, S. Liberati et al.[78–81] further extended the formalism to take into account the change in the dielectric medium in a more elaborate manner. The photon spectrum has been computed using Bogoliubov coefficients, which connect the quantum field modes before and after the collapse of the bubble in an infinite homogenous dielectric medium. Maxwell's equations in this time dependent dielectric medium become

$$\boldsymbol{\nabla}\cdot(\epsilon(t)\mathbf{E}) = 0, \quad \boldsymbol{\nabla}\times\mathbf{B} = \frac{\partial}{\partial t}(\epsilon(t)\mathbf{E}), \tag{1.83}$$

where the authors have introduced pseudo time defined as $d\tau = dt/\epsilon(t)$, so that the equation of motion for the vector potential becomes

$$\frac{\partial^2}{\partial\tau^2}\mathbf{A} = \epsilon(\tau)\nabla^2\mathbf{A}. \tag{1.84}$$

Which interestingly resembles the dynamical equation derived for a scalar field discussed in [82]. In a similar setting, the authors consider the following time profile of the homogenous dielectric medium,

$$\epsilon(\tau) = a + b\tanh(\tau/\tau_0) = \frac{1}{2}(n_{in}^2 + n_{out}^2) + \frac{1}{2}(n_{in}^2 - n_{out}^2)\tanh(\tau/\tau_0), \tag{1.85}$$

where τ_0 is the time scale over which the dielectric constant varies. Wherein n_{in} and n_{out} represent the refractive index inside and outside the bubble respectively. However, again this setup has led to the divergent total energy flux in the wavenumber as,

$$\mathcal{E} = \frac{1}{16\pi^2}\frac{(n_{out}-n_{in})^2}{n_{in}n_{out}^2}R^3k^4. \tag{1.86}$$

Eberlin's approach: With a more natural coupling of the electromagnetic field to the bubble motion, Eberlin [83, 84] has considered the following Lagrangian,

$$\mathcal{L}(\epsilon,\beta) = -\frac{1}{4}F_{\mu\nu}F^{\mu\nu} - \frac{\epsilon-1}{2}u_\mu F^{\mu\nu}u^\alpha F_{\alpha\nu}, \tag{1.87}$$

where u^μ denotes the four-velocity of the medium, with the time dependent dielectric constant, ϵ taken to be of the form,

$$\epsilon(r, R(t)) = 1 + (n^2 - 1)\theta(r - R(t)), \tag{1.88}$$

where θ denotes the Heaviside step function, and the dielectric constant inside the bubble is taken to be 1 and outside as square of the refractive index n^2 with . The Hamiltonian corresponding to the above Lagrangian turns out as,

$$H = H_0(R(t)) + \Delta H(R(t), \beta) = \int d^3r \left[\frac{1}{2}\left(\frac{\mathbf{D}^2}{\epsilon} + \mathbf{B}^2\right) + \frac{\epsilon - 1}{\epsilon}\beta\hat{\mathbf{r}} \cdot (\mathbf{D} \times \mathbf{B}) + \mathcal{O}(\beta^2)\right], \tag{1.89}$$

where the velocity parameter, $\beta = \dot{R}/c$. Whereas the first term, H_0, in the above equation with electric displacement, $\mathbf{D}$ and magnetic field $\mathbf{B}$ represents the usual Hamiltonian due to Maxwell's action. However, the second, ΔH and higher order terms emerge for considering the interaction of the electromagnetic field with the fluid velocity. Therefore the time dependent Schrödinger equation of the state vector $|\psi(t)\rangle$ of photon can be expressed as

$$\mathrm{i}\frac{\partial}{\partial t}|\psi(t)\rangle = (H_0(R(t)) + \Delta H(R(t), \beta))|\psi(t)\rangle. \tag{1.90}$$

For this Hamiltonian, the transition amplitude has been computed following purely quantum mechanical treatment of time dependent perturbation theory using

$$H_0(R(t))|a(R(t))\rangle = E_a(R(t))|a(R(t))\rangle, \tag{1.91}$$

where $|a(R(t))\rangle$ denotes the eigenvector of the unperturbed Hamiltonian and $E_a(R)$ is the corresponding eigenvalue. Utilizing this eigenvector, the total wave vector for the perturbed Hamiltonian can be computed as

$$|\psi(t)\rangle = \sum_a |a(R)\rangle\langle a(R)|\psi(t)\rangle. \tag{1.92}$$

Note that the summation over "a" should be considered as a summation over discrete quantum modes and integration over continuous quantum modes. All of these quantum modes are supposed to be incorporated in $|a(R)\rangle$. Now the transition amplitude from the vacuum to the excited states, defined as $\langle a|\psi\rangle$ can quantified as,

$$\langle a|\psi\rangle = c_a(t)\, \exp\left[-\mathrm{i}\int_{t_0}^{t} dt' E_a(t')\right]. \tag{1.93}$$

Since the Hamiltonian (1.89) is second order in the fields, the perturbation will induce a transition to the two-photon state $|k, k'\rangle$ of wave number k and k' and using the Shrödinger equation one can compute the time evolution of the coefficient c_a (which for two-photon states denoted by $c_{kk'}$) as,

$$\frac{\partial c_{kk'}(t)}{\partial t} = \langle k, k'|\Delta H|0\rangle, \tag{1.94}$$

Then total energy emitted in one acoustic cycle (T) for this transition becomes,

$$\mathcal{W} = \frac{1}{2}\int d^3k \int d^3k'(\omega+\omega')|c_{kk'}(T)|^2, \tag{1.95}$$

where, ω and ω' are the frequency of the modes k and k' respectively. We refer the reader to [84], for the actual computation, which will lead to the following expression for the total energy,

$$\mathcal{W} = 1.16\frac{n^2-1}{n^2}\frac{1}{480\pi}\int_0^T dt \frac{\partial^5 R^2(t)}{\partial t^5} R(t)\beta(t). \tag{1.96}$$

The remaining task is to find out the time profile of the bubble's surface. Eberlin considers the following analytical form of the radius of the bubble,

$$R^2(t) = R_{\text{eq}}^2 - \frac{(R_{\text{eq}}^2 - R_{min}^2)}{(t/\gamma)^2+1}. \tag{1.97}$$

The value of the parameters, considered by the authors, as $R_{\text{eq}} \sim 10\mu m$, $R_{min} \sim 0.5\mu m$, $n = 1.3$, Eberlin obtained $\mathcal{W} = 2.5\times10^{-16}J$ considering the collapsing time scale, $\gamma \sim 1fs$, which is far too short time scale to be feasible as far as the experimental measurement is concerned. Moreover, [85, 86] pointed out that the velocity of the bubble surface needs to be superluminal in order to match the experimental results.

Milton's argument: Later studies [86–89] have cast doubt on the suitability of formalisms relying on the dynamical Casimir effect in explaining the phenomenon of sonoluminescence. It's important to mention that within all the specified quantum mechanics based models (with the exception of Bremsstrahlung process) the typical photon energy flux was found to diverge in wave number. Therefore, an ad hoc cutoff has been implemented to address these phenomena. Milton's analysis ([87, 88]) also contended that such divergent contributions within the quantum theory framework should vanish through renormalization.

All the quantum mechanical modeling of this phenomena suffers from ultraviolet divergence, and that has not been resolved yet. In this thesis we approach this problem in the proper quantum field (QFT) theory framework and utilize the well known analog spacetime formalism [90] where actual temporal evolution of the bubble surface will be taken into account. We point out the origin of the aforesaid divergence as a generic feature of perturbative QFT. We further argue that the sonoluminescene phenomena is rather non-perturbative in nature which does not give rise to any divergences.

1.3.5 Emergence of the acoustic analog metric for fluctuation in the fluid system

In his famous paper [90], Unruh conjectured that the dynamics of the sound wave in an incompressible fluid mimics the governing equation of a classical field propagating in a gravitational background. For an incompressible and irrotational fluid, the corresponding energy-momentum tensor satisfies the following covariant conservation equation, where,

$$\nabla_\mu T^{\mu\nu} = 0, \quad T^{\mu\nu} = (\rho+P)u^\mu u^\nu + P\eta^{\mu\nu}, \tag{1.98}$$

with ρ and P symbolizing density and pressure respectively and $\eta^{\mu\nu}$ is the Minkowski metric describing the flat space time. Whereas, the four-velocity $u^\mu \equiv (1, \mathbf{v})$. Then the above conservation equation can be expressed in three coupled equations,

$$\boldsymbol{\nabla} \times \mathbf{v} = 0, \tag{1.99}$$

$$\rho \left[\frac{\partial \mathbf{v}}{\partial t} + (\mathbf{v} \cdot \boldsymbol{\nabla})\mathbf{v} \right] = -\boldsymbol{\nabla} p - \rho \boldsymbol{\nabla} \Phi, \tag{1.100}$$

$$\frac{\partial \rho}{\partial t} + \boldsymbol{\nabla} \cdot (\rho \mathbf{v}) = 0. \tag{1.101}$$

Where, the first equation signifies the irrotational nature of the fluid, whereas the subsequent equations represent the Euler equation and the continuity equation, respectively. In the Euler equation, the righthand side asserts that the force present in the medium is due to the pressure, and the external driving force, which is expressed as a gradient of a potential Φ. For irrotational fluid flow the vanishing curl of the velocity prompts us to express the velocity as a gradient of a velocity potential, $\mathbf{v} = \boldsymbol{\nabla}\psi$. Now we simplify the above fluid equation with the help of the following parametrization,

$$g(\zeta) = \int^{e^\zeta} \frac{1}{\rho'} \frac{dp(\rho')}{d\rho'} d\rho', \tag{1.102}$$

where, $\zeta \equiv \log \rho$. Utilizing the above quantity, the set of fluid equation simplifies to

$$\frac{\partial \psi}{\partial t} + \frac{1}{2}\mathbf{v} \cdot \mathbf{v} + g(\zeta) + \Phi = 0, \tag{1.103}$$

and

$$\frac{\partial \zeta}{\partial t} + \mathbf{v} \cdot \boldsymbol{\nabla}\zeta + \boldsymbol{\nabla} \cdot \mathbf{v} = 0. \tag{1.104}$$

With this form of the fluid equations, we proceed to introduce fluctuations in the fluid as

$$\zeta = \zeta_0 + \bar{\zeta}, \quad \psi \to \psi_0 + \bar{\psi}. \tag{1.105}$$

Where the fluctuation in ζ signifies the perturbation to the density ρ. Substituting these perturbed fields in the covariant conservation equation one can derive

$$\frac{\partial \bar{\psi}}{\partial t} + \frac{1}{2}\mathbf{v}_0 \cdot \boldsymbol{\nabla}\bar{\psi} + g'(\zeta)\bar{\zeta} = 0, \tag{1.106}$$

$$\frac{1}{\rho_0}\left[\frac{\partial(\rho_0 \bar{\zeta})}{\partial t} + \boldsymbol{\nabla} \cdot (\rho_0 \mathbf{v}_0 \bar{\zeta}) + \boldsymbol{\nabla} \cdot \left(\rho_0 \boldsymbol{\nabla}\bar{\psi}\right) \right] = 0. \tag{1.107}$$

Note that the external driving potential, Φ being a fixed quantity goes in the background equation [92]. Whereas, the background fluid parameters are $\mathbf{v}_0 = \boldsymbol{\nabla}\psi_0$ and $\rho_0 = e^{\zeta_0}$. The

above two fluctuation equation can be decoupled and the equation governing the fluctuation, $\bar{\psi}$, turns out as[90, 92, 93],

$$\frac{1}{\rho_0}\Bigg[\partial_t\left(\frac{\rho_0}{g'(\zeta_0)}\right)\partial_t\bar{\psi}+\partial_t\frac{\rho_0\mathbf{v}_0}{g'(\zeta_0)}\cdot\boldsymbol{\nabla}\bar{\psi}+\boldsymbol{\nabla}\cdot\left(\frac{\rho_0\mathbf{v}_0}{g'(\zeta_0)}\partial_t\bar{\psi}\right) \\ -\boldsymbol{\nabla}\cdot(\rho_0\boldsymbol{\nabla}\bar{\psi})+\nabla\cdot\left(\mathbf{v}_0\frac{\rho_0}{g'(\zeta_0)}\mathbf{v}_0\cdot\boldsymbol{\nabla}\bar{\psi}\right)\Bigg]=0, \tag{1.108}$$

Interestingly this fluctuation equation mimics a massless scalar field propagating in the following background space time, which is often referred to as analog metric (AM) [90],

$$ds^2_{\rm AM}=\left(\frac{\tilde{\rho}_0}{c^2}\right)^{-1}\left\{\frac{(\rho_0/c^2)}{(c_0/c)^2}\left[-\left(\frac{c_0^2}{c^2}-\frac{\delta_{ij}v_0^iv_0^j}{c^2}\right)c^2\,dt^2-2\frac{v_0^i}{c}\delta_{ij}\,dx^j c\,dt+\delta_{ij}\,dx^i\,dx^j\right]\right\}. \tag{1.109}$$

Where x^i denotes the spatial coordinates under consideration. Whereas v_0^i represents the local velocity of the fluid along x^i. The above analog metric can be thought of as emerging due to the fluctuation in the medium inside the air bubble in the water medium, which constitutes the Sonoluminescence setup. Therefore, the local sound speed denoted by $c_0 \sim g'(\zeta_0) = g'(\ln\rho_0)$ assumes the value corresponding to air, $c_0 \sim 343$ m/s. We have also introduced an arbitrary density parameter $\tilde{\rho}_0$ to attribute a dimension of length to the analog metric, $ds_{\rm AM}$. Note that all the fluid equations are independent of this new arbitrary parameter. Now, we are left with two more fluid parameters, v_0 representing the background velocity and ρ_0 symbolizing the fluid density. Assuming the background flow to be spherically symmetric, we will mainly consider the background velocity, v_0^i to be radial, which is approximately expressed as [4],

$$v_0=\frac{\dot{R}(t)}{R(t)}r, \tag{1.110}$$

with $v_0=\sqrt{\delta_{ij}v_0^iv_0^j}$ representing the background velocity in spherical coordinate. Where $R(t)$ denotes the radius of the air bubble in the water. The above form of the velocity satisfies the conditions, $v_0(r=0)=0$ and $v_0(r=R)=\dot{R}$. With the help of v_0, one can derive the background density from the continuity equation [92], and is given by,

$$\rho_0(t)=\rho_{eq}\frac{R_{\rm eq}^3}{R^3(t)}, \tag{1.111}$$

where, $\rho_{eq}=\rho_0(t\to t_0)$ representing the density of air inside the bubble at any arbitrary time t_0 when the bubble is not dynamical with fixed radius $R_{\rm eq}=R(t\to t_0)$, which we have often referred to as ambient radius. This equilibrium situation motivates us to compare the above equation with the equation of state, expressed as, $\rho_0=\frac{P_{\rm eq}R_{\rm eq}^3}{c_0^2}\frac{1}{R^3}$, with $P_{eq}=\rho_{eq}c_0^2$. Hence, we express the factor involving the background density as $\frac{\tilde{\rho}_0^{-1}\rho_0}{c_0^2}=\frac{\xi^3}{R(t)^3}$, where ξ is

a new arbitrary parameter that includes the old ones. Incorporating this parametrization, we finally express the line element of the acoustic metric in a spherical coordinate as,

$$ds^2_{AM} = \frac{\xi^3}{R(t)^3}\Big[-(c_0^2 - v_0^2)\,dt^2 - 2v_0 dr dt + dr^2 + r^2 d\Omega^2\Big]. \tag{1.112}$$

The expression in the parenthesis originally appeared in the paper of Unruh[91]. Whereas, the overall factor, outside, carries the information of the oscillating bubble in the present context of the fluid system of Sonoluminescence. Our goal would be to utilize this analog metric and study the quantum particle production phenomena which is assumed to be connected to the sonoluminescence we are interested in. For this, we propose that any quantum field see this analog metric as a fluctuating part of the following effective spacetime background,

$$ds^2 = \left(-\frac{dt^2}{\epsilon} + dr^2 + r^2\,d\Omega^2\right) + \frac{\xi^3}{R(t)^3}\Big[-(c_0^2 - v_0^2)\,dt^2 - 2v_0 dr dt + dr^2 + r^2 d\Omega^2\Big]. \tag{1.113}$$

The dielectric constant ϵ is associated with the air medium inside the bubble. This metric can be rewritten in a compact form,

$$ds^2 = -f(t,r)dt^2 + 2g(t,r)drdt + p(t)\left(dr^2 + r^2 d\Omega^2\right), \tag{1.114}$$

with the essential matrix elements given as,

$$\begin{aligned} p(t) &= 1 + \frac{\xi^3}{R^3}, \\ f(t,r) &= 1 + \frac{\xi^3}{R^3}\left(c_0^2 - \frac{\dot{R}^2}{R^2}r^2\right), \\ g(t,r) &= -\frac{\dot{R}\xi^3}{R^4}r. \end{aligned} \tag{1.115}$$

However, one can get rid of the off-diagonal term by transforming the radial coordinate in the following manner,

$$\frac{d\bar{r}}{1/p^{1/6}} = \sqrt{p}\,dr + \frac{g}{\sqrt{p}}\,dt. \tag{1.116}$$

The above equation can be integrated (see Appendix.C) to obtain the scaling in the radial coordinate, $\bar{r} = rp^{1/3}$. Utilizing this redefined radial coordinate we recast the effective metric as,

$$ds^2 = -\left(f + \frac{g^2}{p}\right)dt^2 + p^{1/3}\left(d\bar{r}^2 + \bar{r}^2\,d\Omega^2\right). \tag{1.117}$$

This form of the acoustic metric can be further simplified by taking into account the fact that experimental measurement suggests that the photon flux is emitted as the bubble

comes to its minimum radius [4, 59]. Hence one can impose a limit $r \to 0$ in the fluctuation part of the metric. In this limit the metric coefficients (1.115) become,

$$\begin{aligned} p(t) &= 1 + \frac{\xi^3}{R^3}, \\ f(t) &= 1 + \frac{\xi^3}{R^3} c_0^2 \\ g &= 0. \end{aligned} \tag{1.118}$$

This leads to the following simplified form of the acoustic metric,

$$ds^2 = -f(t)\, dt^2 + p^{1/3}(t) \left(d\bar{r}^2 + \bar{r}^2\, d\Omega^2 \right). \tag{1.119}$$

Due to the spherically symmetric nature, the spatial section of the above metric can also be recast into Cartesian coordinates (x, y, z),

$$ds^2 = -f(t) dt^2 + p^{1/3}(t) \left(dx^2 + dy^2 + dz^2 \right) \tag{1.120}$$

This time dependent form of the effective acoustic metric will lead to particle production if coupled with a matter field.

1.3.6 Formalism of particle production in a time dependent background

Quantum field theory plays a significant role in understanding the subatomic world [94]. The standard model of particle physics has been built on the premise of interacting quantum field theory in flat space time [95]. However, in the presence of curved space time, various new phenomena arise [82]. The analysis primarily involves quantization of the matter field while keeping the gravitational background as classical. This semi-classical treatment has been very successful, specifically in the context of structure formation in early universe cosmology [6] and also in the scenario of black hole evaporation [43]. The primary distinction from flat space time is the departure from Lorentz invariant structure in the vacuum states of the matter field. Hence, the vacuum state cannot be uniquely determined for general background space time and may appear differently to different observers [96].

Much of the primary steps in the formulation of quantum field theory in curved space time follow from its classical version [97]. First one needs to find out a complete set of classical mode functions, which satisfies certain orthonormalization conditions. To see that, let us start with a minimally coupled action for a real massive scalar field,

$$\mathcal{A} = -\frac{1}{2} \int \sqrt{-g} d^4x \ \left[\partial_\mu \phi \partial^\mu \phi + m_\phi^2 \phi \right]. \tag{1.121}$$

By varying the action one will obtain the equation of motion for the scalar field,

$$-\frac{1}{\sqrt{-g}} \partial_\mu \left(\sqrt{-g} \partial^\mu \phi \right) + m_\phi^2 \phi = 0. \tag{1.122}$$

Now the inner product of the fields is defined as [98],

$$(\phi_1, \phi_2) = \int_\Sigma d^3x\sqrt{|h|}n^\mu(\phi_2^*\nabla_\mu\phi_1 - \phi_1^*\nabla_\mu\phi_2), \tag{1.123}$$

where Σ is the space like hypersurface, n^μ is the future directed normal to the hypersurface, and h is the determinant of the induced metric $h_{\mu\nu} = g_{\mu\nu} - n_\mu n_\nu$. Taking the hypersurface as space like, t=const., $n^\mu = (n^0, 0, 0, 0)$ and $g_{00}n^0n^0 = 1$, which leads to the following expression of the inner product,

$$(\phi_1, \phi_2) = \int_\Sigma \sqrt{-g}d^3x g^{00}(\phi_2^*\partial_t\phi_1 - \phi_1^*\partial_t\phi_2) \tag{1.124}$$

This inner product can be shown to be independent of the choice of the space like hypersurface, Σ. Therefore one defines the following orthonormalization conditions to be satisfied by mode functions

$$(\phi_i, \phi_j) = \delta_{ij}, \quad (\phi_i^*, \phi_j^*) = -\delta_{ij}, \quad (\phi_i, \phi_j^*) = 0 \tag{1.125}$$

δ_{ij}, Kronecker delta for discrete quantum numbers and Dirac delta functions for continuous quantum numbers. With this generic discussion, we now resort to spatially flat spacetime case which is our primary interest (see Eq.1.120). For spatially flat space time, we can now promote the classical field in quantum field operator and expand the fields in Fourier modes in the following manner,

$$\phi(t, \mathbf{x}) = \int \frac{d^3k}{(2\pi)^3}[\hat{c}_\mathbf{k}\phi(t, \mathbf{k})e^{\mathrm{i}\mathbf{k}\cdot\mathbf{x}} + \hat{c}_\mathbf{k}^\dagger\phi^*(t, \mathbf{k})e^{-\mathrm{i}\mathbf{k}\cdot\mathbf{x}}], \tag{1.126}$$

where, $\hat{c}_\mathbf{k}$ and $\hat{c}_\mathbf{k}^\dagger$ satisfy the usual harmonic oscillator commutation relation

$$\left[\hat{c}_\mathbf{k}, \hat{c}_{\mathbf{k}'}^\dagger\right] = (2\pi)^3\delta^3(\mathbf{k} - \mathbf{k}'), \quad [\hat{c}_\mathbf{k}, \hat{c}_{\mathbf{k}'}] = 0, \quad \left[\hat{c}_\mathbf{k}^\dagger, \hat{c}_{\mathbf{k}'}^\dagger\right] = 0. \tag{1.127}$$

Now from the Lagrangian density of the scalar field, one can obtain the conjugate momentum as,

$$\Pi = \frac{\partial\mathcal{L}}{\partial(\partial_t\phi)} = -\sqrt{-g}g^{00}\partial_t\phi. \tag{1.128}$$

Imposing the canonical commutation relation

$$[\phi(t, \mathbf{x}), \Pi(t, \mathbf{y})] = \mathrm{i}\int \frac{d^3k}{(2\pi)^3}e^{\mathrm{i}\mathbf{k}\cdot(\mathbf{x}-y)} \tag{1.129}$$

Let's write the Fourier mode expansion of (1.130) as

$$\phi(t, \mathbf{x}) = \int \frac{d^3k}{(2\pi)^3}\hat{\chi}(t, \mathbf{k})e^{\mathrm{i}\mathbf{k}\cdot\mathbf{x}} \tag{1.130}$$

where,

$$\hat{\chi}(t, \mathbf{k}) = \hat{c}_\mathbf{k}\phi(t, k) + \hat{c}_{-\mathbf{k}}^\dagger\phi^*(t, k), \quad \hat{\pi}(t, \mathbf{k}) = -\sqrt{-g}g^{00}[\hat{c}_\mathbf{k}\phi'(t, k) + \hat{c}_{-\mathbf{k}}^\dagger\phi'^*(t, k)] \tag{1.131}$$

Introducing another set of time dependent creation and annihilation operators as

$$\hat{d}_{\mathbf{k}}(t) \equiv \sqrt{\frac{\omega_k}{2}}\hat{\chi}(t,\mathbf{k}) + \frac{\mathrm{i}}{\sqrt{2\omega_k}}\hat{\pi}(t,\mathbf{k}), \quad \hat{d}^{\dagger}_{\mathbf{k}}(t) \equiv \sqrt{\frac{\omega_k}{2}}\hat{\chi}(t,-\mathbf{k}) - \frac{\mathrm{i}}{\sqrt{2\omega_k}}\hat{\pi}(t,-\mathbf{k}) \tag{1.132}$$

where, $\omega_k = \sqrt{k^2 + m_\phi^2}$. We connect the two sets of creation and annihilation operators in terms of Bogoliubov coefficients as

$$\hat{d}_{\mathbf{k}}(t) = \alpha_k(t)\hat{c}_{\mathbf{k}} + \beta_k^*(t)\hat{c}^{\dagger}_{-\mathbf{k}}, \quad \hat{d}^{\dagger}_{\mathbf{k}}(t) = \alpha_k^*(t)\hat{c}^{\dagger}_{\mathbf{k}} + \beta_k(t)\hat{c}_{-\mathbf{k}} \tag{1.133}$$

where the time dependent Bogoliubov coefficients are given by

$$\begin{aligned} \alpha_k(t) &= \left(\sqrt{\frac{\omega_k}{2}}\phi(t,k) - \frac{\mathrm{i}}{\sqrt{2\omega_k}}\sqrt{-g}g^{00}\phi'(t,k)\right), \\ \beta_k(t) &= \left(\sqrt{\frac{\omega_k}{2}}\phi(t,k) + \frac{\mathrm{i}}{\sqrt{2\omega_k}}\sqrt{-g}g^{00}\phi'(t,k)\right) \end{aligned} \tag{1.134}$$

From the quantization condition (1.129) we can obtain the following relation of Bogoliubov coefficients

$$|\alpha_k(t)|^2 - |\beta_k(t)|^2 = 1 \tag{1.135}$$

If the Heisenberg picture is adapted to describe the quantum dynamics, then $|0_{in}\rangle$ is the state of the system for all time. However, the physical number operator which counts particles in the out-region is $N_{\mathbf{k}} = \hat{d}^{\dagger}_{\mathbf{k}}\hat{d}_{\mathbf{k}}$, which acting on the initial vacuum state gives,

$$\langle N_{\mathbf{k}}\rangle = \langle 0_{in}|\hat{d}^{\dagger}_{\mathbf{k}}\hat{d}_{\mathbf{k}}|0_{in}\rangle = |\beta_k|^2 \tag{1.136}$$

The quantity β_k^2 denotes the particle number density in the mode k. The usual explanation [82] for particle production is that initial vacuum states appear as excited states to an observer at a later time. To determine $|\beta_k|^2$, the primary challenge one encounters involves determining the mode function for a generic time-dependent background. In the majority of the cases [99], numerical computation with appropriate boundary or initial conditions is necessary. In some cases, one may be able to find out the solution to the equation of motion analytically following the perturbative expansion of the mode function in high frequency range. However, it is well known that the perturbative approach leads to very low production, which is a natural outcome for high frequency modes. Therefore for significant production, one needs to find out the mode function in the low to medium frequency range, we have to perform numerical computation.

1.4 Outline of the thesis

The entire thesis is segmented into six chapters including the introduction and conclusions. Motivated by the interesting aspects of time dependent systems, we have studied observable quantities in two different scenarios. The first involves astrophysical systems, with a focus

on oscillating black holes (BHs), while the second entails investigating particle production due to an oscillating air bubble in water.

In the first case, our focus has been specifically directed towards the evaluation of the absorption cross section of Schwarzschild BH as it rings down after the merging phase (we have referred to this BH as ringing BH). In chapter 2, we have considered a scalar field propagating on this ringing BH with minimal interaction. We have formally treated this scalar field as an axion. Due to the quadrupole fluctuation (GWs) in the background space time, the scalar field obtains nontrivial dynamics. Particularly, quasinormal modes (QNMs) of GWs enter into the evolution of the scalar field. To bypass the difficulty associated with the definition of absorption cross section as the ringing BHs lack the asymptotic flatness, we have introduced a hypothetical interaction surface. With this setup, we have been able to compute the absorption cross section, which turns out to be oscillating quasi-periodically with negative values during some parts of its evolution. We have argued that these negative values are arising due to the superradiant enhancement of the outgoing flux. Interestingly, it appears that the decay time scale of this time dependent superradiant feature in the absorption cross section matches with decay time scale of the QNMs. It is well known that the detection of axion is difficult. Therefore, to measure the enhanced flux, we have proposed a scenario, where an incoming light ray is interacting with this axion, which carries the GW induced fluctuation. Then, we have obtained an interesting feature in the rotation of the plane of polarization of the passing light ray. Next, we have discussed various existing experiments where this rotation angle can be measured.

In chapter.3, we have extended the formalism of the previous study on the scattering of fields in the ringing BH for the case of electromagnetic fields. The main motivation is associated with the greater prospect of observability as compared to the scalar field case. All the basic formalisms remain the same as before. However, to avoid complicacy regarding the gauge choice of the EM field, we have developed our framework in terms of gauge invariant variables. It is found that electromagnetic fields are also similarly amplified due to the ringing of BHs. There are existing ground based detectors which measure EM flux of various frequency ranges. We deduce the frequency ranges within which the amplified EM signal may be observed, and it turns out to be inversely proportional to the mass of the BH. Considering solar mass BHs, we have estimated that superradiant amplification happens for EM waves with a frequency around 10 kHz. This is below the existing Low Frequency Array (LOFAR) telescopes' operating range, $10 - 240$MHz. Hence, to be able to connect with the experiments, we need to consider less than solar mass BHs. Interestingly, such a low mass BH indeed arises in the early universe cosmology and those are called primordial BHs (PBHs). We briefly discuss the possible mass range of those PBHs which are assumed to be formed after merging and their observational prospects.

In the second scenario, in chapter.4, we have considered an oscillating bubble in a fluid medium, firstly to explain a light-emitting phenomena called Sonoluminescence. We have utilized the effective acoustic metric that emerges analogously in the context of fluid due to fluctuation induced by sound waves. Then we have coupled the EM field with this acoustic metric, which can be recast into a conformally flat metric. It is well known that the minimally coupled EM field in four dimensions is conformal invariant. Therefore we

have introduced nonminimal coupling of EM field to the analog acoustic metric through the corresponding Ricci curvature scalar. This conformal breaking coupling leads to photon production. We have presented our numerical findings, which demonstrate that due to the oscillating nature of the background acoustic metric, particles such as photons will be produced via parametric resonant amplification from the quantum vacuum. We further computed the power spectrum of the produced particle and compared it with the the experimental results.

The production of particles in the presence of time dependent background is a ubiquitous phenomena. Motivated by this, in chapter 5, we have put forward a proposal for fermion production in a very similar manner to photon production from the oscillating air bubble of Sonoluminescence. Minimally coupled massless fermionic action in four dimensions is also a conformally invariant theory in the presence of a conformally flat space time. However, massive fermion breaks this invariance. Hence, following the methodology discussed for the photon we have computed the power spectrum of the produced fermions. The mass range for which we have calculated the spectrum is within $10^{-10} - 10^{-5}$ eV, which suggests that the fermion could be very well treated as a Neutrino. However, with the present coupling prescription the magnitude of the produced flux appears to be extremely low.

In the concluding chapter 6, we summarize the key findings of our analysis for the two time-dependent systems: ringing BH in the context of an astrophysical scenario and oscillating bubble in the case of fluid systems. This section also serves to list all the important issues pertaining to the works presented in the thesis. We will also briefly discuss how these issues can be addressed in the future. Then we will end with the possible future outlook and extensions of the present analysis.

Superradiant scattering of scalar field from ringing black holes 2

"In space, no one can hear you scream; and in a black hole, no one can see you disappear."

— *Stephen Hawking, Black Holes: The Reith Lectures*

2.1 Introduction

The first observation of gravitational waves (GWs) by LIGO [1] in 2016 is such a remarkable achievement as it confirms the predictions of Einstein's general theory of relativity. Moreover, it establishes the existence of compact objects, such as black holes (BHs) and neutron stars (NSs) in our universe. Importantly, GW signals encode the quasinormal mode (QNMs) ringing in the merging event of binary BH (BBH) [1], BH-NS [100] and NS-NS [24]. In addition, these QNMs carry the information on the intrinsic parameters of BHs, such as mass, charge and spin[1]. Therefore, an elaborate study of the merging phase is very motivating. This may lead to theoretical predictions of new signatures in the observed signal, either through the emission of GWs or via scattering of fundamental fields from the compact object undergoing the merging phase. However, the transient gravitational wave (GW) signals that have been detected so far, match very well with the predicted waveform of the merging event, which consists of inspiral, merger and ringdown [1]. Hence, it is very significant to investigate the possibility of a complementary prediction of gravitational waves via scattering of fundamental fields.

As a first case study, we have mainly focussed on the ringdown phase, the last phase of the merging event. Particularly we have considered a scalar field being scattered by the BH as it rings down (which we referred to as ringing BH). Investigation of the possibility

of a complementary prediction of GWs requires exploration of the observable phenomena, apart from gravitational waves (GW). To serve this purpose, the absorption cross section of the ringing BH for the scalar field could be a potential physical quantity. Moreover, the dissipative nature of a system may lead to a superradiant absorption cross section as we have argued in the Introduction chapter of this thesis. During the ringdown phase, the black hole undergoes damped oscillation which has been extensively studied using the method of BH perturbation theory. Because of inherent dissipation, the oscillation frequency is quasi-normal. Therefore, if superradiance indeed appears in the absorption cross section of ringing BH, the observation of the enhanced scattered flux of the scalar field is more viable.

The superradiantly amplified flux can act as a complementary observable along with the gravitational waves during the ringing phase of the black holes. The focus of this study will be confined to the ultralight scalar field, which can be described as axions or axion-like particles. Axion holds significant importance as a potential candidate for dark matter. The detectability of dark matter remains a pressing concern, prompting numerous proposals and experiments [101–103]. We have examined various observables that capture the distinctive signature of the oscillating scalar field, which encodes information on the ringdown phase of the BH. Detecting such a time-varying effect would be more feasible.

2.2 Background and Framework

We start with the Ringing Schwarzschild BH metric, $g_{\mu\nu} = g^0_{\mu\nu} + h_{\mu\nu}$, where $g^0_{\mu\nu}$ is the standard Schwarzschild metric and the fluctuation part $h_{\mu\nu}$ can be expressed in radiation gauge in the following manner as discussed in (1.2.1) putting together the odd and even parity perturbation, specifically choosing quadrupole mode,

$$h_{\mu\nu} = \frac{e^{-i\omega t}}{2}\begin{pmatrix} \tilde{H}_{20}(\omega,r)f(r)Y_{20} & \tilde{H}^{(1)}_{20}(\omega,r)Y_{20} & 0 & 0 \\ \tilde{H}^{(1)}_{20}(\omega,r)Y_{20} & \tilde{H}_{20}(\omega,r)f(r)^{-1}Y_{20} & \tilde{h}^{(1)(e)}_{20}(\omega,r)\partial_\theta Y_{20} & \tilde{h}^{(1)(o)}_{20}(\omega,r)s_\theta\partial_\theta Y_{20} \\ 0 & \tilde{h}^{(1)(e)}_{20}(\omega,r)\partial_\theta Y_{20} & r^2\mathcal{D}_{20}(\omega,r,\theta) & \frac{1}{2}\tilde{h}^{(2)}_{20}(\omega,r)\mathcal{C}_{20}(\theta) \\ 0 & \tilde{h}^{(1)(o)}_{20}(\omega,r)s_\theta\partial_\theta Y_{20} & \frac{1}{2}\tilde{h}^{(2)}(\omega,r)\mathcal{C}_{20}(\theta) & r^2 s^2_\theta\tilde{\mathcal{D}}_{20}(\omega,r,\theta) \end{pmatrix} + c.c. \tag{2.1}$$

where, symbols are, $\mathcal{C}_{20} = (c_\theta\partial_\theta Y_{20} - s_\theta\partial^2_\theta Y_{20})$, $\mathcal{D}_{20} = \tilde{K}_{20}Y_{20} + \tilde{G}_{20}\partial^2_\theta Y_{20}$, and $\tilde{\mathcal{D}}_{20} = \tilde{K}_{20}Y_{20} + \cot\theta\tilde{G}_{20}\partial_\theta Y_{20}$. $s_\theta = \sin\theta$, $c_\theta = \cos\theta$. Note that we have added the complex conjugate (c.c.) part to make the fluctuation, $h_{\mu\nu}$ real. Our goal is to compute the absorption cross-section of the ultra-light scalar field in this ringing Schwarzchild background. The equation of motion of a minimally coupled scalar field on this background is given by,

$$\Box_g\phi + \mu^2\phi = 0. \tag{2.2}$$

where μ is the mass of the scalar field. Importantly, in our analysis, we can always maintain scalar field amplitude $\phi < h^\mu_\mu$ by multiplying a small number as (2.2) remains invariant under constant scaling. Using such scaling, the scalar energy momentum tensor can always

be made subleading compared to that of the GW background. With this assumption, we solve the scalar field perturbatively in terms of GW fluctuation, $h_{\mu\nu}$. For simplicity, most of our discussion will be for $\mu \approx 0$. One of the potential candidate scalar fields could be ultra-light axion which is of interest as a potential dark matter candidate. Considering the spherical harmonic expansion of the scalar field, $\phi = \sum \mathcal{N}_{lm}\xi^{lm}(t,r)Y_{lm}(\theta,\phi)$, where $\mathcal{N}_{lm}$ being normalization constant, utilizing (2.2), the mode equation becomes,

$$\mathcal{L}_0\xi^{lm}(t,r) + \mathcal{P}_{lmc\gamma}(h)\xi^{c\gamma}(t,r) + \bar{\mathcal{P}}_{lmc\gamma}(h^*)\xi^{c\gamma}(t,r) = 0, \tag{2.3}$$

with $\mathcal{L}_0$ symbolizing the radial differential operator corresponding to static Schwarzschild space-time ;

$$\mathcal{L}_0\xi^{lm} = -\partial_t^2\xi^{lm}(t,r) + f(r)\frac{1}{r^2}\partial_r\{r^2 f(r)\partial_r\xi^{lm}(t,r)\} - f(r)\frac{l(l+1)}{r^2}\xi^{lm}(t,r).$$

Note that repeated indices have been assumed to be summed over. Whereas $\mathcal{P}_{lmc\gamma}, \bar{\mathcal{P}}_{lmc\gamma}$, (see Appendix.B.1 for detail expression) are the differential operators dependent on the first-order complex and its conjugate part of the metric fluctuation "h" respectively. Gravitational-wave background naturally breaks spherical symmetry, due to which different angular momentum modes of the scalar field will be coupled to each other. Following perturbative approach, the field ξ^{lm} is expanded as,

$$\xi^{lm}(t,r) = \xi^{lm}_{(0)}(t,r) + \xi^{lm}_{(1)}(t,r) + \mathcal{O}([h_{\mu\nu}]^2), \tag{2.4}$$

where the successive terms represent the gauge field in the order of $[h_{\mu\nu}]$. Field variables with subscript "(0)" denote the solution for the static background and the same with subscript "(1)" denote the same corresponding to the perturbed part. Substituting the above expansion in (2.3) we obtain the linearized equations of motion, up to $\mathcal{O}([h_{\mu\nu}]^0)$,

$$\mathcal{L}_0(t,r)\xi^{lm}_{(0)}(t,r) = 0, \tag{2.5}$$

and up to $\mathcal{O}([h_{\mu\nu}])$,

$$\mathcal{L}_0(t,r)\xi^{lm}_{(1)}(t,r) + \mathcal{P}_{lmc\gamma}(h)\xi^{c\gamma}_{(0)}(t,r) + \bar{\mathcal{P}}_{lmc\gamma}(h^*)\xi^{c\gamma}_{(0)}(t,r) = 0. \tag{2.6}$$

By using the properties of the inhomogeneous differential equation, we have decomposed the perturbed part of the scalar field, $\xi^{lm}_{(1)}(t,r) = \xi^{lm}_1(t,r) + \bar{\xi}^{lm}_1(t,r)$, such that,

$$\mathcal{L}_0\xi^{lm}_1(t,r) + \mathcal{P}_{lmc\gamma}(h)\xi^{c\gamma}_{(0)}(t,r) = 0 \ ; \ \mathcal{L}_0\bar{\xi}^{lm}_1 + \bar{\mathcal{P}}_{lmc\gamma}(h^*)\xi^{c\gamma}_{(0)}(t,r) = 0 \tag{2.7}$$

The above set of equations can be thought of as scalar waves propagating in the static Schwarzschild ($g^0_{\mu\nu}$) background with oscillatory source term.

2.3 How the GW-QNMs manifest in the scalar field

The zeroth order part of the scalar field $\xi_0^{c\gamma}(t,r)$ being the solution for static Schwarzschild BH, we can rewrite it as,

$$\xi_{(0)}^{c\gamma}(t,r) = \int d\mathrm{k}\; e^{-\mathrm{i}\mathrm{k}t}\xi_{(0)}^{c\gamma}(\mathrm{k},r) \tag{2.8}$$

with k representing the corresponding frequency. Now, recall that the time dependence of the ringing fluctuation (2.1) is dictated by $e^{-\mathrm{i}\omega t}$ so that, one will be able to extract it out of $(\mathcal{P}_{lmc\gamma})$ and $(\bar{\mathcal{P}}_{lmc\gamma})$. The preceding two arguments help us to express (2.7) as,

$$\begin{aligned}
&\mathcal{L}_0(t,r)\xi_{(1)}^{lm}(t,r) + \int d\mathrm{k}\; e^{-\mathrm{i}(\mathrm{k}+\omega)t}\mathcal{P}_{lmc\gamma}(\mathrm{k},\omega,r)\xi_{(0)}^{c\gamma}(\mathrm{k},r) = 0,\\
&\mathcal{L}_0(t,r)\bar{\xi}_{(1)}^{lm}(t,r) + \int d\mathrm{k}\; e^{-\mathrm{i}(\mathrm{k}-\omega^*)t}\bar{\mathcal{P}}_{lmc\gamma}(\mathrm{k},\omega^*,r)\xi_{(0)}^{c\gamma}(\mathrm{k},r) = 0,
\end{aligned} \tag{2.9}$$

We only consider the particular solution for the $\xi_{(1)}^{lm}(t,r)$ and $\bar{\xi}_{(1)}^{lm}(t,r)$, hence, it is plausible to consider the following decomposition,

$$\xi_{(1)}^{lm}(t,r) = \int d\mathrm{k}\; e^{-\mathrm{i}(\mathrm{k}+\omega)t}\xi_{(1)}^{lm}(\mathrm{k},r), \tag{2.10}$$

and, in the same fashion, we can express,

$$\bar{\xi}_{(1)}^{lm}(t,r) = \int d\mathrm{k}\; e^{-\mathrm{i}(\mathrm{k}-\omega^*)t}\bar{\xi}_{(1)}^{lm}(\mathrm{k},r) \tag{2.11}$$

Substituting these above forms of the fields' decomposition, we obtain from (2.9),

$$\begin{aligned}
&\mathcal{L}_0(\mathrm{k},\omega,r)\xi_{(1)}^{lm}(\mathrm{k},r) + \mathcal{P}_{lmc\gamma}(\mathrm{k},\omega,r)\xi_{(0)}^{c\gamma}(\mathrm{k},r) = 0,\\
&\mathcal{L}_0(\mathrm{k},\omega^*,r)\bar{\xi}_{(1)}^{lm}(\mathrm{k},r) + \bar{\mathcal{P}}_{lmc\gamma}(\mathrm{k},\omega^*,r)\bar{\xi}_{(0)}^{lm}(\mathrm{k},r) = 0,
\end{aligned} \tag{2.12}$$

Where,

$$\mathcal{L}_0(\mathrm{k},\omega,r) = f(r)\partial_r(f(r)\partial_r) + (\mathrm{k}+\omega)^2 - f(r)\frac{l(l+1)}{r^2}, \tag{2.13}$$

and

$$\mathcal{L}_0(\mathrm{k},\omega^*,r) = f(r)\partial_r(f(r)\partial_r) + (\mathrm{k}-\omega^*)^2 - f(r)\frac{l(l+1)}{r^2}, \tag{2.14}$$

can be derived by acting $\mathcal{L}_0(t,r)$ on (2.10) and (2.11). To solve the above set of differential equations we fix the following ingoing initial boundary condition near the horizon of the static black hole,

$$\xi_0^{lm} = \mathcal{N}_0\left(\zeta_0^{lm} + (r-2M)\frac{(16M^2\mathrm{k}^2 - l(l+1))}{2M(4\mathrm{i}M\mathrm{k}-1)}\zeta_0^{lm} + ...\right) \tag{2.15}$$

with arbitrary normalization constant ζ_0^{lm}. $\mathcal{N}_0 = e^{-i\mathrm{k}t}f(r)^{-2\mathrm{i}M\mathrm{k}}$, which corresponds to the ingoing mode near the Schwarzschild horizon of momentum k.

2.4 Defining the absorption cross section

Usually one defines the absorption cross-section in the asymptotic flat space region. To compute such quantity for the ringing black hole we propose the following method: the spatial section is divided into region-**I** (shaded) with the ringing background and region-**II** with pure Schwarzschild (see Fig.2.1). Between the regions, a hypothetical surface, named as an "interaction surface", is defined at $r = r_{int}$, where at $t = t_{int} = r^*_{int}$, the incoming scalar wave interacts with the gravitational wave. Considering Eq.(2.15), we numerically solve for each mode (k) of the scalar field up to the first order in h in the region-**I** described as,

$$\xi^{klm}_{\mathbf{I}}(t,r) = e^{-\mathrm{i}\mathrm{k}t}\xi^{lm}_0(\mathrm{k},r) + e^{-\mathrm{i}(\mathrm{k}+\omega)t}\xi^{lm}_1(\mathrm{k},r) + e^{-\mathrm{i}(\mathrm{k}-\omega^*)t}\bar{\xi}^{lm}_1(\mathrm{k},r) \tag{2.16}$$

In region-**II**, since we consider the pure Schwarzschild background, the solution will be

$$\xi^{klm}_{\mathbf{II}}(t,r) = \xi^{klm}_0(t,r) \quad \text{with} \quad \mathcal{L}_0(t,r)\xi^{klm}_0(t,r) = 0, \tag{2.17}$$

We want to clarify that the notation used to denote the fields with subscript "0" *in the exterior of interaction surface in contrast to the same quantity with the subscription* "(0)" *(see the discussion below (2.4)), which represents the solution for the static Schwarzchild BH without the prior fluctuation.* The primary motivation for complicating the subscription of the variable, ξ, rather than using different variables altogether is to convey the fact that they represent the same physical quantity in various circumstances. Now, the above second order partial differential equation involving two variables (t, r) requires four boundary conditions. Therefore, in Region-**II**, the appropriate boundary/initial condition would be as follows: we provide two spatial initial conditions at the interaction surface r_{int},

$$\begin{aligned} \xi^{klm}_{\mathbf{II}}(t,r)|_{\forall t, r\to r_{int}} &= \xi^{klm}_{\mathbf{I}}(t,r)|_{\forall t, r\to r_{int}} \\ \partial_r\xi^{klm}_{\mathbf{II}}(t,r)|_{\forall t, r\to r_{int}} &= \partial_r\xi^{klm}_{\mathbf{I}}(t,r)|_{\forall t, r\to r_{int}} \end{aligned} \tag{2.18}$$

while we provide the time conditions as boundary conditions at $t \to \infty$,

$$\begin{aligned} \xi^{klm}_{\mathbf{II}}(t,r)|_{t\to\infty,\forall r} &= \xi^{klm}_0(t,r)|_{t\to\infty,\forall r} \\ \partial_t\xi^{klm}_{\mathbf{II}}(t,r)|_{t\to\infty,\forall r} &= -\mathrm{i}\mathrm{k}\xi^{klm}_0(t,r)|_{t\to\infty,\forall r} \end{aligned} \tag{2.19}$$

Within the lightcone, the quasi-normal oscillation is exponentially decaying in time. Hence, in $t \to \infty$ fluctuation part of the scalar field $(\xi^{lm}_1, \bar{\xi}^{lm}_1)$ at the interaction surface vanishes. This essentially sets our last two boundary conditions which make sure that the scalar field absorption cross-section of ringing BH boils down to static Schwarzschild value within the characteristic time scale of the oscillation $\tau \sim 2\pi/\omega$. Using the boundary condition Eq.2.18, we solve Eq.2.19 within the region $t \geq r_*$, of the box bounded in (r, t) plane as $([r_{int}, \infty], [t_{int}, \infty])$. Asymptotically, the gravitational wave propagates along the outgoing null coordinate. Hence, once the solution is obtained, we transform it into outgoing null coordinate $(t, r) \to (u = t - r^*, r)$ and define the absorption cross-section, which will naturally be r_{int} dependent.

2.4.1 Energy Flux:

In our framework, the procedure to determine the absorption cross section for an oscillating black hole arises from the definition followed (1.2.3) in the case of static and stationary black holes. For

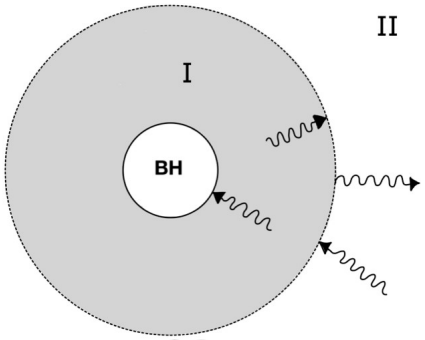

FIGURE 2.1: Interaction of the scalar wave with the gravitational wave. The shaded region(**I**) represents the spatial extent of ringing fluctuation, outside (**II**) is considered to be static Schwarzschild space-time.

this, we first study the case of static and stationary black holes in (u, r) coordinate, and then we extend the formalism to the oscillating black hole. To proceed we write down the covariant conservation equation on a generic spacetime background with the associated Killing vector, ξ^μ, as [7],

$$\nabla_\mu \left(\mathscr{T}^\mu{}_\nu \xi^\nu\right) = 0, \tag{2.20}$$

which can be explicitly checked using the covariant conservation of the symmetric stress energy tensor, $\nabla_\mu \mathscr{T}^\mu{}_\nu = 0$, and the killing equation $\nabla^\mu \xi^\nu + \nabla^\nu \xi^\mu = 0$. Let us symbolize the quantity inside the parenthesis of the above equation as the generalized four momentum, $P^\mu = \mathscr{T}^\mu{}_\nu \xi^\nu$. To determine the conserved quantity, one needs to find out the allowed Killing vectors. For example, the static spherically symmetric (Schwarzschild type black hole) spacetime, in $(u = t - r_*, r)$,

$$ds^2 = -f(r)du^2 - 2dudr + r^2(d\theta^2 + \sin^2\theta d\phi^2), \tag{2.21}$$

This metric allows one of the time like Killing vectors as $\xi_0 = \delta^\mu_0 \partial_\mu$. For this particular Killing vector, the associated conserved quantity turns out to be

$$\mathcal{F} = \int d^3x \sqrt{-g_0(u,r)} P^0, \tag{2.22}$$

Where, $g_0(u, r)$ is the determinant of metric given in (2.21). The above statement also implies, $\partial_u \mathcal{F} = 0$. Taking the time derivative on both sides of the above equation we get

$$\partial_u \mathcal{F} = \int d^3x \partial_u \left(\sqrt{-g_0(u,r)} P^0\right) = -\int d^3x \partial_i \left(\sqrt{-g_0(u,r)} P^i\right). \tag{2.23}$$

By choosing a r-constant hypersurface and applying the divergence theorem in the above equation one will arrive at

$$\partial_u \mathcal{F} = -\int r^2 d\Omega P^r \Big|_{r_h}^{\infty} = -\int r^2 d\Omega \mathscr{T}^r{}_u \xi^u \Big|_{r_h}^{\infty} = -\left[\int r^2 d\Omega \mathscr{T}^r{}_u \Big|_{r\to\infty} - \int r^2 d\Omega \mathscr{T}^r{}_u \Big|_{r_h}\right]. \tag{2.24}$$

Where, $d\Omega \equiv \sin\theta d\theta d\phi$. We can see that two terms in the last equality of the above equation are equal by the fact that $\partial_u \mathcal{F} = 0$, as mentioned previously. Therefore, one may infer that the energy

being absorbed by the black hole horizon per unit time could be equated with, $\partial_u \mathcal{F}_{r\to\infty}$. Now, the definition of the absorption cross section [34] is the amount of energy being absorbed by the black hole horizon divided by the incident energy density. We define the incident energy density as, $\partial_u \mathcal{G} = \mathscr{T}^z{}_u$, which sometimes called as energy density current [35]. Utilizing this technology we obtain the absorption cross section in terms of the stress-energy tensor of the fields as,

$$\sigma^{kl}_{\rm ring}(u, r_{\rm int}) \equiv \frac{\partial_u \mathcal{F}^{\rm kl}}{\partial_u \mathcal{G}^{\rm k}}\bigg|_{r\to\infty} = \frac{\int r^2 d\Omega \mathscr{T}^r{}_u}{\mathscr{T}^z{}_u}\bigg|_{r\to\infty}. \tag{2.25}$$

This expression, in principle, should be evaluated at spatial infinity (one may look at eq.(23) of [122] for a similar definition using current density). For practical purposes, we have presented our results considering $r = 75r_h$, however, we have checked that all the results are stable with $r = 50r_h - 100r_h$. The subsequent part of the analysis very much follows from the discussion given in the Introduction chapter.(1.2.3). We have to first substitute the scalar field $\phi = \sum \mathcal{N}_{\rm klm}\xi^{klm}(u, r)Y_{lm}(\theta, \phi)$ in the stress energy tensor of the above definition of absorption cross section using the numerical solution of $\xi^{klm}(u, r)$. The procedure to find out the mode solution, $\xi^{klm}(u, r)$, has been discussed in the preceding section. However, to figure out the normalization factor $\mathcal{N}_{klm}$, we should reiterate that we have solved the scalar field modes starting from the black hole horizon to the interaction surface (r_{int}) with an ingoing boundary condition. For this, the ringing Schwarzschild metric is playing as a source. Then using that solution as the time dependent initial condition at the interaction surface, we solve the same mode equation in the static Schwarzschild background. This procedure renders it difficult to identify the plane wave component at the asymptotic infinity, thereby finding the normalization factor $\mathcal{N}_{klm}$. We proceed by considering an approximate asymptotic solution of the scalar field as,

$$\xi^{klm}_0(t, r) = \mathcal{N}_{\rm klm}\left(\frac{\mathcal{I}^{\rm k}_{lm}(u, r_{int})}{r}e^{-{\rm ik}(u+2r_*)} + \frac{\mathcal{R}^{\rm k}_{lm}(u, r_{int})}{r}e^{-{\rm ik}u}\right). \tag{2.26}$$

Due to the oscillating nature of the ringing black hole background, the ingoing/outgoing coefficients ($\mathcal{I}^{\rm k,\omega}_{lm}/\mathcal{R}^{\rm k,\omega}_{lm}$) naturally become time dependent and the dependency on the r_{int} appears for the initial condition set at the interaction surface. Following the standard procedure [34], the assumption of incoming plane wave along the z-direction in the asymptotic infinity sets the constant normalization factor. Therefore, to identify the incoming scalar wave propagating along 'z-direction, we first use the well known Rayleigh expansion of the plane wave in terms of the partial wave as

$$e^{-{\rm ik}(u+z_*)}e^{-{\rm ik}z_*} \sim \sum e^{-{\rm ik}(u+r_*)}\frac{e^{-{\rm ik}r_*}}{2{\rm ik}r}\sqrt{4\pi(2l+1)}Y^0_l(\Omega) + \text{Outgoing} \tag{2.27}$$

where $z_* = r_* \cos\theta$ (recall that we have transformed, $t \to u + z_*$). Considering the asymptotic solution Eq.(2.26), we first choose the time independent normalization condition as,

$$\mathcal{N}_{\rm klm} = \frac{\sqrt{4\pi(2l+1)}}{2{\rm ik}\mathcal{I}^{\rm k}_{lm}(u\to\infty, r_{int})}\delta^0_m. \tag{2.28}$$

The ingoing/outgoing coefficients ($\mathcal{I}^{\rm k,\omega}_{lm}/\mathcal{R}^{\rm k,\omega}_{lm}$) will match with that of the static Schwarzschild case in $u \to \infty$ limit. Using the above normalization factor, the ingoing plane wave at the asymptotic infinity is assumed as,

$$\phi_{in} \sim \frac{\int \sum \mathcal{N}_{\rm klm}\mathcal{I}^{\rm k}_{lm}(u, r_{int})Y_{lm}(\Omega)d\Omega}{\int \sum \sqrt{4\pi(2l+1)}Y^0_l(\Omega)d\Omega}2{\rm ik}e^{-{\rm ik}(u+2z_*)}. \tag{2.29}$$

Where time dependent amplitude is averaged over angle. This amplitude is defined in such a way that in the $u \to \infty$ limit, it reduces to unity. With this approximated ϕ_{in}, we obtain the total rate of ingoing flux for a given mode k by substituting it in the stress energy tensor in the denominator of the definition (2.25) of absorption cross section. With all these ingredients we have been able to numerically compute the absorption cross-section $\sigma^{kl}_{\rm ring}$. In the following section, we have discussed our numerical results of $\sigma^{kl}_{\rm ring}(u, r_{int})$, which is the partial absorption cross section.

2.5 Numerical Computation of $\sigma^{\rm kl}_{\rm ring}$

As mentioned earlier, the gravitational wave background is assumed to be quadrupole oscillation (2.1) with the QNMfrequency $\omega = (0.74734 - {\rm i}\ 0.17792)(r_h)^{-1}$ [16], where, Schwarzschild horizon radius $r_h = 2M$. We express all physical parameters in units of r_h. Ringdown phase in general should contain all possible QNM modes[15]. However, we consider the one which is long-lived. The background ringing field solutions are so chosen that the perturbativeness defined as $\delta g/g_0 \propto h^\mu_\mu \ll 1$ is maintained for a wide range of initial parameters. Given the ringing black hole background with a specific QNM frequency, we solve for the scalar field (2.3). Importantly, we should reproduce the well known static value of the absorption cross-section (1.2.3.a) associated with Schwarzschild black hole in the limit, $\lim_{u\to\infty} \sigma^{kl}_{\rm ring}(u, r_{int}) = \sigma^0({\rm k}, l)$. Hence, before the static limit is reached over the time scale $\tau \sim 40$, $\sigma^{kl}_{\rm ring}(u, r_{int})$ will also undergo a ring down phase. It is during the ring-down phase when the superradiance is observed.

Elaborating more on the numerics, our final solutions have been observed to be stable for a wide range of initial conditions parametrized by ζ^{lm}_0 within $\sim 10^{-2} - 20$. Up to a small fluctuation, our results are also stable for a range of asymptotic radial infinity within $r = 75r_h - 100r_h$. This fluctuation may be arising due to our approximate normalization. Nonetheless, the characteristic features of absorption cross-section for different angular momentum modes have been observed to be the same. Hence, we particularly focus on $l = 0$ mode. As emphasized in the beginning the most important characteristic that emerged from our study is the super-radiant(negative) absorption cross-section in its ringing phase for all angular momentum modes (see Figs.2.2, 2.3, 2.4).

We identify five main theory parameters of our interest $({\rm k}, l, r_{\rm int})$ and the GW amplitudes $(\mathcal{E}_h, \mathcal{O}_h)$ (1.2.1). We have considered the following fixed values of the parameters for our analysis, $\mathcal{E}_h \simeq \mathcal{O}_h \sim 10^{-3}$ and $r_{int} = 20$, as well as have investigated the effect due to their variation. For the given ω and $(\mathcal{E}_h, \mathcal{O}_h)$, the maximum super-radiant absorption cross-section amplitude symbolized as $\sigma^{kl}_{\mathbf{maxN}}({\rm k})$, decreases with increasing momentum k. We also derived a fitting formula $\sigma^{kl=0}_{\mathbf{maxN}}({\rm k}) = -1021 + 20065{\rm k} - 131798{\rm k}^2 + 292061{\rm k}^3$, withing the range $({\rm k} = 0.06 \to 0.14)$. Following our expectation, we observe the existence of a maximum value of k_{max} above which super-radiance vanishes. However, the absorption cross-section will still remain oscillatory with a positive magnitude and attain its static Schwarzschild value in the ringdown time scale (see Fig.2.2). The physical reason behind the vanishing of superradiance can be attributed to the decoupling of higher momentum modes from the gravitational wave fluctuations. Our numerical analysis provides: $l = 0, {\rm k}_{max} \sim 0.13$; $l = 1, {\rm k}_{max} \sim 0.45$; $l = 2, {\rm k}_{max} \sim 1.0$; $l = 3, {\rm k}_{max} \sim 1.5$; $l = 4, {\rm k}_{max} \sim 1.8$. Of course, decreasing the background amplitude would make k_{max} lower.

As our methodology suggests, the ringing phase of the absorption cross-section and its amplitude depend on the location of the interaction surface r_{int} shown in Fig.(2.2). For each $(l, {\rm k})$

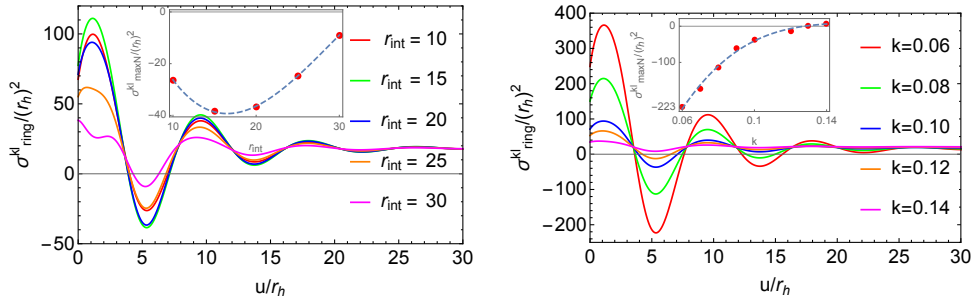

FIGURE 2.2: Left panel: we have plotted σ^{kl}_{ring} with respect to time considering $l = 0, k = 0.1$ for different r_{int}. In the inset the variation of **max**imum **N**egative value symbolized as $\sigma^{kl}_{\mathbf{maxN}}$ is plotted with respect to r_{int} Right panel: we have plotted the same for $l = 0$ and vary k. The inset shows the variation of maximum negative value $\sigma^{kl}_{\mathbf{maxN}}(k)$ with respect to k. All plots are from $\mu = 0$.

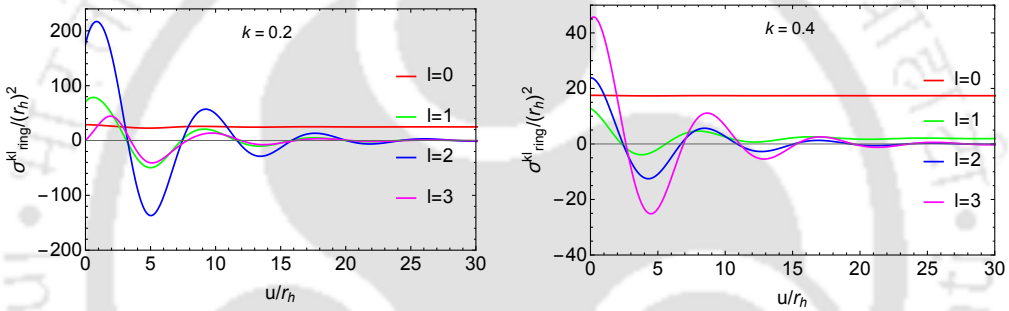

FIGURE 2.3: The partial absorption cross-section is plotted with respect to time for two frequencies k = 0.2(left) and k = 0.4(right) for different l. All plots are from $\mu = 0$.

value, there exists a maximum possible super-radiant amplitude ($\sigma^{kl}_{\mathbf{maxN}}(r_{int})$) as one varies r_{int}. For example, for $l = 0$ it occurs approximately at $r_{int} \sim 20$, for higher range k values. In the low k region this location of maximum super-radiant amplitude shifts towards higher $r_{int} \sim 30 - 40$. This behavior can again be fitted as $\sigma^{kl=0}_{\mathbf{maxN}}(r_{int}) = 63.7 - 14.4 r_{int} + 0.6 r^2_{int} - 0.007 r^3_{int}$ within the range ($r_{int} = 10 \to 30$). Each super-radiant mode has been observed to be saturated to a particular negative value of the absorption cross-section for large r_{int}. So far we discussed the absorption cross-section for a fixed value of $\mathcal{E}_h \simeq \mathcal{O}_h \sim 10^{-3}$. However, background gravitational wave amplitude plays a crucial role in enhancing the outgoing amplitude of the scalar wave compared to the incoming one. This fact motivates us to look into the variation of σ^{kl}_{ring} with respect to $(\mathcal{E}_h, \mathcal{O}_h)$ as shown Fig.(2.4). Decreasing background amplitude of $(\mathcal{E}_h, \mathcal{O}_h)$ reduces the overall amplitude of σ^{kl}_{ring} in its ringing phase as shown in the Fig.(2.4), and finally super-radiance ceases to exist at around $\mathcal{E}_h, \mathcal{O}_h = 10^{-4}$(in units of black hole mass) for $l = 0$. This conclusion has been observed to be true for higher l mode as well. Thus far we discussed a particular angular momentum mode $l = 0$. Behavior of $\sigma^{kl}_{ring}(u, r_{int})$ for different l is important. For a given location of the interaction surface ($r_{int} = 20$), the left panel of Fig.2.3 shows that in the lower momentum region (k = 0.2) the super-radiant amplitude first increases up to $l = 2$ and then become suppressed after $l = 3$. This does not hold for all the momentum modes as can be seen in the right panel of Fig.2.3 for k = 0.4.

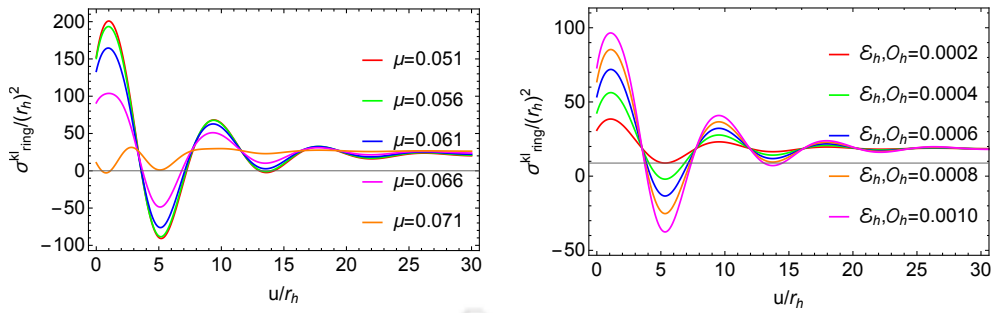

Figure 2.4: Left panel:we have plotted $\sigma^{kl}_{\rm ring}$ with respect to time for $l = 0, \sqrt{k^2+\mu^2} = 0.1, r_{int} = 20$ for different mass of the scalar field. Right panel: we have plotted the same for $l = 0, k = 0.1, r_{int} = 20$ and vary $\mathcal{E}_h = \mathcal{O}_h$ for massless case, $\mu = 0$.

Because of the non-trivial dependence on r_{int} described before, maximum super-radiant amplitude happens to be at different locations of the interaction surface r_{int} for different (l, k). Hence, overall our study suggests that with increasing l the enhancement of super-radiance amplitude can be attributed to "mode-mixing" and an increasing number of modes contributing as a background source term in Eq.2.12. A similar kind of feature has been observed for moving black holes where absorption cross-section has been shown to diverge logarithmically with angular momentum l [35].

Finally, we perform preliminary analysis for (Fig.(2.4)) massive scalar. What we observed is that for a given mode, $(\tilde{\omega} = \sqrt{\mathrm{k}^2+\mu^2}, l)$ and r_{int}, as we increase the mass of the scalar field, superradiant amplitude increases towards a maximum value and then after it decreases towards zero for a critical value of $\mu_{cri} < \tilde{\omega}$. For example $\mu_{cri} \sim 0.071$ in (Fig.2.4) for $l = 0, \tilde{\omega} = 0.1, r_{int} = 20$. Our primary observation is that along with the increasing l, the μ_{cri} is increasing approximately linearly. Detailed study for the massive scalar and its bound needs further analysis, which will be an important future project.

2.6 Mean absorption cross section and Energy extraction at spatial infinity

To find out the absorption cross section in a time-dependent background, such as that of a ringing black hole, we introduced the concept of the interaction surface. As a computational tool, the position of the interaction surface, $r_{\rm int}$ should not turn up in the final result. Although the reader has already noticed that the absorption cross section significantly depends on $r_{\rm int}$, this does not provide the complete picture. This is because the incoming wave, in principle, interacts with the gravitational background at every point. Therefore we further compute the mean value of the absorption cross section, which is independent of the position of the interaction surface, $r_{\rm int}$, by integrating over $r_{\rm int}$, and dividing by a large spatial domain in the following manner,

$$\bar{\sigma}^{kl}_{\rm ring}(u) = \frac{\int \sigma^{kl}_{\rm ring}(u, r_{\rm int}) dr_{\rm int}}{\int dr_{\rm rint}}. \tag{2.30}$$

Although this definition, a priori, may seem arbitrary, it correctly reproduces the standard result for the absorption cross section of a static Schwarzschild black hole in the expected limit as $u \to \infty$.

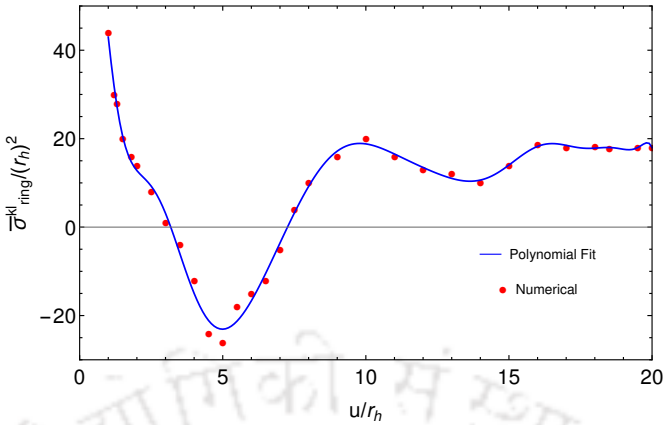

FIGURE 2.5: Mean absorption cross section has been plotted with time by averaging over the position of the interaction surface, $r_{\rm int}$ for a fixed frequency, k $= 0.1 r_h^{-1}$ and $l = 0$.

To numerically evaluate the above quantity, first, we have obtained the absorption cross section at a particular instant of time for $r_{\rm int} \in (5r_h, 50r_h)$. In this interval, we have fitted the points using Polynomial fit, which will provide a functional form of the absorption cross section in terms of the $r_{\rm int}$ and integrated it in the same interval. Repeating this procedure for various instants of time, we have generated the plot of Fig.2.5. One may extend the domain of $r_{\rm int}$, but that will negligibly affect the result as we have already seen in Fig.2.2 that the maximum amplitude occurs at $r_{int} \sim 20r_h$ and decreases on both sides. The mean absorption cross section presented in Fig.2.5, thus independent of $r_{\rm int}$, however, shares very much the same feature as given in Fig.2.2 and Fig.2.3.

Energy Extraction: By definition, the absorption cross section entails the fractional energy gain (see [123]), if it happens so, as can be realized by looking at the numerator in the definition (2.25), expanding which in terms of the fields, we obtain,

$$\begin{aligned}\int r^2 d\Omega \mathcal{T}^r{}_u &\sim \Big[\, |\mathcal{N}_{klm}|^2 \left(|\mathcal{I}^{\rm k}_{lm}(u)|^2 - |\mathcal{R}^{\rm k}_{lm}(u)|^2\right)\Big], \\ &\sim (\partial_u E^{tot}_{\rm in} - \partial_u E^{tot}_{\rm out}),\end{aligned} \tag{2.31}$$

where, $E_{\rm in}$ and $E_{\rm out}$ represents respectively the total ingoing and outgoing energy flux, which can be obtained by substituting (2.26) in the numerator of (2.25). Note that there will be additional terms in the first line of the above equation, however, the contribution of them turns out to be negligibly small. Nevertheless, the negative values of the absorption cross section thus imply, $\partial_u E^{tot}_{\rm in} < \partial_u E^{tot}_{\rm out}$, which happens in certain time intervals as shown in Fig.2.2,2.3 and Fig.2.5. In these durations energy will be extracted by the scalar field from the ringing BH. Of course, the positive part of the absorption cross section, presented in Fig.2.2, Fig.2.3 and Fig.2.5 suggest that there will be absorption in some intervals. However, the superradiance will happen in the rest of the intervals within the decay time scale of the ringdown phase. An observer sitting at spatial infinity will receive this amplified scalar wave as a repeated flash, which eventually decays, exhibiting the transient nature of the ringing phase of the BH.

2.7 Observables effects of the oscillating scalar field

Superradiance phenomena is known to occur in the context of static Kerr and charged black hole [42]. However, a most striking feature of our present study is its oscillatory nature which is observed to carry the information of black holes through their quasi-normal modes. Any time varying observable is always physically motivating when it comes to observation compared to the static one. Identifying the ringing scalar field as axion, we calculate multiple observables, which can in principle be observed in the laboratory [104, 105].

Rotation of the plane of polarization of a photon beam: Treating the axion field as time varying background, we consider the well known Chern-Simons, axion-photon interaction,

$$S = \int \sqrt{-g} d^4x [-\frac{1}{2}(\partial_\mu\phi\partial^\mu\phi + m_\phi^2\phi^2) - \frac{1}{4}F_{\mu\nu}F^{\mu\nu} - \frac{1}{4}g_{\phi\gamma\gamma}\phi F_{\mu\nu}\tilde{F}^{\mu\nu}] \tag{2.32}$$

where, $g_{\phi\gamma\gamma}$ is the axion-photon coupling costant. Choosing the radiation gauge, $\boldsymbol{\nabla}\cdot\mathbf{A} = 0, A_0 = 0$, both the scalar and Maxwell equation can be simplified as,

$$\begin{aligned} -\partial_t^2\phi + \nabla^2\phi - m_\phi^2\phi + g_{\phi\gamma\gamma}\mathbf{B}\cdot\partial_t\mathbf{A} = 0 \\ \partial_t\mathbf{E} - \boldsymbol{\nabla}\times\mathbf{B} - g_{\phi\gamma\gamma}\mathbf{B}\partial_t\phi - g_{\phi\gamma\gamma}\boldsymbol{\nabla}\phi\times\mathbf{E} = 0 \end{aligned} \tag{2.33}$$

Having a time varying axion background the evolution of the electric field will be affected due to the presence of the term involving time derivative of axion in the above second equation. Actual calculation (see Appendix.B.2) shows that this interaction will induce rotation of the plane of polarization of photons, which can be expressed as,

$$\theta = -\mathrm{i}(\tilde{\Delta}_\phi - \tilde{\Delta}_\phi^*) \sim g_{\phi\gamma\gamma}\ \phi(t) \tag{2.34}$$

Where, $\tilde{\Delta}_\phi = \int^t \frac{\mathrm{i}}{2} g_{\phi\gamma\gamma}\ \partial_{t'}\phi$, with axion-photon coupling taken as, $g_{\phi\gamma\gamma} \sim 10^{-13} - 10^{-14}$ GeV^{-1} [106]. Experimental searches of such rotation due to background axion have been extensively studied in the literature [107, 108]. Our analysis suggests that there would be an extra time varying contribution (see Fig.2.6) originating from the ringing oscillation, which can in principle be observed in the near future.

Nucleon electric dipole moment: The time varying nucleon electric dipole moment (N_{edm}), is calculated as $N_{edm} = h\,\phi(t)$, considering the following nucleon(N)-axion-photon interaction $\mathcal{L} \sim -\frac{\mathrm{i}}{2}h\phi\bar{N}\sigma_{\mu\nu}\gamma_5 N F^{\mu\nu}$. The value of axion-nucleon coupling h is typically set from decay constant for QCD axion [103]. The time profile of the two observables mentioned above is depicted in the left panel of Fig.2.6 for different momentum of the axion.

Precession of the spin of fermion: Finally we consider axial axion-fermion type coupling $\mathcal{L} \sim -\frac{\mathrm{i}}{2}\zeta\partial_\mu\phi\bar{\psi}\gamma^\mu\gamma^5\psi$, which describes a physical system where spin of the fermion will be precessing around the direction of local momentum, $\mathbf{v}\,\partial_t\phi$, of the axion, as can be seen from the Hamiltonian arising due to this coupling, $H \sim \zeta\partial_t\phi\,\mathbf{v}\cdot\boldsymbol{\sigma}_\psi$, where $\boldsymbol{\sigma}_\psi$ is the fermion spin operator. That leads to a shift in the energy levels of the fermions (nuclear or electron), $\Delta E_{nm}(t) \sim \zeta|\mathbf{v}|\partial_t\phi$ due to its axial moment. The coupling parameter $\zeta \sim 10^{-9}$ GeV^{-1}, [109] is constrained from supernova cooling rates, and $\mathbf{v}$ is the relative velocity (in astrophysical context galactic virial velocity $|\mathbf{v}| \sim 10^{-3}$ may be used) between axion and fermion [103]. The time variation of this energy shift is shown in the right panel of Fig.2.6. Detecting such extra time varying contribution to the energy shift is promising given the several existing proposals of measuring those quantities

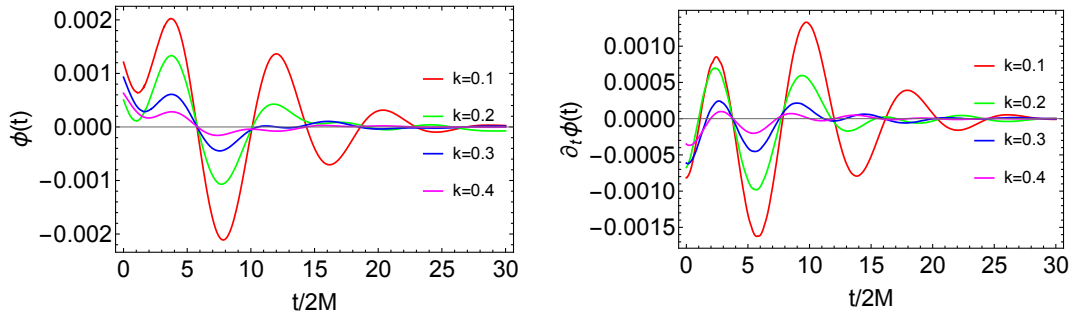

FIGURE 2.6: Real part of the outgoing axion wave, subtracting the contribution of the static black hole, has been plotted in the left panel, with respect to time for a fixed frequency, k = (0.1, 0.2, 0.3, 0.4). The time derivative of the same quantity has been plotted in the right panel. Time is measured from a point $t_{inf} = r_{inf}$ on the light cone. The location of the interaction surface is taken as $r_{int} = 30$

[110] using the method of "Precision magnetometry" using cold molecules [111]. In order to show the oscillating features of all the observables, we consider the s-wave($l = 0$) outgoing mode of the ringing axion and subtract the effect due to the static black hole. Time is measured from a point $t_{inf} = r_{inf}$ on the light cone, where the detector is assumed to be placed [112, 113].

2.8 Summary And Discussion

Despite being widely discussed in the literature, recent observation of GWs has led to a resurgence of exploring the phenomena of black hole superradiance in a more general gravitational setting. Such phenomena were so far shown to exist in Kerr and charged black hole background. In this study, we have worked out for the first time that the black hole in its ringing phase can also lead to superradiance when interacting with an incoming scalar wave. Apart from detecting gravitational waves, our present study opens up interesting possibilities of observing black hole merging phenomena through complementary observables in terms of other fundamental fields. The basic mechanism behind this superradiance is simple. When an incoming scalar wave passes through the ringing GW background, gravitational energy can be transferred into the scalar wave leading to the enhancement of its outgoing flux. This is precisely what makes the scalar field absorption cross-section σ^{kl}_{ring} also go through the ringing phase. Before settling down to its standard Schwarzschild value, σ^{kl}_{ring} in its ringing phase assumes the negative value indicating the superradiance phenomena in the ringing black hole background. Finally, we computed different possible time varying observables through axion-photon and axion-fermion coupling. All the observables namely, rotation of photon polarization ($\theta(t)$), nucleon electric dipole moment ($N_{edm}(t)$) and shifting of the energy levels ($\Delta E_{nm}(t)$) due to fermionic axial moment are found to naturally encode the ringing oscillation through the axion. However, this complicacy of the indirect approach of obtaining the superradiant signature straightforwardly drives us to investigate the scattering of the electromagnetic field itself in the ringing black hole background. This scenario is more motivating as the scattered electromagnetic field can be directly observed in existing ground based detectors. This particular aspect will be the topic of our discussion in the next chapter.

Superradiant scattering of electromagnetic field due to ringing black hole 3

"The main thing in science is the effort to discover truth; the mode in which this is done constitutes art"

James Clerk Maxwell

3.1 Introduction

In the previous chapter, we investigated the scattering of an ultralight scalar field with a ringing Schwarzschild BH and demonstrated that the field may experience superradiant scattering, particularly in the infrared regime. However, the detection of such transient superradiant signals in the scalar sector is experimentally challenging. In this chapter, we investigate instead the scattering of electromagnetic (EM) fields which is experimentally more relevant. Apart from direct gravitational waves, any complementary signature such as time dependent superradiant scattering of EM waves from ringing BH could be of paramount importance in light of the recent spate of research activity on the aspects of black holes, and gravitational waves in particular. Thus the question of obtaining a detectable complimentary signature of the black hole ringdown phase and for that matter superradiant enhancement has motivated us to extend our previous analysis of the scalar field to the electromagnetic field.

On the observational front, the dynamics of fundamental fields in time dependent background have been the subject of investigation in recent times[114], where the superradiant evolution leads to significant enhancement in the emitted flux. The dynamical character of the superradiance very often gives rise to interesting effects in BH shadow[115, 116] and polarization [117, 118]. In the present analysis, we initiate a novel study of electromagnetic wave scattering through the ringing black hole background. Moreover, there are existing ground-based Low Frequency Array (LOFAR), radio telescopes which are currently operational and receiving electromagnetic signals

in the radio frequency range. Therefore it would be an interesting premise to understand different observables in relation to BHs which could be relevant for future observation.

3.2 Minimally coupled gauge field in the ringing BH background

The minimally coupled EM field on the ringing BH background (2.2) satisfies the standard equation of motion as,

$$\partial_\mu(\sqrt{-g}g^{\mu\alpha}g^{\nu\beta}F_{\alpha\beta}) = 0. \tag{3.1}$$

It is important to understand that one can always maintain the amplitude of the EM field, $F_{\mu\nu} < h^\mu{}_\mu$ with an overall multiplication by a small number as (3.1) remains invariant. This way we can make the energy momentum tensor of the EM field subleading with respect to that of the ringing background. To construct a linearized version of the equation of motion (3.1), up to $\mathcal{O}(h)$, we consider the determinant of the metric as, $\sqrt{-g} = \sqrt{-g_0}(1 + h^\mu{}_\mu/2)$, with the trace of the metric taken to be $h^\mu{}_\mu = g_0^{\mu\nu}h_{\mu\nu}$. For the same purpose, we express the inverse metric as, $g^{\mu\nu} = g_0^{\mu\nu} - h^{\mu\nu}$. With this setup, the equation of motion can be expressed up to linear order in fluctuation ($\mathcal{O}(h)$) as,

$$\begin{aligned}&\partial_\mu(\sqrt{-g_0}g_0^{\mu\alpha}g_0^{\nu\beta}F_{\alpha\beta})\\&+\partial_\mu\left[\sqrt{-g_0}\left(\frac{h^\gamma{}_\gamma}{2}g_0^{\mu\alpha}g_0^{\nu\beta} - g_0^{\mu\alpha}h^{\nu\beta} - h^{\mu\alpha}g_0^{\nu\beta}\right)F_{\alpha\beta}\right] = 0.\end{aligned} \tag{3.2}$$

Notice that the first part of the above equation describes the governing equation of the EM field for the static Scwarzschild BH, while the second part corresponds to that for the leading order ringing fluctuation. Since the non-ringing part of the background is spherically symmetric, we decompose the EM field components as [48]

$$\begin{aligned}A_t(t,\mathbf{r}) &= \sum_{lm} b^{lm}(t,r)Y_{lm}(\Omega),\\A_r(t,\mathbf{r}) &= \sum_{lm} d^{lm}(t,r)Y_{lm}(\Omega),\\A_s(t,\bar{r}) &= \sum_{lm}\left[k_{lm}(t,r)\Psi_s^{lm}(\Omega) + a_{lm}(t,r)\Phi_s^{lm}(\Omega)\right],\end{aligned} \tag{3.3}$$

where we have used the well known orthogonal vector spherical harmonic basis [119, 120] for the azimuthal field components,

$$\begin{aligned}\Psi_s^{lm} &= \partial_s Y_{lm},\\\Phi_s^{lm} &= \epsilon_{ss'}\partial^{s'}Y_{lm}.\end{aligned} \tag{3.4}$$

Here, and throughout the paper, s, s' indices correspond to angular coordinates (θ, ϕ). Levi-Civita symbols, $\epsilon_{\theta\theta} = \epsilon_{\phi\phi} = 0, \epsilon_{\theta\phi} = -\epsilon_{\phi\theta} = \sin\theta$. In our analysis, we work with the following gauge invariant variables,

$$\begin{aligned}\chi_1^{lm} &= \frac{r^2}{l(l+1)}(\partial_t d^{lm} - \partial_r b^{lm}) \quad ; \quad \chi_2^{lm} = a^{lm},\\\chi_3^{lm} &= d^{lm} - \partial_r k^{lm} \quad ; \quad \chi_4^{lm} = b^{lm} - \partial_t k^{lm},\end{aligned} \tag{3.5}$$

(see Appendix.D of [48] for stationary BHs), which can be obtained from (3.3) utilizing the gauge transformation $A_\mu \to A_\mu - \partial_\mu(\Xi(t,r)Y_{lm}(\theta,\phi))$, with Ξ representing some arbitrary function. With this setup the governing dynamical equation (3.2) can be expressed in the following simplified form in terms of gauge invariant variables (3.5) up to linear order in fluctuations,

$$\begin{aligned}\mathcal{L}_0(t,r)\chi_1^{lm} + \mathcal{Q}^i_{lmc\gamma}(h)\chi_i^{c\gamma} + \bar{\mathcal{Q}}^i_{lmc\gamma}(h^*)\chi_i^{c\gamma} = 0,\\ \mathcal{L}_0(t,r)\chi_2^{lm} + \mathcal{R}^i_{lmc\gamma}(h)\chi_i^{c\gamma} + \bar{\mathcal{R}}^i_{lmc\gamma}(h^*)\chi_i^{c\gamma} = 0,\end{aligned} \tag{3.6}$$

with $\mathcal{L}_0(t,r)$ representing a Klein-Gordon operator for static Schwarzschild BH,

$$\mathcal{L}_0(t,r) = f(r)\partial_r(f(r)\partial_r) - \partial_t^2 - f(r)\frac{l(l+1)}{r^2}, \tag{3.7}$$

where $i \to (1,2,3,4)$. All the repeated indices are assumed to be summed over. Whereas $\mathcal{Q}^i_{lmc\gamma}, \mathcal{R}^i_{lmc\gamma}$ (for detailed expression see the appendix B.3), are the differential operators depending on the first complex part of the fluctuation metric, while $\bar{\mathcal{Q}}^i_{lmc\gamma}, \bar{\mathcal{R}}^i_{lmc\gamma}$ corresponds to the differential operators for the complex conjugate (as the metric in (2.1) is expressed terms of complex quantities) part of the fluctuation metric (reason for h^* in the parenthesis). The new index c and γ represent the orbital and azimuthal angular momentum modes respectively, in a similar manner as l and m. Therefore we use these sets ((l,m) and (c,γ)) of indices interchangeably.

The ringing background is constructed out of quadrupole perturbation, and hence the spherical symmetry of the system under study is naturally lost. As a consequence, different angular modes of the EM field are now coupled to each other. Therefore, to make the the equation (3.6) solvable we proceed via considering perturbative expansion of the field χ^{lm} as,

$$\chi_i^{lm}(t,r) = \chi^{lm}_{i(0)}(t,r) + \chi^{lm}_{i(\mathrm{p})}(t,r) + \mathcal{O}([h_{\mu\nu}]^2), \tag{3.8}$$

where the successive terms represent the gauge field in the order of $[h_{\mu\nu}]$. Field variables with subscript "(0)" denote the solution for the static background and the same with subscript "(p)" denote the same corresponding to the perturbed part. Substituting the above expansion in (3.6) we obtain the linearized equations of motion, up to $\mathcal{O}([h_{\mu\nu}]^0)$,

$$\begin{aligned}\mathcal{L}_0(t,r)\chi^{lm}_{1(0)} = 0,\\ \mathcal{L}_0(t,r)\chi^{lm}_{2(0)} = 0,\\ .\end{aligned} \tag{3.9}$$

and up to $\mathcal{O}([h_{\mu\nu}])$,

$$\begin{aligned}\mathcal{L}_0(t,r)\chi^{lm}_{1(\mathrm{p})} + \mathcal{Q}^i_{lmc\gamma}(h)\chi^{c\gamma}_{i(0)} + \bar{\mathcal{Q}}^i_{lmc\gamma}(h^*)\chi^{c\gamma}_{i(0)} = 0\\ \mathcal{L}_0(t,r)\chi^{lm}_{2(\mathrm{p})} + \mathcal{R}^i_{lmc\gamma}(h)\chi^{c\gamma}_{i(0)} + \bar{\mathcal{R}}^i_{lmc\gamma}(h^*)\chi^{c\gamma}_{i(0)} = 0.\end{aligned} \tag{3.10}$$

Once again we neglect the $\mathcal{O}([h_{\mu\nu}]^2)$ terms given the amplitude of the ringing fluctuation very small with respect to the background. Nevertheless, the remaining two gauge-invariant variables χ_3^{lm} and χ_4^{lm} also lead to similar equations, however, it will not be required to find out the solution directly, as we will see in the later sections. Now, using the properties of the nonhomogeneous

differential equation, we now simplify the above equations (3.9)(3.10), with the decomposition of the fields taken as, $\chi^{lm}_{1(\mathrm{p})} = \chi^{lm}_{1,\mathrm{p}} + \bar{\chi}^{lm}_{1,\mathrm{p}}$ and $\chi^{lm}_{2(\mathrm{p})} = \chi^{lm}_{2,\mathrm{p}} + \bar{\chi}^{lm}_{2,\mathrm{p}}$, such that,

$$\begin{aligned}\mathcal{L}_0(t,r)\chi^{lm}_{1,\mathrm{p}} + \mathcal{Q}^{i}_{lmc\gamma}(h)\chi^{c\gamma}_{i(0)} = 0\\ \mathcal{L}_0(t,r)\bar{\chi}^{lm}_{1,\mathrm{p}} + \bar{\mathcal{Q}}^{i}_{lmc\gamma}(h^*)\chi^{c\gamma}_{i(0)} = 0\end{aligned} \tag{3.11}$$

and

$$\begin{aligned}\mathcal{L}_0(t,r)\chi^{lm}_{2,\mathrm{p}} + \mathcal{R}^{i}_{lmc\gamma}(h)\chi^{c\gamma}_{i(0)} = 0\\ \mathcal{L}_0(t,r)\bar{\chi}^{lm}_{2,\mathrm{p}} + \bar{\mathcal{R}}^{i}_{lmc\gamma}(h^*)\chi^{c\gamma}_{i(0)} = 0.\end{aligned} \tag{3.12}$$

In the next section, we will discuss the procedure to solve these equations.

3.3 How the GW-QNMs manifest in the EM field

The above set of equations can be thought of as EM waves propagating in the static Schwarzchild ($g^s_{\mu\nu}$) background with oscillatory source term. Moreover, $\chi^{c\gamma}_{i(0)}(t,r)$ being the solution for static Schwarzschild BH, we can rewrite it as,

$$\chi^{c\gamma}_{i(0)}(t,r) = \int d\mathrm{k}\; e^{-\mathrm{i}\mathrm{k}t}\chi^{c\gamma}_{i(0)}(\mathrm{k},r) \tag{3.13}$$

with k representing the corresponding frequency. Now, recall that the time dependence of the ringing fluctuation (2.1) is dictated by $e^{-\mathrm{i}\omega t}$ so that, one will be able to extract it out of $(\mathcal{Q}_{lmc\gamma}, \mathcal{R}_{lmc\gamma})$ and $(\bar{\mathcal{Q}}_{lmc\gamma}, \mathcal{R}_{lmc\gamma})$. The preceding two arguments help us to express (3.11) and (3.12) as,

$$\begin{aligned}\mathcal{L}_0(t,r)\chi^{lm}_{1,\mathrm{p}} + \int d\mathrm{k}\; e^{-\mathrm{i}(\mathrm{k}+\omega)t}\mathcal{Q}^{i}_{lmc\gamma}(\mathrm{k},\omega)\chi^{c\gamma}_{i(0)}(\mathrm{k},r) = 0,\\ \mathcal{L}_0(t,r)\bar{\chi}^{lm}_{1,\mathrm{p}} + \int d\mathrm{k}\; e^{-\mathrm{i}(\mathrm{k}-\omega^*)t}\bar{\mathcal{Q}}^{i}_{lmc\gamma}(\mathrm{k},\omega^*)\chi^{c\gamma}_{i(0)}(\mathrm{k},r) = 0,\end{aligned} \tag{3.14}$$

and

$$\begin{aligned}\mathcal{L}_0(t,r)\chi^{lm}_{2,\mathrm{p}} + \int d\mathrm{k}\; e^{-\mathrm{i}(\mathrm{k}+\omega)t}\mathcal{R}^{i}_{lmc\gamma}(\mathrm{k},\omega)\chi^{c\gamma}_{i(0)}(\mathrm{k},r) = 0\\ \mathcal{L}_0(t,r)\bar{\chi}^{lm}_{2,\mathrm{p}} + \int d\mathrm{k}\; e^{-\mathrm{i}(\mathrm{k}-\omega^*)t}\bar{\mathcal{R}}^{i}_{lmc\gamma}(k,\omega^*)\chi^{c\gamma}_{i(0)}(\mathrm{k},r) = 0.\end{aligned} \tag{3.15}$$

We only consider the particular solution for the $\chi^{lm}_{1,\mathrm{p}}, \bar{\chi}^{lm}_{1,\mathrm{p}}$ and $\chi^{lm}_{2,\mathrm{p}}, \bar{\chi}^{lm}_{2,\mathrm{p}}$, hence, it is plausible to consider the following decomposition,

$$\chi^{lm}_{1,\mathrm{p}}(t,r) = \int d\mathrm{k}\; e^{-\mathrm{i}(\mathrm{k}+\omega)t}\chi^{lm}_{1,\mathrm{p}}(\mathrm{k},r) \tag{3.16}$$

and similar expressions for $\chi^{lm}_{2,\mathrm{p}}$ is understood. In the same fashion,

$$\bar{\chi}^{lm}_{1,\mathrm{p}}(t,r) = \int d\mathrm{k}\; e^{-\mathrm{i}(\mathrm{k}-\omega^*)t}\bar{\chi}^{lm}_{1,\mathrm{p}}(\mathrm{k},r) \tag{3.17}$$

and similar expressions for $\bar{\chi}^{lm}_{2,\mathrm{p}}$ is understood. Substituting these forms of the fields, we obtain from (3.14)(3.15),

$$\begin{aligned}\mathcal{L}_0(\mathrm{k},\omega,r)\chi^{lm}_{1,\mathrm{p}}(\mathrm{k},r) + \mathcal{Q}^{i}_{lmc\gamma}(\mathrm{k},\omega)\chi^{c\gamma}_{i(0)}(\mathrm{k},r) = 0,\\ \mathcal{L}_0(\mathrm{k},\omega^*,r)\bar{\chi}^{lm}_{1,\mathrm{p}}(\mathrm{k},r) + \bar{\mathcal{Q}}^{i}_{lmc\gamma}(\mathrm{k},\omega^*)\chi^{c\gamma}_{i(0)}(\mathrm{k},r) = 0,\end{aligned} \tag{3.18}$$

and

$$\begin{aligned}\mathcal{L}_0(\mathrm{k},\omega,r)\chi^{lm}_{2,\mathrm{p}}(\mathrm{k},r)+\mathcal{R}^{i}_{lmc\gamma}(\mathrm{k},\omega)\chi^{c\gamma}_{i(0)}(\mathrm{k},r)=0\\ \mathcal{L}_0(\mathrm{k},\omega^*,r)\bar{\chi}^{lm}_{2,\mathrm{p}}(\mathrm{k},r)+\bar{\mathcal{R}}^{i}_{lmc\gamma}(\mathrm{k},\omega^*)\chi^{c\gamma}_{i(0)}(\mathrm{k},r)=0.\end{aligned} \tag{3.19}$$

Where,

$$\mathcal{L}_0(\mathrm{k},\omega,r)=f(r)\partial_r(f(r)\partial_r)+(\mathrm{k}+\omega)^2-f(r)\frac{l(l+1)}{r^2}, \tag{3.20}$$

and

$$\mathcal{L}_0(\mathrm{k},\omega^*,r)=f(r)\partial_r(f(r)\partial_r)+(\mathrm{k}-\omega^*)^2-f(r)\frac{l(l+1)}{r^2}, \tag{3.21}$$

can be derived by acting $\mathcal{L}_0(t,r)$ on (3.17) and other components. Finally, we are left with (3.18)(3.19), which describe a nonhomogeneous differential equation with spatial variable, r. To solve these equations, we will mainly focus on the source contribution, i.e., the second term in each equation of (3.18) and (3.19). Following the property of a nonhomogenous differential equation, fixing the initial condition for $\chi^{lm}_{i(0)}$ would be sufficient, as the source term depends (along with the ringing metric components) on the zeroth order solution of the EM field. To find out the zeroth order solution of all the gauge invariant variables, $\chi^{lm}_{i(0)}(\mathrm{k},r)$ we solve $\chi^{lm}_{1(0)}(\mathrm{k},r)$ and $\chi^{lm}_{2(0)}(\mathrm{k},r)$ first, by setting the ingoing boundary condition near the horizon of the static BH, as, $\chi^{lm}_{1(0)}(\mathrm{k},r)|_{r\to 2M}=\zeta^{lm}_1 f(r)^{-2\mathrm{i}M\mathrm{k}}$ and $\chi^{lm}_{2(0)}(\mathrm{k},r)|_{r\to 2M}=\zeta^{lm}_2 f(r)^{-2\mathrm{i}M\mathrm{k}}$, with arbitrary constant ζ^{lm}_1 and ζ^{lm}_2. Although our final results do not depend on these overall constants, we have obtained stable solutions for a range of values, $(\zeta^{lm}_1,\zeta^{lm}_2)\sim 10^{-3}-1$. Once the solution of $\chi^{lm}_{1(0)}$ and $\chi^{lm}_{2(0)}$ are obtained, we find out the solution of the remaining gauge invariant variables, $\chi^{lm}_{3(0)}$ and $\chi^{lm}_{4(0)}$ using the following coupled equation,

$$\begin{aligned}f(r)\partial_r\chi^{lm}_{1(0)}+\chi^{lm}_{4(0)}=0,\\ \partial_t\chi^{lm}_{1(0)}+f(r)\chi^{lm}_{3(0)}=0,\end{aligned} \tag{3.22}$$

which are the governing equations (see appendix.B.5 for the derivation) of the electromagnetic field for static Schwarzschild BH space time. Once all the zeroth order solutions are obtained we substitute these solutions in the source terms of the nonhomogeneous eq. (3.11) and (3.12) and again solve these nonhomogeneous differential equations numerically using “StiffnessSwitching" method built in Mathematica.

3.4 Setting up the boundary condition

In the static Schwarzschild space time, asymptotic flatness helps us to normalize the field solution such that an incoming wave of unit amplitude from infinity gets scattered by the BH potential. Such normalization is used to define [34] the absorption cross section of a static BH. For our present case, however, the ringing BH background being oscillatory in nature does not have the same asymptotic structure. Further, due to quadrupole perturbation, spherical symmetry is also lost. Therefore, to compute the absorption cross section for such a case, we proposed a methodology in the previous chapter (2) for the scattering of the scalar field, we have outlined the important steps here. We introduce a hypothetical surface Fig.(2.1), in a very similar manner to the scalar case, at some radial distance $r=r_{\mathrm{int}}$ from the BH event horizon calling it an interaction

surface. The wave coming towards the black hole is assumed to perceive the presence of ringing BH once it hits the interaction surface. Outside the surface $r > r_{\rm int}$, the spacetime is assumed to be approximately static Schwarzschild BH, and this is the approximation which helps us to appropriately define the normalization of the incoming wave. We label the region inside the interaction surface as region-**I**, and outside as region-**II**. With this setup, the individual mode (corresponding to k) of the EM wave solution in region-**I** will assume,

$$\chi^{{\rm k}lm}_{j[\mathbf{I}]}(t,r) = e^{-{\rm i}{\rm k}t}\chi^{lm}_{j(0)}({\rm k},r) + e^{-{\rm i}({\rm k}+\omega)t}\chi^{lm}_{j,{\rm p}}({\rm k},r) + e^{-{\rm i}({\rm k}-\omega^*)t}\bar{\chi}^{lm}_{j,{\rm p}}({\rm k},r) \tag{3.23}$$

where, $j \equiv (1,2)$, i.e. the expansion of both $\chi^{{\rm k}lm}_{1[\mathbf{I}]}$ and $\chi^{{\rm k}lm}_{2[\mathbf{I}]}$ in the region-**I**. In the region-**II**, it would be in the background of static Schwarzschild BH, hence, the mode functions can be expressed as,

$$\chi^{lm}_{j[\mathbf{II}]}(t,r) = \chi^{lm}_{j,0}(t,r) \quad \text{with} \quad \mathcal{L}_0(t,r)\chi^{lm}_{j,0}(t,r) = 0. \tag{3.24}$$

We want to clarify that the notation used to denote the fields with subscript $\{j,0\}$ in the exterior of interaction surface in contrast to the same quantity with the subscription $\{j(0)\}/\{i(0)\}$ (see the discussion below (3.8)) which represents the solution for the static Schwarzchild BH without the prior fluctuation. The primary motivation for complicating the subscription of the variable, χ, rather than using different variables altogether is to convey the fact they represent the same physical quantity in various circumstances. Important to note that due to the interaction surface, the evolution of $\chi^{{\rm k}lm}_{j,0}$ in the exterior of the interaction surface will be different as compared to the situation of the usual static Schwarzschild background. Therefore, the interaction surface will naturally provide for the first two boundary conditions (3.25). However, the above second order partial differential equation involving two variables (t,r)(the field solution at the interaction surface may not be separable in space and time) requires four boundary conditions. Therefore, in region-**II**, the appropriate boundary condition would be as follows: we provide two spatial initial conditions at the interaction surface r_{int},

$$\begin{aligned}
\chi^{{\rm k}lm}_{j[\mathbf{II}]}(t,r)|_{\forall t, r\to r_{\rm int}} &= \chi^{{\rm k}lm}_{j[\mathbf{I}]}(t,r)|_{\forall t, r\to r_{\rm int}}, \\
\partial_r\chi^{{\rm k}lm}_{j[\mathbf{II}]}(t,r)|_{\forall t, r\to r_{\rm int}} &= \partial_r\chi^{{\rm k}lm}_{j[\mathbf{I}]}(t,r)|_{\forall t, r\to r_{\rm int}},
\end{aligned} \tag{3.25}$$

and the remaining two conditions for the time we provide as boundary conditions at $t\to\infty$ as,

$$\begin{aligned}
\chi^{{\rm k}lm}_{j[\mathbf{II}]}(t,r)|_{t\to\infty,\forall r} &= e^{-{\rm i}{\rm k}t}\chi^{{\rm k}lm}_{j(0)}(r)|_{t\to\infty,\forall r}, \\
\partial_t\chi^{{\rm k}lm}_{j[\mathbf{II}]}(t,r)|_{t\to\infty,\forall r} &= -{\rm i}{\rm k}e^{-{\rm i}{\rm k}t}\chi^{{\rm k}lm}_{j(0)}(r)|_{t\to\infty,\forall r}.
\end{aligned} \tag{3.26}$$

Where the last two boundary conditions arise due to the following reason: at a fixed distance from the black hole r, ringing oscillation amplitude decays exponentially with time due to its quasinormal nature. Therefore, in $t\to\infty$ limit, the perturbative components of the gauge field, $(\chi^{{\rm k}lm}_{({\rm p})}, \bar{\chi}^{{\rm k}lm}_{({\rm p})})$ which are the explicit function of $h_{\mu\nu}$ must also be vanishing at the interaction surface. Such a condition will naturally ensure the calculated absorption cross-section of ringing BH reducing to its static Schwarzschild value within the characteristic time scale of the oscillation $\tau \sim 2\pi/\omega$. By employing the boundary condition described in Eq.3.25, we proceed to solve Eq.3.24 in the domain, $([r_{\rm int},\infty],[t_{\rm int},\infty])$ lying inside light cone, $t \geq r_*$. For solving the partial differential equation, we have used the "PDEDiscretization" method built in Mathematica. Whereas the convergence criteria for the solutions have been taken care of by setting the Accuracy goal (AG) and Precision goal (PG), which ensure that the solution, $\chi^{{\rm k}lm}_{j,0}(t,r)$, is obtained as far as the

absolute error, Er $< 10^{-\mathrm{AG}} + |\chi^{klm}_{j,0}(t,r)| \times 10^{-\mathrm{PG}}$ [121] is maintained. We have checked by varying (AG,PG) from $(8,8)$ to $(12,12)$ that the results remain stable with the specified error tolerance.

The asymptotic nature of the GWs is better expressed in the outgoing null coordinates. Therefore, after obtaining the solution, we perform a transformation into the outgoing null coordinate system. $(t,r) \to (u = t - r_*, r)$ using $\tilde{A}_\mu(x') = (\partial x^\nu / \partial x'^\mu) A_\nu(x)$ [7] and define the absorption cross-section accordingly as described in the following section.

3.5 Defining Absorption Cross Section

We follow the definition of the absorption cross section as discussed in the previous chapter (2) for the scalar field. Of course, for an electromagnetic field, the evaluation will be more complicated as compared to the scalar case. Nevertheless, to evaluate the absorption cross section (2.25) we start with the total energy being absorbed by the ringing BH per unit time that can be expressed in terms of gauge invariant variables as,

$$\partial_u \mathcal{F}^{\mathrm{kl}} = l(l+1)\Big[\frac{1}{2}\Big\{\tilde{\chi}^{klm}_{3,0}(u,r)\tilde{\chi}^{klm^*}_{4,0}(u,r) + \tilde{\chi}^{klm}_{4,0}(u,r)\tilde{\chi}^{klm^*}_{3,0}(u,r) + \partial_r\tilde{\chi}^{klm}_{2,0}(u,r)\partial_u\tilde{\chi}^{klm^*}_{2,0}(u,r) + \partial_u\tilde{\chi}^{klm}_{2,0}(u,r)\partial_r\tilde{\chi}^{klm^*}_{2,0}(u,r)\Big\} - \Big\{\tilde{\chi}^{klm}_{4,0}(u,r)\tilde{\chi}^{klm^*}_{4,0}(u,r) + \partial_u\tilde{\chi}^{klm}_{2,0}(u,r)\partial_u\tilde{\chi}^{klm^*}_{2,0}(u,r)\Big\}\Big]. \tag{3.27}$$

Note that to define the absorption cross-section we used ingoing light-cone coordinate (u,r), in which all the field variables are expressed in "tilde" when transforming from $(t,r) \to (u,r)$ (see Appendix.B.6 for detailed derivation). Coming to the evaluation of the above expression, we find out the solution of $\tilde{\chi}^{klm}_{1,0}(u,r)$ and $\tilde{\chi}^{klm}_{2,0}(u,r)$ by transforming the solution obtained in (t,r) (3.24), whereas for the solution of the remaining gauge invariant variables, we use the following coupled equation,

$$\begin{aligned} \tilde{\chi}^{lm}_{3,0}(u,r) &= -\partial_r\tilde{\chi}^{lm}_{1,0}(u,r) \\ \tilde{\chi}^{lm}_{4,0}(u,r) &= \partial_u\tilde{\chi}^{lm}_{1,0}(u,r) + \tilde{\chi}^{lm}_{3,0}(u,r), \end{aligned} \tag{3.28}$$

which are the governing equations (see appendix.B.6 for the derivation) of the electromagnetic field for static Schwarzschild BH space time in (u,r) coordinate. The procedure outlined above supports our earlier assertion that there's no need to directly solve all the gauge invariant variables. This justifies our previous claim about obtaining the energy flux in terms of the two gauge invariant variables, $\chi^{lm}_{1,0}(u,r)$ and $\chi^{lm}_{2,0}(u,r)$. Now, the incident energy density per unit time for a plane EM wave propagating in the z-direction is constructed as before (2.25),

$$\partial_u \mathcal{G}^{\mathrm{k}} = \mathcal{T}^{z}{}_{u}. \tag{3.29}$$

Having evaluated the solution of the EM wave in spherical coordinates with a damped oscillating time dependent feature we find it convenient to recast the expression for incident energy density in the spherical coordinates as (one may look at (B.36) and (B.38)),

$$\partial_u \mathcal{G}^{\mathrm{k}} = \Big\{\frac{1}{2} g_0^{ss}(u,r)(\partial_u A_s - \partial_s A_u)(\partial_r A^*_s - \partial_s A^*_r) + c.c.\Big\} - g_0^{ss}(u,r)(\partial_u A_s - \partial_s A_u)(\partial_u A^*_s - \partial_s A^*_u). \tag{3.30}$$

Once again "s" represents coordinates, (θ,ϕ), as before. Also, notice that all the raising and lowering of indices have been done with respect to $g_0^{\mu\nu}(u,r)$ (2.21), keeping in mind that the

incident energy density should be evaluated at a considerable distance from the interaction surface, i.e. in the exterior region where spacetime is characterized as Schwarzschild. With the help of (3.3) and (3.5) one can express (of course, one has to take care of the coordinate transformation from (t, r) to (u, r)) the field combinations of (3.30) in terms of the invariant variables as,

$$\begin{aligned}\partial_u A_s - \partial_s A_u &= \sum_{lm}\left[\left(\partial_r \tilde{\chi}^{klm}_{1,0} - \partial_u \tilde{\chi}^{klm}_{1,0}\right)\Psi^{lm}_s(\Omega) + \partial_u \tilde{\chi}^{klm}_{2,0}\Phi^{lm}_s(\Omega)\right],\\ \partial_r A_s - \partial_s A_r &= \sum_{lm}\left[\partial_r \tilde{\chi}^{klm}_{1,0}\Psi_s + \partial_r \tilde{\chi}^{klm}_{2,0}\Phi_s\right].\end{aligned} \tag{3.31}$$

The remaining task is to figure out the incident part of EM wave, $\tilde{\chi}^{klm}_{1,0}$ and $\tilde{\chi}^{klm}_{2,0}$ that can be obtained by assuming an approximate asymptotic form,

$$\begin{aligned}\tilde{\chi}^{klm}_{1,0}(u, r) &= \mathcal{N}^{klm}_1[\mathcal{I}_1(u)e^{-\mathrm{ik}(u+2r_*)} + \mathcal{R}_1(u)e^{-\mathrm{ik}u}],\\ \tilde{\chi}^{klm}_{2,0}(u, r) &= \mathcal{N}^{klm}_2[\mathcal{I}_2(u)e^{-\mathrm{ik}(u+2r_*)} + \mathcal{R}_2(u)e^{-\mathrm{ik}u}],\end{aligned} \tag{3.32}$$

where the coefficients, $(\mathcal{I}_1(u), \mathcal{R}_1(u))$ and $(\mathcal{I}_2(u), \mathcal{R}_2(u))$ are related to ingoing (incident) and outgoing (reflected) wave amplitude of $\tilde{\chi}^{lm}_{1,0}(u, r)$ and $\tilde{\chi}^{lm}_{2,0}(u, r)$ respectively. We evaluate these amplitudes numerically from the solutions of $\tilde{\chi}^{lm}_{1,0}(u, r)$ and $\tilde{\chi}^{lm}_{2,0}(u, r)$. Now comparing the above two expressions with the same quantities constructed (see Appendix.B.4) for circularly polarized incident plane EM wave we derive the normalization factors as [124],

$$\begin{aligned}\mathcal{N}^{klm}_1 &= -\mathrm{i}(-1)^{l+1}\delta_{m1}\sqrt{\frac{4\pi(2l+1)}{l(l+1)}}\frac{1}{2\mathrm{k}\mathcal{I}_1(u\to\infty)},\\ \mathcal{N}^{klm}_2 &= (-1)^{l}\delta_{m1}\sqrt{\frac{4\pi(2l+1)}{l(l+1)}}\frac{1}{2\mathrm{k}\mathcal{I}_2(u\to\infty)}.\end{aligned} \tag{3.33}$$

Where δ_{m1} appears due to the fact that the EM field potentials, $A_\mu(x)$, transforms as a vector, and that shows up in the spherical wave expansion of the incident circularly plane polarized EM wave (see details in the appendix B.4) coming from z-direction, with azimuthal index $m = 1$ [122, 124] similar to that of scalar field analysis where δ_{m0} appears due its spin zero property[35]. We also normalize the combinations of (3.31) by dividing the right hand side with $\sum_{lm}(-1)^{l+1}\delta_{m1}\sqrt{\frac{4\pi(2l+1)}{l(l+1)}}[\Phi^{lm}_s(\Omega) + \mathrm{i}\Psi^{lm}_s(\Omega)]$, consequently the gauge invariant combinations finally become,

$$\begin{aligned}\partial_u A_s - \partial_s A_u &= \xi_{us}(\mathrm{k}, u)(-\mathrm{ik}A'_s(u, \mathbf{r})),\\ \partial_r A_s - \partial_s A_r &= \xi_{rs}(\mathrm{k}, u)(-2\mathrm{ik}A'_s(u, \mathbf{r})),\end{aligned} \tag{3.34}$$

with the nontrivial time dependent coefficients, $\xi_{us}(\mathrm{k}, u), \xi_{rs}(\mathrm{k}, u)$ with the property that they become unity as the static limit, $u \to \infty$, of the ringing BH is approached (for details one may look at Appendix.B.4). Importantly, the sum in (3.31)with normalization factors exhibits a convergent nature for increasing l having alternative $+/-$ sign in the summation, therefore, we have taken up to $l = 6$ for our numerical analysis. Whereas, $A'_s(u, \mathbf{r})$, denotes the spherical polar expansion [122] of the incident circularly polarized EM wave, which can be suitably factored out from the expression of the incident energy density. Now, we have all the tools required to evaluate the absorption cross section (2.25) for the EM field and we have provided our numerical findings in the next section.

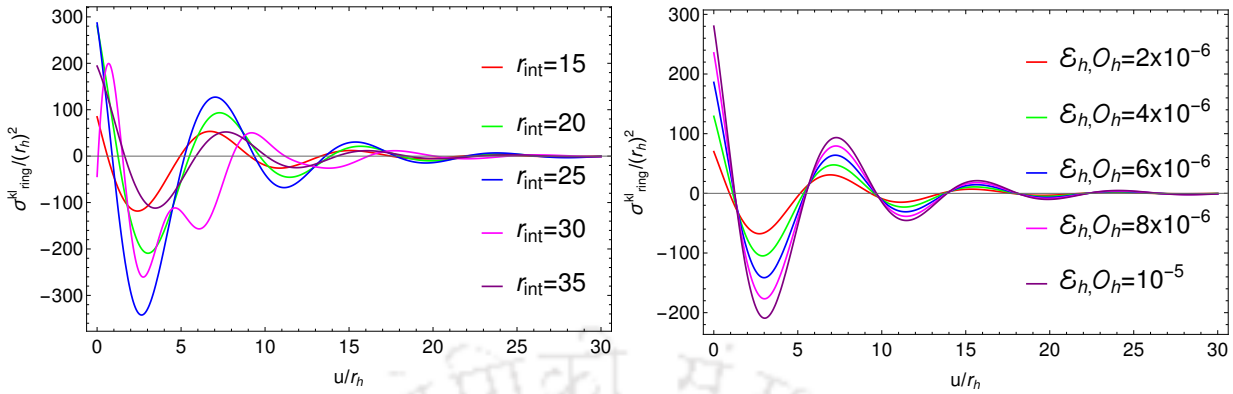

FIGURE 3.1: On the left panel absorption cross section of the ringing BH for the EM field has been plotted with time, u, for various interaction surfaces, r_{int}, considering frequency, $\mathrm{k} = 0.1 r_h^{-1}$ and $l = 1$. On the right panel, we have plotted the same by varying the background amplitude, $\mathcal{E}_h, \mathcal{O}_h$, considering frequency, $\mathrm{k} = 0.1 r_h^{-1}$ and $l = 1$ at a particular interaction surface $r_{int} = 20 r_h$. All the parameters written inside the plots are in units of r_h.

3.6 Numerical Results

As previously mentioned, the ringing BH background is constructed taking only the quadrupole oscillation [10] or the lowest $l(=2)$ mode with the corresponding quasinormal frequency $\omega = (0.74734 - \mathrm{i}\ 0.17792)(r_h)^{-1}$ [16, 18]. $r_h = 2M$ is the horizon radius for the Schwarzschild BH. The chosen frequency is known to be the long-lived one among all the other modes. Further, the frequency for both even and odd parity perturbation was found to be the same as per the existing literature [15, 16, 18]. All physical quantities and associated parameters have been made dimensionless utilizing the characteristic scale, r_h. We consider the solution of the background ringing field for which the perturbative scheme is valid ensuring $\delta g/g_0 \propto h^{\mu}_{\mu} \ll 1$ for a diverse range of initial parameters. Once the solution for the ringing black hole background is obtained, we solve for the EM field Eq.3.24. Unless stated throughout our presentation we have shown the results for a fixed background amplitude, $\mathcal{E}_h, \mathcal{O}_h \sim 10^{-5}$ within the perturbative limit. As mentioned earlier, as a consistency check we also reproduce the well studied static limit of the absorption cross-section [124] of Schwarzschild BH for EM field in the limit, $\lim_{u\to\infty} \sigma^{kl}_{\mathrm{ring}}(u, r_{\mathrm{int}}) = \sigma^0(\mathrm{k}, l)$.

We evaluate the absorption cross section at $r \sim 75 r_h$ and further numerically ensure that all the necessary results remain intact even afterwards, apart from very small fluctuations induced by numerical precisions due to the extension of the domain of the solutions. Our final results are summarized in Fig.3.1 and 3.2.

According to our construction, time dependent boundary conditions at the interaction surface would introduce time varying features in the absorption cross section. Such transient nature of the GWs is clearly seen to be imprinted in the behaviour of EM absorption cross section and exhibits the quasi-periodic oscillation along with its characteristic time scale. One can indeed observe that within the GW time scale $\tau_{\mathrm{GW}} \sim 35 r_h$ associated with the quasinormal frequency $\omega = (0.74734 - \mathrm{i}\ 0.17792)(r_h)^{-1}$, the EM absorption cross section $\sigma^{kl}(u, r_{\mathrm{int}})$ undergoes a time dependent oscillation, which can assume large negative values, and this negative amplitude of the

absorption corss-section precisely signifies the phenomena of superradiant scattering.

We identify five main theory parameters of our interest $(\mathrm{k}, l, r_{\mathrm{int}})$ and the GW amplitudes $(\mathcal{E}_h, \mathcal{O}_h)$ (1.2.1). However, for all our practical purposes we choose both the GW amplitudes to be the same. With decreasing GW amplitude the EM superradiant amplitude is expected to decrease which we have consistently observed in our numerical results, and indeed be seen in the second panel of the Fig. 3.1. This also provides us confidence as a consistency check of our numerical methodology.

Interaction surface: We provide the plots choosing the interaction surface located at $r_{\mathrm{int}} \sim 20 r_h$. Interestingly, the superradiant amplitude turned out to be maximum at $r_{\mathrm{int}} \sim 20 - 25 r_h$ for all angular modes, l and frequency, k that we have considered. For example $\sigma \sim -354 r_h^2$ is the maximum value for $l = 1$ at frequency $\mathrm{k} \sim 0.1 r_h^{-1}$ and $r_{\mathrm{int}} \sim 25 r_h$. As it turns out the final results are significantly dependent on r_{int}. Moreover, the matter field, being coupled with the ringing black hole background, interaction with space-time should be taken throughout the region from the horizon to the spatial infinity. This fact points out that the value of r_{int} is not a choice. Hence, the robust approach would be to integrate out the r_{int}, accounting for the aggregated effect. With our present numerical methodology, we find it difficult to perform this numerical integration. However, the characteristics exhibited by the absorption cross section at r_{int} corresponding to the maximum enhancement bear the features of the aggregated result. This is exactly the reason for demonstrating our results for the r_{int} corresponding to the maximum enhancement. Moreover, the time profile of the absorption cross section for different r_{int} suggests that the aggregated effect may not vanish.

In the perturbative framework, the scatter solution of a particular order depends on the GW background and lower order EM solution as the source. Particularly when the maximum amplitude of the lower order EM solution appears away from the BH, GW amplitude is always maximum near the horizon. The resultant of those two contributing factors effectively decides the location of the interaction surface for which superradiant amplitude is maximized. This is reminiscent of much studied [48, 125] superradiance from rotating BHs whose effective potential maximizes itself a little away from the event horizon.

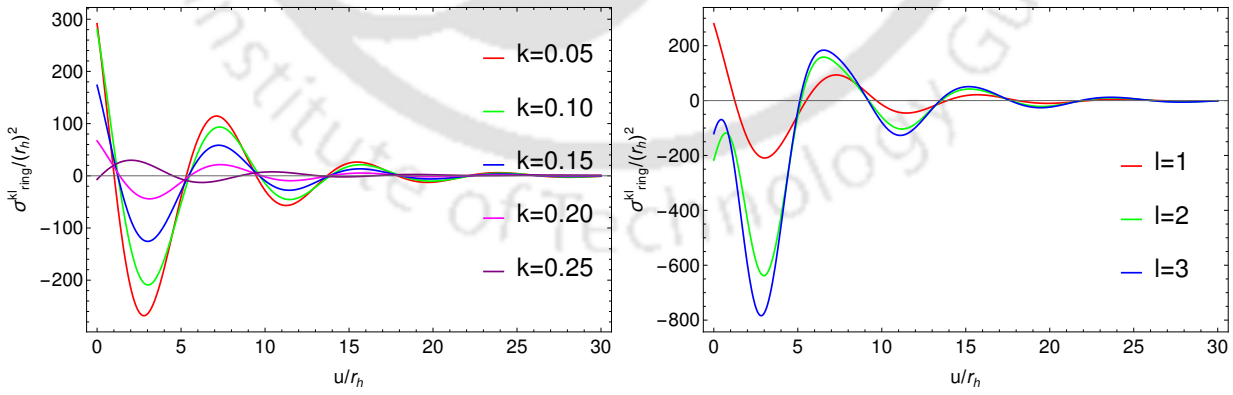

FIGURE 3.2: On the left panel absorption cross section of the ringing black hole for the EM field has been plotted with time, u, by varying the frequency, k, of the EM field considering $l = 1$. On the right panel, we have plotted the same various angular modes, l, of the EM field considering $\mathrm{k} = 0.1 r_h^{-1}$. All the parameters written inside the plots are in units of r_h.

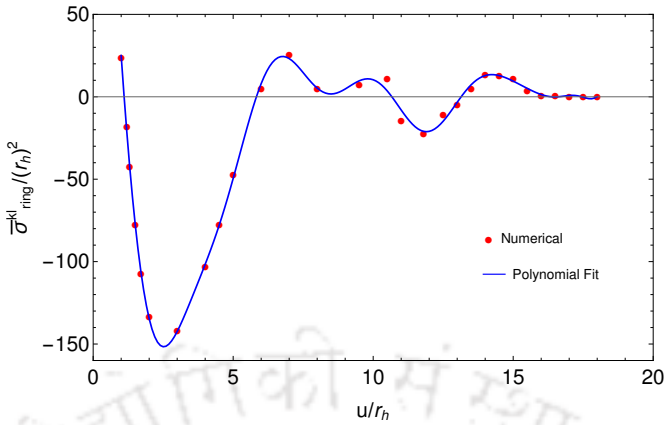

FIGURE 3.3: Mean absorption cross section has been plotted with time by averaging over the position of the interaction surface, $r_{\rm int}$ for a fixed frequency, $\mathrm{k} = 0.1 r_h^{-1}$ and $l = 1$.

In Fig.3.2 we have shown the behaviour of the superradiant absorption cross section with different frequencies. Like the usual case of static charged or rotating BHs [126], a ringing BH also exhibits superradiance at low frequency with distinct time varying features induced by the GWs. We have obtained the expected cut-off frequency beyond which the superradiance ceases to exist for different angular momentum (l). For example, we obtain $\mathrm{k}_{\rm max} = 0.28 r_h^{-1}$ for $l = 1$ above which superradiance vanishes, and similarly for $l = 2, \mathrm{k}_{\rm max} \sim 0.55 r_h^{-1}$, and $l = 3, \mathrm{k}_{\rm max} \sim 0.8 r_h^{-1}$. A non-trivial point to note is that for the higher angular momentum mode the cut-off frequency $\mathrm{k}_{\rm max}$ increases contrary to the usual expectation as exciting higher frequency mode would be difficult. For example, only long wavelength modes are amplified in the usual superradiance phenomena from black hole [124, 126–128]. For the ringing case, however, the reason could be due to complicated mode coupling and their competition in the source terms (see details in the Appendix.B.3). Our result seems to suggest that the perturbative scheme may not be valid above certain angular modes which could be further inferred from the increasing superradiant amplitude for higher angular mode l shown in Fig.3.2. However, this is not a unique feature to the ringing case, for the moving BH system similar behaviour in the absorption cross-section has been observed shown in [35]. Nonetheless, further details need to be investigated to decode such behaviour, and that is beyond the scope of our present study.

3.7 Mean absorption cross section and Energy extraction at spatial infinity

Following the analysis performed for the scalar field in Sec.2.6 to compute the mean absorption cross section, we have also evaluated the same quantity for the EM field. The mean absorption cross section presented in Fig.3.3, is independent of $r_{\rm int}$, moreover, it shares very much the same feature as given in Fig.3.1 and Fig.3.2. This average quantity will be the actual physical outcome, as observed by an asymptotic observer. As found in the scalar case, the black hole in the ringdown phase, therefore, also exhibits the superradiance effect for the EM field.

Energy Extraction: In a similar fashion to the scalar field fractional energy gain can be quantified for the EM field (see [123]), by looking at the numerator in the definition (2.4), expanding which in terms of the EM fields, we obtain,

$$\begin{aligned}\int r^2 d\Omega \mathcal{T}^r{}_u &\sim \Big[\left|\mathcal{N}_1^{klm}\right|^2 \left(|\mathcal{I}_1(u)|^2 - |\mathcal{R}_1(u)|^2\right) + \left|\mathcal{N}_2^{klm}\right|^2 \left(|\mathcal{I}_2(u)|^2 - |\mathcal{R}_2(u)|^2\right) \Big], \\ &\sim (\partial_u E_{\rm in}^{tot} - \partial_u E_{\rm out}^{tot}),\end{aligned} \tag{3.35}$$

where, $E_{\rm in}$ and $E_{\rm out}$ represent respectively the total ingoing and outgoing energy flux. Note that there will be additional terms in the first line of the above equation, however, their contribution turns out to be negligibly small as discussed for the scalar field. Nevertheless, the negative values of the absorption cross section thus imply, $\partial_u E_{\rm in}^{tot} < \partial_u E_{\rm out}^{tot}$, which happens in certain time intervals as shown in Fig.3.1,3.2 and Fig.3.3. In these durations, the electromagnetic field will extract energy from the ringing BH. Of course, the positive part of the absorption cross section, presented in Fig.3.1,3.2 and Fig.3.3 suggest that there will be the absorption of radiation in some intervals. However, the superradiance will happen in the rest of the intervals within the decay time scale of the ringdown phase. An observer sitting at spatial infinity will receive this amplified radiation as a repeated flash, which eventually decays, exhibiting the transient nature of the ringing phase of the BH.

3.8 Observability

The evaluated flux of EM waves with enhanced amplitude could be detected in low frequency ground-based observatories. From our analysis, the cutoff frequency for the occurrence of superradiance turned out to be, $\omega \sim 10^5 k_{\rm max}\,(M_\odot/M)\,$Hz, where, $M_\odot$ is the solar mass and M is the BH mass under consideration. Whereas, $\mathrm{k_{max}}$ is the dimensionless cutoff frequency discussed before. As an example for a solar mass BH, with EM field parameters $l = 1$, $\mathrm{k_{max}} = 0.28$, we obtain $\omega \sim 10^4$Hz in the very low radio frequency range below which we would expect to observe the superradiant scattering.

The Existing ground-based observatories such as LOFAR (Low Frequency Array), are sensitive to the EM wave within the frequency band, $10 - 240$MHz, or wavelength $\sim 30 - 1.2m$ [129, 130]. Converting this experimental range of frequency in our present context, we obtain the required BH mass range would be within $M \sim 10^{-2} - 10^{-1} M_\odot$, from which superradiant scattering of EM field could be relevant for detection. However, the smallest compact object in the binary coalescence found by LIGO, VIRGO [28] is $M \sim 2.6 M_\odot$, which falls in the mass gap region of a neutron star and very light black hole. Further, for the astrophysical BHs, the lower limit of mass is set by Chandrasekhar limit $M \sim 1.4 M_\odot$ [131, 132]. Therefore, to be able to observe any superradiant scattering of the EM field, the required mass of the BHs should not be of astrophysical origin. The interesting way out appears to be primordial BHs (PBHs) which have garnered a lot of interest in the recent past, particularly in cosmology [133, 134]. At this point, we should mention there are some interesting studies already [135–137] on superradiance from PBHs.

PBHs are assumed to form due to gravitational collapse during the usual cosmological evolution if the density perturbation is very large in some spatial region (details of the formation mechanism can be found in [138–141] and for observational perspective [142, 143]). If the universe is radiation-dominated, and density perturbation satisfies the appropriate condition, the PBH formation mass

Observatory	Frequency range	Precision time
LOFAR	$10-240$MHz	$\sim 0.1ns$
GMRT	50MHz $-$ 1.5GHz	$\sim 81\mu s$
VLA	74MHz - 50GHz	$\sim 5ms$
BH mass range	Superradiant frequency	$\sigma^{kl}_{\rm ring}$ time scale (τ)
$0.1M_\odot - 0.01M_\odot$	1MHz $-$ 10MHz	$20\mu s - 2\mu s$

Table 3.1: The frequency and precision-time-scale of existing observatories along with the same quantities corresponding to EM absorption cross-section for a particular range of detectable BH mass range

can be estimated from [141]

$$M \sim M_{\rm pl}^2 H^{-1} \tag{3.36}$$

where the Hubble radius $H = \sqrt{\rho_r/3M_{\rm pl}^2}$, $M_{\rm pl}$ is the reduced Planck mass. Whereas, radiation energy density $\rho_r = (\pi^2 g_*/30)T^4$. T is the radiation temperature and g_* is the effective number of relativistic degrees of freedom. Utilizing these expressions we can estimate the early universe temperature when a BH of particular mass is formed, $T^2 \sim M_{\rm pl}^3\sqrt{90/(\pi^2 g_*)}/M$. For example the BH of mass $M \sim 10^{-2}M_\odot$ at present is formed when the temperature of the universe was $T \sim 128$ GeV. If we have a large number of such PBHs formed in the early epoch of the universe, their merger can go through the ringing phase leading to superradiant amplification within the detectable range of frequency as mentioned. Moreover, it can be shown that if the PBHs mass $M \lesssim 10^{15}$ gram, those will evaporate by now given the age of the universe $\sim 10^9 yr$ [43, 144, 145]. Therefore, in principle, one can extend the mass range of the PBH within $10^{-1}M_\odot > M > 10^{-18}M_\odot$, that can survive till now and merge. Depending upon their merger rate and distribution, they can in principle lead to superradiant scattering within a wide observable frequency range 10^6 Hz $< \omega < 10^{22}$ Hz. However, it is important to note that cross-section being $\sigma \propto r_h^2 \propto M^2$, lowering the mass naturally reduces the superradiant signal strength. Therefore, BH mass within the range $M \sim 10^{-1}M_\odot - 10^{-2}M_\odot$ could be of importance from the observational point of view. Several ground-based radio observatories are fully operational to explore EM signals, such as the Giant Metrewave Radio Telescope (GMRT) with frequency range, $\omega \gtrsim 50$MHz [146–148], Square Kilometer Array (SKA)[149], and Very Large Array (VLA) [150] other than LOFAR (already mentioned). Moreover, the latest addition, LOTAAS (LOFAR Tied-Array All-Sky Survey)[151–154] is capable of receiving signals throughout the northern hemisphere.

To this end, we must point out the time scale of the evolving superradiant amplitude $\tau \sim 200(M/M_\odot)\mu s$ which is of the order of GW oscillation time scale. Therefore, to measure such a signal the sensitivity in the time measurement is extremely important, and in this range with,

$M \sim 10^{-2} M_\odot$, implying $\tau \sim 2\mu s$, only LOFAR with precision ~ 0.1 ns [130], could detect those. To put the above estimates in perspective, in the Table.3.1 we provide the frequency range and precision-time-scale of the existing observatories along with the frequency ranges corresponding to superradiant absorption cross-section and its oscillation time scale, (τ) for a range of BH mass. Our findings may open up an enormous opportunity to explore the prospect of direct detection of the superradiance phenomena, and a new way of observing the PBHs of cosmological origin.

3.9 Summary And Discussion

To summarize, we have achieved superradiant scattering for the EM field during the ringing phase of the black hole. Unlike the static case, GW-induced superradiance phenomena are transient in nature and the time scale is directly proportional to the GW oscillation time scale. We have interpreted the negative values of the absorption cross section during the course of its fast evolution as superradiant scattering. *Our analysis reveals that superradiance phenomena arise not only in the presence of rotating horizon [49], EM wave scattered through the ringing fluctuation of BH can also undergo superradiant enhancement.* Detecting the BH superradiance itself is difficult because of its extremely weak signal. GW induced time varying superradiance signal, in principle, should be easier to detect than the static one. For such a case, though, the challenge arises due to its very short time scale of oscillation. We further would like to point out that BH-BH or BH-Neutron star mergers detected by LIGO, Virgo and KAGRA [1, 19–32] should have produced such transient superradiant EM signals. However, due to their mass $> M_\odot$ the wavelength of the signal they produced is very large of $\gtrsim 10$ km, and observing such EM waves is far from any present day experimental limit. This immediately suggests us to look for the BH mass which should be very low $M < M_\odot$ and consequently they can produce a detectable superradiant signal in the radio or higher frequency range. Interestingly those mass ranges should be of primordial origin that has gained widespread interest in the recent past as an alternative to dark matter candidate. We found within the existing experimental setup LOFAR may have the potential to detect such a radio signal within its existing sensitivity limit.

To this end, we must reiterate the significance of our outcome which is its complementary nature as a potential observable signature of the ringdown phase of BHs. Along with our previous findings for the scalar field (2), the effect on the EM field analyzed in the present chapter establishes a generic feature of the ringing BHs of having the superradiant scattering of any fundamental field. Although, fermions have been shown not to exhibit superradiant enhancement [48, 155] in case of a rotating BH, existing studies point out that certain BHs, such as extremal BH [156] or in case of charged AdS BH [156, 157], it may be possible for the fermions to develop superradiant instability. In our future publication, we would like to take up these issues along with their direct detection prospects.

Photon production from oscillating bubble in fluid: Sonoluminescence 4

"...Let there be sound, and there was sound
Let there be light, and there was light..."

AC/DC, Let There Be Rock

4.1 Introduction

The fascinating phenomena of Sonoluminescence due to a quasi-periodically oscillating air bubble reveal another aspect of the dissipative systems, albeit in a fluid medium. Instead of amplifying fluctuations, this light-emitting event can be viewed as an energy conversion process, wherein energy carried by the sound wave trapped within the bubble transforms into light. However, the exact mechanism leading to the light emission in Sonoluminescence remains debatable, as we have discussed in the Introduction chapter of the thesis. There are broadly two lines of approaches in the existing proposals, classical models based on shockwave Bremsstrahlung process (1.3.3) and quantum mechanical models based on dynamical Casimir effect (1.3.4). In our proposal, we will be particularly following the quantum mechanical production. In this framework of quantum field theory where fields, such as photons, are excited from the quantum vacuum due to time dependent background.

Important to note that in all the stated (1.3.4) quantum mechanical formulations, typical photon energy flux turned out to be divergent in wave number. Hence adhoc cut-off has been introduced to account for the produced power spectrum. In our framework, we indeed show that this divergent contribution can be easily accounted for in the perturbatve QFT framework which generically comes as k^2 divergence, and has been interpreted as the produced flux, as has been argued by Milton [87, 88]. We also argue that it is the non-perturbative parametric resonance which may be an appropriate mechanism that can explain the sonoluminescence.

We utilize the well known analog spacetime formalism [90] taking into account the actual temporal evolution of the bubble surface by solving the well known Rayleigh-Plesset (RP)[4, 62, 63] equation. We couple the Ricci scalar curvature, $\mathcal{R}$, of the analog geometry with an EM field preserving Lorentz symmetry following the idea that has been widely used in cosmology. This scalar curvature acts as a conformal breaking factor leading to the production of photons, which is otherwise absent in conformal space time [82].

Though we do not claim to explain sonoluminescence in the observed frequency range [59, 61], present theoretical results, however, seem to suggest that our framework for quantum mechanical particle production in time dependent analog spacetime may well be an interesting avenue to explore. Due to our present numerical limitation, we could not reach the actual frequency range of observation. However, we certainly obtained the photon spectrum in the lower frequency with reasonable magnitude which could be extrapolated to match the observation.

4.2 General formalism

Simply keeping the Lorentz invariance intact, generically, one can couple the EM field to the background space time in the linear order in curvature as shown below [158, 159],

$$\mathcal{L} = -\frac{\sqrt{-g}}{4}\Big[F_{\mu\nu}F^{\mu\nu} + \chi^{\mu\nu\alpha\beta}(q_1 F_{\mu\nu}F_{\alpha\beta} + q_2 F_{\mu\nu}\tilde{F}_{\alpha\beta})\Big], \tag{4.1}$$

with

$$\chi^{\mu\nu\alpha\beta} = \alpha_1\mathcal{R}(g^{\mu\alpha}g^{\nu\beta} - g^{\mu\beta}g^{\nu\alpha}) + \alpha_2(R^{\mu\alpha}g^{\nu\beta} - R^{\mu\beta}g^{\nu\alpha} + R^{\nu\beta}g^{\mu\alpha} - R^{\nu\alpha}g^{\mu\beta}) + \alpha_3 R^{\mu\nu\alpha\beta}, \tag{4.2}$$

where $F_{\mu\nu}$ is the field strength tensor of the EM field and $\tilde{F}^{\mu\nu} = \epsilon^{\mu\nu\alpha\beta}F_{\alpha\beta}/2$ is the dual tensor. Whereas, (q_1, q_2) and $(\alpha_1, \alpha_2, \alpha_3)$ are arbitrary constants need to be fixed. Here, $\mathcal{R}, R^{\mu\nu}$ and $R^{\mu\nu\alpha\beta}$ represent the Ricci scalar, Ricci tensor and Riemann tensor of the background metric (1.120) respectively. Now the metric (1.120) can be recast into a conformally flat form as,

$$ds^2 = p(\tau)^{\frac{1}{3}}(-d\tau^2 + dx^2 + dy^2 + dz^2), \tag{4.3}$$

with conformal time $d\tau = dt\sqrt{f/p^{1/3}}$. Keeping the symmetry intact, we have used Cartesian coordinate to describe the spatial part of the metric to simplify the analysis. Throughout our analysis, we will work assuming the parameter, $\xi = 0.2R_{\rm eq}$, where $R_{\rm eq} = 4.5\mu m$ is the ambient radius of the bubble (1.3.1), such that $\xi/R(t) < 1$, which compels us to consider $\tau \simeq t$, i.e. conformal time approximated as real time. Important to note that having this conformally flat metric, the first term in the given Lagrangian does not lead to any real particle production as the minimally coupled action of the EM field in this space time is conformally invariant [160, 161]. The rest of the terms in the Lagrangian represent non-minimal coupling and lead to particle production. Furthermore, the coupling with the dual tensor $(F\tilde{F})$ signifies a parity breaking term that leads to the production of the helical EM field (one may look at [162–165], where such considerations are often studied in the context of magnetogenesis in early universe cosmology). We do not consider such terms leading to non zero helicity which may interesting in the context of observation, and we will consider this in our future course of study. Therefore we will put $q_2 = 0$ for the present work. The coupling with Reimann tensor and Ricci tensor, however, is equally

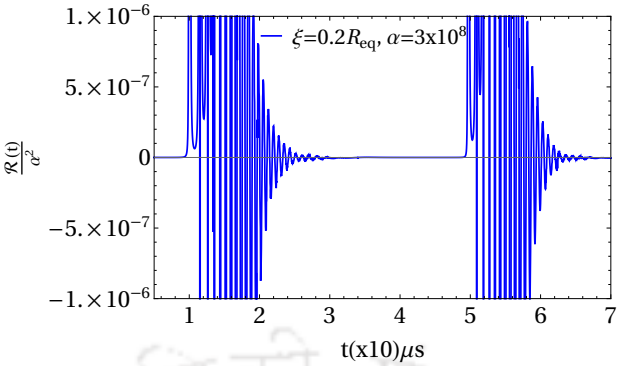

FIGURE 4.1: Evolution of the curvature scalar of the analog metric, with time

important as the Ricci coupling with the FF. For the simplification of the numerical computation, we restrict ourselves to the Ricci coupling only, for the present analysis, keeping $\alpha_2 = \alpha_3 = 0$ (otherwise, the equation of motion of the EM field will involve 4 non-zero components of the Ricci tensor and 12 non-zero components of the Riemann tensor for the metric under consideration). The analysis with consideration of these other couplings, we leave for our future work.

4.2.1 Quantization of the EM field

We consider the following Lagrangian for the Maxwell field with conformal symmetry breaking coupling,

$$\mathcal{L} = -\frac{\sqrt{-g}}{4}\left[F_{\mu\nu}F^{\mu\nu} + \frac{\mathcal{R}(t)}{\alpha^2}F_{\mu\nu}F^{\mu\nu}\right], \tag{4.4}$$

where $\alpha^2 \equiv 1/(\alpha_1 q_1)$ from (4.1). The Ricci scalar of the background metric turns out to be,

$$\mathcal{R}(t) \simeq -3\frac{\xi^3}{R^3}\left[\frac{\partial_t^2 R}{R} - 4\left(\frac{\partial_t R}{R}\right)^2\right], \tag{4.5}$$

which captures the oscillating features of the bubble, as can be seen from Fig.(4.1). α is a controlling parameter of mass dimension unity. We ignore all the higher order ξ^n, $n > 3$ coupling. We symbolize the conformal breaking coupling factor as $\mathcal{I}(t) = 1 + \mathcal{R}(t)/\alpha^2$. Throughout our analysis, we fix $\alpha = 3 \times 10^8$ in the unit of Ricci scalar, $\mathcal{R}$, such that $|\mathcal{I}(t) - 1| < 1$. We should also mention that breaking the conformal invariance, considering such a coupling prescription is not totally new, as one may find in [162–165], and the formulations of non-perturbative production in curved space time are also well studied [99]. However, to the best of our knowledge, we have not found any work where such analyses have been performed in the context of analog systems.

With this setup, one obtains the equation of motion from the Lagrangian (4.4),

$$\partial_\mu\left(\sqrt{-g}g^{\mu\alpha}g^{\nu\beta}\mathcal{I}(t)F_{\alpha\beta}\right) = 0. \tag{4.6}$$

The spatial part of the metric being flat (4.3), we can suitably choose the Coulomb gauge condition,

$$A_t = 0, \quad \boldsymbol{\nabla}\cdot\mathbf{A} = 0. \tag{4.7}$$

Only with time-dependent coupling, we can expand the vector potential in Fourier mode in the following manner,

$$A_i(t,\bar{x}) = \int \frac{d^3k}{(2\pi)^3}[c_{\bar{k}}A_i(t,k)e^{i\bar{k}\cdot\bar{x}} + c^*_{\bar{k}}A^*_i(t,k)e^{-i\bar{k}\cdot\bar{x}}], \tag{4.8}$$

where $c_{\bar{k}}$, and $c^*_{\bar{k}}$ are some arbitrary constants for the time being. Substituting the above mode expansion of the EM field in (4.6) we arrive at,

$$\partial_t^2 A_i(t,k) + \frac{\partial_t\mathcal{I}(t)}{\mathcal{I}(t)}\partial_t A_i(t,k) + |\mathbf{k}|^2 A_i(t,k) = 0, \tag{4.9}$$

where we have used $g^{nl}\partial_n A_l = 0$, i.e. the gauge condition and $k^2 = |\bar{k}|^2 = \delta^{nl}k_n k_l$ denotes the square of the amplitude of wave vector, $\mathbf{k}$. In the following discussion, we demonstrate the quantization procedure of this classical field.

4.2.2 Calculation of Bolgoliuobov coefficients

We now write the classical EM field (4.8) in polarization basis and promote it to the quantum field operator by making the constants, $c_{\bar{k}}, c^*_{\bar{k}}$, as creation and annihilation operator respectively,

$$A_i(t,\bar{x}) = \sum_{\lambda=1,2}\int \frac{d^3k}{(2\pi)^3}\epsilon_i^\lambda(\bar{k})[\hat{c}^\lambda_{\bar{k}}A_\lambda(t,k) + \hat{c}^{\lambda\dagger}_{-\bar{k}}A^*_\lambda(t,k)]e^{-i\bar{k}\cdot\bar{x}}, \tag{4.10}$$

where, $\hat{c}^\lambda_{\bar{k}}$ and $\hat{c}^{\lambda\dagger}_{\bar{k}}$ satisfy the usual harmonic oscillator commutation relation,

$$\begin{aligned}&[\hat{c}^\lambda_{\bar{k}}, \hat{c}^{\lambda'}_{\bar{k}'}] = 0, \quad [\hat{c}^{\lambda\dagger}_{\bar{k}}, \hat{c}^{\lambda'\dagger}_{\bar{k}'}] = 0,\\ &[\hat{c}^\lambda_{\bar{k}}, \hat{c}^{\lambda'\dagger}_{\bar{k}'}] = (2\pi)^3\delta^{\lambda\lambda'}\delta^3(\bar{k}-\bar{k}').\end{aligned} \tag{4.11}$$

Whereas orthonormalized polarization basis vectors satisfy the following relation

$$\begin{aligned}&\epsilon_i^\lambda(\bar{k})\cdot k_i = 0, \quad \epsilon_i^\lambda(\bar{k})\epsilon_i^{\lambda'}(\bar{k}) = \delta_{\lambda\lambda'},\\ &\sum_{\lambda=1,2}\epsilon_i^\lambda(\bar{k})\epsilon_\lambda^j(\bar{k}) = \delta_i^j - \frac{k_i k^j}{k^2}.\end{aligned} \tag{4.12}$$

From the Lagrangian (4.4) the canonically conjugate momentum of $A_i(t,\mathbf{x})$ turns out to be,

$$\Pi^i = -\sqrt{-g}\mathcal{I}(t)g^{00}g^{ij}\partial_\eta A_j = \mathcal{I}(t)\delta^{ij}\partial_t A_j. \tag{4.13}$$

Imposing the equal time canonical commutation relation between the EM potentials and their conjugate momentum we obtain

$$[A_i(t,\mathbf{x}), \Pi^j(t,\mathbf{y})] = \mathrm{i}\int \frac{d^3k}{(2\pi)^3}e^{i\mathbf{k}\cdot(\mathbf{x}-\mathbf{y})}\epsilon_i^\lambda(\mathbf{k})\epsilon_\lambda^j(\mathbf{k}). \tag{4.14}$$

where, $\epsilon_i^\lambda(\bar{k})\epsilon_\lambda^j(\bar{k}) = \left(\delta_i^j - \frac{k_i k^j}{k^2}\right)$. From this commutation relation we can deduce the quantization condition for the EM potentials as [166],

$$A_\lambda(t,k)A'^*_\lambda(t,k) - A^*_\lambda(t,k)A'_\lambda(t,k) = \frac{i}{\mathcal{I}(t)}, \tag{4.15}$$

where, $A'_\lambda(t,k) = \partial_t A_\lambda(t,k)$ also $\delta^{ij}\epsilon_i^\lambda(\bar{k})\epsilon_j^{\lambda'}(-\bar{k}) = \delta_{\lambda\lambda'}$. We assume each mode starts its journey from the quantum vacuum with no particle state at an initial time, $\hat{c}_{\bar{k}'}^{\lambda'\dagger}|0\rangle = 0$, which is quite similar to the Bunch-Davies[82, 167] vacuum considered in cosmology. The associated mode function takes the form, $A_\lambda(t,k) \sim N_k e^{-ikt}$, with positive frequency outgoing mode, and the initial normalization can be fixed using Eq.4.15, as $N_k = 1/\sqrt{2k\mathcal{I}(t_0)}$. Let's write the Fourier mode terms of (4.10) as

$$\begin{aligned}\hat{B}_\lambda(t,\mathbf{k}) &= \hat{c}_{\mathbf{k}}^\lambda A_\lambda(t,k) + \hat{c}_{-\mathbf{k}}^{\lambda\dagger} A_\lambda^*(t,k),\\ \hat{\pi}_\lambda(t,\mathbf{k}) &= \mathcal{I}(t)[\hat{c}_{\mathbf{k}}^\lambda \dot{A}_\lambda(t,k) + \hat{c}_{-\mathbf{k}}^{\lambda\dagger}\dot{A}_\lambda^*(t,k)].\end{aligned} \tag{4.16}$$

Introducing another set of time dependent creation and annihilation operators in terms of the above field operators as,

$$\begin{aligned}\hat{d}_{\bar{k}}^\lambda(t) &\equiv \sqrt{\frac{\mathcal{I}(t)k}{2}}\hat{B}_\lambda(t,\bar{k}) + \frac{\mathrm{i}}{\sqrt{2\mathcal{I}(t)k}}\hat{\pi}_\lambda(t,\bar{k}),\\ \hat{d}_{\bar{k}}^{\lambda\dagger}(t) &\equiv \sqrt{\frac{\mathcal{I}(t)k}{2}}\hat{B}_\lambda(t,-\bar{k}) - \frac{\mathrm{i}}{\sqrt{2\mathcal{I}(t)k}}\hat{\pi}_\lambda(t,-\bar{k}),\end{aligned} \tag{4.17}$$

we define late time creation and annihilation operators expressed in terms of respective initial time operators and time dependent Bogoliubov coefficients [82] in the following manner:

$$\begin{aligned}\hat{d}_{\bar{k}}^\lambda(t) &= \alpha_k^\lambda(t)\hat{c}_{\bar{k}}^\lambda + \beta_k^{\lambda^*}(t)\hat{c}_{-\bar{k}}^{\lambda\dagger},\\ \hat{d}_{\bar{k}}^{\lambda\dagger}(t) &= \alpha_k^{\lambda*}(t)\hat{c}_{\bar{k}}^{\lambda\dagger} + \beta_k^\lambda(t)\hat{c}_{-\bar{k}}^\lambda.\end{aligned} \tag{4.18}$$

The time dependent Bogoliubov coefficients are given by [168, 169],

$$\begin{aligned}\alpha_k^\lambda(t) &= \sqrt{\mathcal{I}(t)}\Big(\sqrt{\frac{k}{2}}A_\lambda(t,k) + \frac{\mathrm{i}}{\sqrt{2k}}A'_\lambda(t,k)\Big),\\ \beta_k^\lambda(t) &= \sqrt{\mathcal{I}(t)}\Big(\sqrt{\frac{k}{2}}A_\lambda(t,k) - \frac{\mathrm{i}}{\sqrt{2k}}A'_\lambda(t,k)\Big).\end{aligned} \tag{4.19}$$

From the quantization condition (4.15) one can derive the following constrained relation of the Bogoliubov coefficients,

$$|\alpha_k^\lambda(t)|^2 - |\beta_k^\lambda(t)|^2 = 1. \tag{4.20}$$

Now using the expression of $\beta_k^\lambda(t)$ (4.19) and with the relation (4.15) we obtain

$$|\beta_k^\lambda(t)|^2 = \frac{\mathcal{I}(t)}{2}\Big(k|A_\lambda(t,k)|^2 + \frac{|A'_\lambda(t,k)|^2}{k}\Big) - \frac{1}{2}, \tag{4.21}$$

which physically represents the photon number density produced from the quantum vacuum due to time dependent background [97].

In the following discussion, we will analyze the time evolution of this quantity and present the interpretation of the produced photon flash from the growth of $|\beta_k^\lambda(t)|^2$. In our framework, we have introduced two arbitrary parameters α and ξ. Depending upon those parameter values, we show particles can be produced both through perturbative and non-perturbative processes.

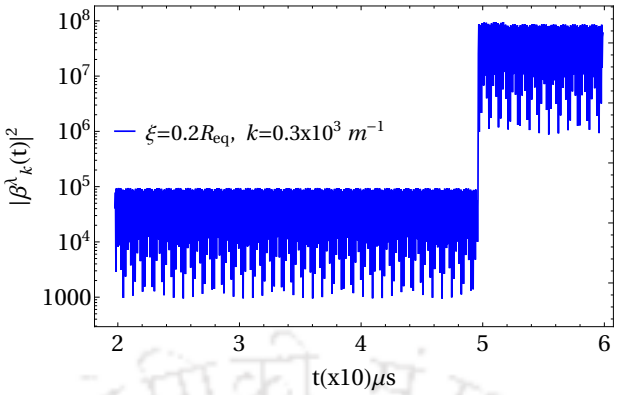

FIGURE 4.2: Spectral number density has been plotted with time for a fixed $k = 0.3 \times 10^3\ m^{-1}$. In the Y-axis we have used a log scale.

However, it is generically true and also we show that for the perturbative process, the particle production is insignificant, and it is the non-perturbative resonance due to the oscillating bubble background which will contribute the most. To study this analogy, we proceed by numerically finding out the solution of the EM field from the equation of motion (4.9). It is important to note that the extreme stiffness of the Ricci scalar and its time derivative, make this equation very stiff. When dealing with stiff ordinary differential equations, it is well known that implicit numerical methods, characterized by a greater number of discretization steps, work better than explicit methods in ensuring stable solutions [170, 171]. Naturally, this advantage comes at the cost of increased time consumption. For our present analysis, we have used such an implicit, Cranck-Nicholson method[172, 173] (see also Appendix.C.1).

Using the solution of the EM field in the expression (4.21) we have plotted $|\beta^{\lambda}_{k}(t)|^2$ with time in Fig.4.2 for a fixed frequency. It is indeed observed that at the moment say $t = 50\mu$s when the bubble comes to its minimum radius (Fig.1.5) a sudden enhancement in the photon number density appears. Most importantly, the enhancement gets repeated with the time period of the bubble shrinking to its minimum radius. This indeed indicates parametric resonance due to the breakdown of adiabaticity. We interpret this enhancement of the energy density at each successive period as the indicator of the periodically emitted photon flux as observed in the experiment [59–61]. The sudden growth of number density at the time of collapse is expected to occur within a specific frequency band which is a typical feature of the Floquet system [174], and this is indeed a significant result of our present proposal accounting for the experimental findings[61]. The particle production happens at the moment when the bubble comes to its minimum radius. Therefore, by tuning (α, ξ) values where the effect is maximized, surprisingly we obtain the magnitude of the number spectrum $|\beta_k|^2$ very close to that of the experimentally observed value, as we will see in a moment.

Under our adopted numerical method, we could get the spectrum in the range $(1, 10^5)$ m^{-1} of k, as shown in blue dotted points Fig.4.3. On the same plot we also provide data for the experimentally observed frequency ranges [61] around 10^7 m^{-1} that extend from visible to ultraviolet range reviling the broadband nature of the spectrum, and is shown in purple dots. As previously stated, the implicit numerical method might be the most effective approach. However, even following such a numerical technique, the Crank-Nicholson method, we could not get a reliable

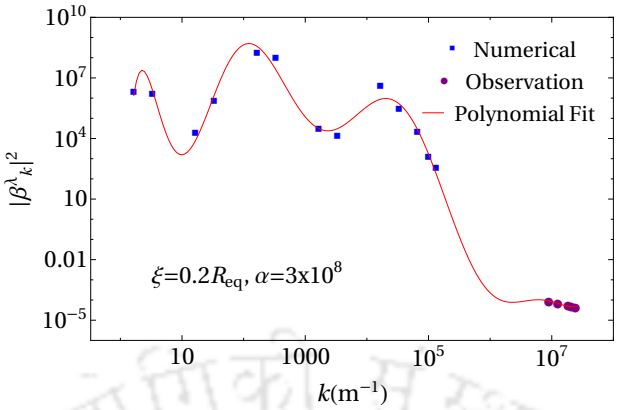

FIGURE 4.3: The spectral number density is plotted with frequency using a log scale for both axes. The experimental data is given along with the data numerically calculated from our model for comparison. We have fitted both results using Polynomial fit in Mathematica.

solution for $k > 10^5$ m^{-1}. Nevertheless, the trend of the numerically obtained photon number appears to indicate that our analog metric framework could explain the actual observation. This motivated us to extrapolate our results taking into account the experimentally measured data using the Polynomial fit (look at Appendix.C.2 for the fitting function), which is highlighted in red coloured line in Fig.4.3. The nice fitting of the extrapolated curve accounting for the experimental data seems to suggest that vacuum production through parametric resonance could be a possible mechanism of sonoluminescence. To this end, we should mention that addressing the relevant numerical challenges requires a thorough investigation into more robust numerical analysis techniques, such as implementations of the implicit methods discussed in [175–177]. In particular, the Parallelization technique presented in [175], aimed at addressing time consumption in the implicit method, could be a suitable approach. By employing these methods, it may become possible to address the stiffness problem in the model equations, thereby obtaining a stable solution within the experimentally observed frequency range. Then, it will be possible to confirm whether the current formulations are capable of accurately reproducing the fitted line in the high-frequency range, aligning with the actual measured data, or if they might deviate from it. In the next section, we calculate photon energy flux that has also been experimentally measured.

4.2.3 Photon Energy Flux

To connect with the experimental observation we evaluate the spectral energy density (energy density per k mode) from the Hamiltonian that can be calculated from the Lagrangian (4.4). The final expression for Hamiltonian in terms of creation and annihilation operators (with the help of (4.17)) can be expressed as,

$$H = \sum_{\lambda=1,2} \int \frac{d^3k}{(2\pi)^3}\, k \hat{d}^{\lambda\dagger}_{\vec{k}}(t) \hat{d}^{\lambda}_{\vec{k}}(t). \tag{4.22}$$

The expectation value of this Hamiltonian operator on the initial vacuum state discussed in Sec.4.2.1, turns out as,

$$\langle H\rangle = \sum_{\lambda=1,2}\int \frac{d^3k}{(2\pi)^3}\; k|\beta_k^\lambda(t)|^2\delta^3(0), \tag{4.23}$$

where $\delta^3(0)$ = Volume in the above equation appears from the commutators of the creation and annihilation operators, signifies infinite spatial volume emerging due to the quantization of the EM field throughout the space-time [97]. Therefore, the energy density comes out to be,

$$\mathcal{E} = \frac{\langle H\rangle}{\delta^3(0)} = \sum_{\lambda=1,2}\int dk\; 4\pi k^3|\beta_k^\lambda(t)|^2, \tag{4.24}$$

and the associated spectral energy density assumes the following form,

$$\frac{\partial\mathcal{E}}{\partial\ln k} = \sum_{\lambda=1,2} 4\pi k^4|\beta_k^\lambda(t)|^2. \tag{4.25}$$

The dimension of the above quantity is simply energy per unit volume. Converting this into the unit of experimentally measured quantity as

$$\frac{\text{Flux}}{s\times\text{nm}} = \frac{\partial\mathcal{E}}{\partial\ln k}\times\frac{4\pi(0.2\mu\text{m})^2}{50\text{ps}}\left[\frac{\text{Watt}}{\text{nm}}\right], \tag{4.26}$$

where, the typical radius of the bubble at the time of the emission is considered as $\sim 200nm$[178], and we have used experimentally measured pulse width $\sim$ 50ps [61]. we numerically evaluate the above expression using (4.21), and plotted in Fig.4.4. Interestingly, one can see the increasing trend in the flux, shown in blue dotted points, with the wave number k. The nature of the spectrum indicates that it sufficiently produces the required amount of flux which is close to the observed one, shown in purple dotted points. For example, we obtained the maximum numerical value of flux, 1.5×10^{-14}Watt/nm for a frequency $\sim 0.7\times10^5\text{m}^{-1}$. The upward trend of the flux seems to suggest that by invoking an improved numerical method one can indeed reach the level of experimentally observed amplitude $\sim 5\times10^{-12}$ Watt/nm near around $k\sim10^7\text{m}^{-1}$ since the production is mainly driven by parametric resonance. It might also happen that in the observed frequency range, our model could not reach the measured amplitude of the photon flux (the same issue discussed in the previous subsection with the possible way out). Whether the nature of our results can have the potential to match the experimentally observed flux, we have extrapolated our results including measured data points, utilizing the polynomial fit used in Fig.4.3, and highlighted the fitting function with a red solid line in Fig.4.4.

4.3 Perturbative spectrum at high-Frequency: analytical Estimation

In this section, we discuss perturbative photon production in the high frequency limit. We use the well known WKB method to get the analytic spectrum and also show the emergence of divergent contributions if the conformal property of the EM field is not appropriately taken into account.

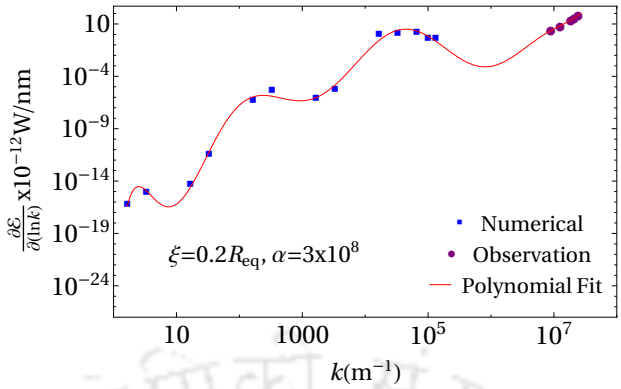

FIGURE 4.4: The power spectrum of the photon emission from the sono bubble is demonstrated using a log scale for both axes. The experimental data is given along with the data numerically calculated from our model for comparison. We have fitted both results using Polynomial fit in Mathematica.

To use the WKB method we rewrite the EM mode Eq. (4.9) in terms of newly defined field, $\tilde{A}_i(t,k) = \sqrt{\mathcal{I}(t)}A_i(t,k)$, and obtain the modified field equation as,

$$\partial_t^2 \tilde{A}_i(t,k) + \omega_k^2(t)\tilde{A}_i(t,k) = 0, \tag{4.27}$$

where the time dependent frequency is expressed as

$$\omega_k^2(t) = \frac{\dot{\mathcal{I}}^2(t)}{4\mathcal{I}^2(t)} - \frac{\ddot{\mathcal{I}}(t)}{2\mathcal{I}(t)} + \epsilon(t)k^2 \equiv \mathcal{J}(t) + \epsilon(t)k^2, \tag{4.28}$$

with $\mathcal{J}(t) \equiv \frac{\dot{\mathcal{I}}^2(t)}{4\mathcal{I}^2(t)} - \frac{\ddot{\mathcal{I}}(t)}{2\mathcal{I}(t)}$. While the factor $\epsilon(t)$ multiplied with k is the time dependent dielectric constant of the fluid inside the oscillating bubble. In our previous analysis, we assumed it to be unity. This particular time dependent term can be identified with the conformal modification of the flat Minkowski background, as it can always be absorbed into the modified time. However, without any time modification, we argue that the presence of such a term will always lead to divergent contributions indicating the non-physical contribution to the photon flux.

Remembering the well known WKB method in the high frequency limit, the temporal part of the EM field $\tilde{A}_i(t,\mathbf{k})$ is expressed as[179],

$$\tilde{A}_\lambda(t,k) = \frac{\gamma_k^\lambda(t)}{\sqrt{2\omega_k(t)}} e^{-\mathrm{i}\int \omega_k(t)\ dt} + \frac{\rho_k^\lambda(t)}{\sqrt{2\omega_k(t)}} e^{\mathrm{i}\int \omega_k(t)\ dt}. \tag{4.29}$$

Utilizing this the original EM field mode assumes,

$$A_\lambda(t,k) = \frac{\gamma_k^\lambda(t) e^{-\mathrm{i}\int \omega_k(t)\ dt}}{\sqrt{2\mathcal{I}(t)\omega_k(t)}} + \frac{\rho_k^\lambda(t) e^{\mathrm{i}\int \omega_k(t)\ dt}}{\sqrt{2\mathcal{I}(t)\omega_k(t)}}. \tag{4.30}$$

Comparing the above expression with (4.19) we deduce the expression for the Bogoliubov coefficients as,

$$\begin{aligned} \alpha_k^\lambda(t) &= \gamma_k^\lambda(t)\sqrt{\frac{k}{\omega_k(t)}} e^{-\mathrm{i}\int \omega_k(t)\ dt}, \\ \beta_k^\lambda(t) &= \rho_k^\lambda(t)\sqrt{\frac{k}{\omega_k(t)}} e^{\mathrm{i}\int \omega_k(t)\ dt}. \end{aligned} \tag{4.31}$$

Finally, the EM field equation can be equivalently written in terms of WKB functions from (4.27) as the following first order differential equations [179],

$$\begin{aligned}\dot{\gamma}_k^\lambda(t) &= \frac{\dot{\omega}_k(t)}{2\omega_k(t)} e^{2\mathrm{i}\int^t \omega_k(t')dt'} \rho_k^\lambda(t),\\ \dot{\rho}_k^\lambda(t) &= \frac{\dot{\omega}_k(t)}{2\omega_k(t)} e^{-2\mathrm{i}\int^t \omega_k(t')dt'} \gamma_k^\lambda(t).\end{aligned} \tag{4.32}$$

The initial no particle state (Bunch-Davis vacuum) can be identified by assuming the condition $\gamma_k^\lambda(t_0) = 1$, $\rho_k^\lambda(t_0) = 0$. As time evolves due to time dependent background particles will be produced. In the perturbative limit, at later time we can assume $\rho_k^\lambda(t) << 1$, and $\gamma_k^\lambda(t) \approx 1$. With this approximation, we get

$$\begin{aligned}\rho_k^\lambda(t) &\sim \frac{1}{2}\int^t dt' \frac{\dot{\omega}_k(t')}{\omega_k(t')} e^{-2\mathrm{i}\int^{t'} \omega_k(t'')dt''}\\ &= \frac{1}{2}\int^t \frac{\dot{\omega}_k(t')}{\omega_k(t')} \frac{1}{(-2\mathrm{i}\omega_k(t'))} d\Big(e^{-2\mathrm{i}\Omega_k(t')}\Big)\\ &= \frac{1}{k}\frac{1}{2}\frac{\dot{\omega}_k(t')}{\omega_k(t')}\frac{1}{(-2\mathrm{i})}\Big(e^{-2\mathrm{i}\Omega_k(t')}\Big)\Big|_{t_0}^t - \frac{1}{k}\int^t \frac{d}{dt'}\Big[\frac{1}{2}\frac{\dot{\omega}_k(t')}{\omega_k(t')}\frac{1}{(-2\mathrm{i})}\Big] e^{-2\mathrm{i}\Omega_k(t')} dt'\\ &\simeq \frac{1}{k}\frac{1}{4}\frac{\dot{\mathcal{J}}(t') + \dot{\epsilon}(t')k^2}{\omega_k^2(t')}\frac{1}{(-2\mathrm{i})}\Big(e^{-2\mathrm{i}\Omega_k(t')}\Big)\Big|_{t_0}^t - \frac{1}{k}\int^t \frac{d}{dt'}\Big[\frac{1}{4}\frac{\dot{\mathcal{J}}(t') + \dot{\epsilon}(t')k^2}{\omega_k^2(t')}\frac{1}{(-2\mathrm{i})}\Big] e^{-2\mathrm{i}\Omega_k(t')} dt',\end{aligned} \tag{4.33}$$

where we have defined $\Omega_k(t') \equiv \int^{t'} \omega_k(t'')dt''$. For such integrals, the leading contribution usually comes from the stationary phase approximation. However, we numerically checked that the phase factor $\Omega_k(t')$ does not have any stationary point within the integration limit of one bubble oscillation. In such a case, integration by parts leading to a series in $1/k$ in the high frequency limit (the Riemann-Lebesgue lemma, look at page.439 of [180]). Therefore, the number density in the high frequency limit up to sub-leading order turns out as,

$$|\beta_k^\lambda(t)|^2 \sim |\rho_k^\lambda(t)|^2 \sim \frac{\dot{\epsilon}^2(t)}{\epsilon^2(t)k^2} + \frac{2\dot{\epsilon}(t)\dot{\mathcal{J}}(t)}{\epsilon^2(t)k^4} e^{\mathrm{i}\chi(t,k)} + \frac{\dot{\mathcal{J}}^2(t)}{\epsilon^2 k^6} \tag{4.34}$$

where, the phase factor, $\chi(t,k)$, arises due to quantum interference [181]. This immediately leads to the following form of the spectral energy density,

$$\frac{\partial\mathcal{E}}{\partial lnk} \sim \frac{\dot{\epsilon}^2(t)k^2}{\epsilon^2(t)} + \frac{2\dot{\epsilon}(t)\dot{\mathcal{J}}(t)}{\epsilon^2(t)} e^{\mathrm{i}\chi(t,k)} + \frac{\dot{\mathcal{J}}^2(t)}{\epsilon^2(t)k^2} \tag{4.35}$$

As stated earlier we indeed see the diverging spectral energy density $\propto k^2$ contribution originated from the time dependent dielectric constant, $\epsilon(t)$ which is due to non-conformal time coordinate. However, if one chooses the conformal time, for example, the case when $\epsilon = 1$, leading order spectral energy density falls as $1/k^2$ in large k. This is the case we have discussed previously.

This particular decaying behaviour of the spectral energy density with the frequency, k, in the high frequency limit infers that the perturbative approach is not sufficient to produce the required amplitude of the sonoluminescence flux that demands an increasing trend with the frequency up to the ultraviolet range. From our crude estimate, in the experimental range, $k \sim 10^7 m^{-1}$, spectral energy density turns out as $\frac{\partial\mathcal{E}}{\partial lnk} \sim 10^{-30}$Watt/nm. This estimated amount of flux is much less compared to the nonperturbative production, which we have obtained in the high frequency near the experimentally observed frequency range.

4.4 Summary And Discussion

Particle production in time dependent background is an intriguing and well-known phenomenon in quantum field theory (QFT) [182–184]. It has been successfully applied in the early universe cosmological scenario. It would indeed be interesting if such phenomena could be observed in a real laboratory system. Sonoluminescence is one such phenomena where quantum photon production is believed to be one of the possible mechanisms. A large number of attempts have been made towards this direction in the past with their own pros and cons. In our analysis, we have attempted to revisit this event to understand the photon production mechanism better. We have to say that in the QFT framework if this phenomena is of quantum mechanical origin the underlying mechanism of production should be non-perturbative in nature.

We have modelled the oscillating bubble as an analog geometric system and proposed a nonminimal coupling prescription of the EM field with the analog geometry through the Ricci scalar. Due to oscillating bubble dynamics, the Ricci scalar plays the role of periodic time dependent coupling, and that also breaks the underlying conformal invariance of the EM field. Due to the periodic nature of the Ricci scalar source, and the appropriate values of the coupling parameters, the EM field is observed to show parametric amplification and that can seen as the production of photons flux from the quantum vacuum. Throughout our analysis, we stress the fact that it is this parametric resonance which could be the potential mechanism to explain the observed sonoluminescence phenomena.

We have computed the photon flux in the parametric resonance regime in the experimental unit. Whereas the experimentally observed frequency is around $k \sim 10^7 \mathrm{m}^{-1}$, due to our numerical limitation and high stiffness of the Ricci scalar function, we could obtain the flux in the low frequency region up to $\sim 10^5 \mathrm{m}^{-1}$. Interestingly magnitude of the produced flux in terms of frequency (k) turned out to be in the required order which may reach the experimental value with good numerical technique. For completeness, we further computed the analytic photon spectrum in the perturbative framework and showed that the produced amplitude of the flux is very low as expected.

Our model thus suggests that quantum production might be the actual mechanism responsible for photon production in contrast to the existing model on thermal production. Hence, the promising next step would be to analyse the quantumness of the produced spectrum by defining quantum observables, such as Poincare's sphere [185, 186], which utilizes time dependent squeezing parameter (one may look at [185]) for such dynamical systems. Squeezing parameters are connected to the Bogoliuobov coefficients, however, the analysis could be performed in a somewhat, independent manner (see [187, 188]), which can also provide for a consistency check of our model.

In the end, we should mention that the phenomena of sonoluminescence is sensitive to the nature of the gas inside the bubble. In this regard, we want to point out that the theory proposed here is very much dependent on the bubble dynamics including all the parameters of the medium inside the bubble. Hence, it will be our next task to take into account different experimental issues in the future [59, 61].

Neutrino production from oscillating bubble in fluid: Sononeutrinoescence 5

"The career of a young theoretical physicist consists of treating the harmonic oscillator in ever-increasing levels of abstraction."

Sidney Coleman

5.1 Introduction

We have seen in the previous chapter that the formalism of particle production in the time dependent background plays a very crucial role in realizing the photon emission in the sonoluminescence. However, particle production in the time dependent background is a universal phenomena in the sense that one can talk about the production of other fundamental particles in the same context. This particular aspect has motivated us to look for the possibility of producing neutrino, which may be emitted due to the oscillating bubble in the fluid, along with the photon.

In accordance with the formalism developed in the previous chapter for photons, we have also proposed here the same non-perturbative mechanism to produce particles from the effective time dependent acoustic metric that emerged due to the fluctuation in the oscillating bubble in water. However, in the present case of fermion, we have considered minimal coupling with this time dependent background, which is conformally flat to Minkowski space time. This simplified prescription can give rise to massive fermion production, as the mass of the fermion breaks the conformal symmetry of the action. This is a slightly different way to break the symmetry as compared to the case of photons (4.4), where we chose explicit conformal breaking coupling. Nevertheless, the mass range of the fermions, which could be produced with the minimal coupling prescription, prompts us to treat the fermions as neutrinos. Therefore we call this phenomena of neutrino production from the oscillating bubble in water as Sononeutrinoescence.

In the framework of the standard model of particle physics, Neutrinos are characterized by their weak interaction and definite chirality. Experiments on neutrino oscillations reported [189, 190] their possible mass range, with the upper limit to be ~ 0.5 eV [191, 192], including all the flavors. However, there exists no experimental constraint on the minimum limit of neutrino. Thus, in our analysis, we consider the neutrino mass as a free parameter. There are various scenarios where fermion production in time dependent background has been studied, particularly in the scenario of early universe cosmology, [179, 193–201]. However, the prospect of producing fermions in the analog system is not very intuitive. Therefore our motivation to explore Sononutrinoscence stems from the fact that one may be able to observe neutrinos in the laboratory experiment of sonoluminescence in the near future.

5.2 Neutrinos in analog background: a prescrition

We start with the following action of the neutrino as a massive Dirac fermion ψ, minimally coupled with the acoustic metric (4.3), which we have used in the previous chapter,

$$\mathcal{A} = \int d^4x\sqrt{-g}\bar{\psi}\left[i\gamma^\mu D_\mu - m_\psi\right]\psi, \tag{5.1}$$

where, m_ψ is the mass of the fermion, $\gamma^\mu = e_a{}^\mu\gamma^a$ and covariant derivative $D_\mu = \partial_\mu + \Gamma_\mu$, with, $\Gamma_\mu = \frac{1}{4}\omega_\mu^{ab}\gamma_a\gamma_b$ [179, 197]. Flat space- Gamma matrices satisfy the usual anti commutation relation $\{\gamma^a, \gamma^b\} = 2\eta^{ab}$ with η^{ab} as the Minkowski metric, and the connection to the curved-space gamma matrices are made through the Vierbein, which is chosen as, $e^a{}_\mu \equiv p^{1/6}(t)\delta^a{}_\mu$. With these setup we obtain $\gamma^\mu\Gamma_\mu = \frac{p'(t)}{4p^{7/6}(t)}\gamma^0$. Whereas, gamma matrices, in the Dirac representation, are given by,

$$\gamma^0 = \begin{pmatrix} I & 0 \\ 0 & -I \end{pmatrix}, \quad \gamma^i = \begin{pmatrix} 0 & \sigma^i \\ -\sigma^i & 0 \end{pmatrix}. \tag{5.2}$$

In terms of the rescaled field $\psi(x) = p^{-1/4}(t)\chi(x)$, the equation of motion governing the fermion field can be derived from the action as,

$$\mathrm{i}\gamma^a\partial_a\chi - m_\psi p^{1/6}(t)\chi = 0. \tag{5.3}$$

Conjugate momentum of ψ, ne derived from the action as

$$\Pi_\chi = \frac{\partial(\sqrt{-g}\mathcal{L})}{\partial\dot{\chi}} = \mathrm{i}\bar{\chi}\gamma^0, \qquad \Pi_{\bar{\chi}} = 0. \tag{5.4}$$

We decompose $\chi(x)$ into eigen spinors as,

$$\begin{aligned}
\chi(x) &= \sum_{\lambda=\pm1}\int\frac{d^3k}{(2\pi)^3}\left(\hat{b}_{\mathbf{k},\lambda}\mathcal{U}_{k,\lambda}(t) + \hat{d}^\dagger_{-\mathbf{k},\lambda}\mathcal{V}_{-k,\lambda}(t)\right)e^{\mathrm{i}\mathbf{k}\cdot\mathbf{x}}, \\
\chi^\dagger(x) &= \sum_{\lambda=\pm1}\int\frac{d^3k}{(2\pi)^3}\left(\hat{b}^\dagger_{\mathbf{k},\lambda}\mathcal{U}^\dagger_{k,\lambda}(t) + \hat{d}_{-\mathbf{k},\lambda}\mathcal{V}^\dagger_{-k,\lambda}(t)\right)e^{-\mathrm{i}\mathbf{k}\cdot\mathbf{x}},
\end{aligned} \tag{5.5}$$

where the creation and annihilation operator satisfies the anticommutation relation,

$$\begin{aligned}\left\{\hat{b}_{\mathbf{k},\lambda}, \hat{b}^{\dagger}_{\mathbf{k}',\lambda'}\right\} &= (2\pi)^3\delta(\mathbf{k}-\mathbf{k}')\delta_{\lambda\lambda'},\\ \left\{\hat{d}_{\mathbf{k},\lambda}, \hat{d}^{\dagger}_{\mathbf{k}',\lambda'}\right\} &= (2\pi)^3\delta(\mathbf{k}-\mathbf{k}')\delta_{\lambda\lambda'}.\end{aligned} \tag{5.6}$$

Given the following quantization condition,

$$\{\chi_\alpha(t,\mathbf{x}), \chi^{\dagger}_\beta(t,\mathbf{y})\} = \delta^3(\mathbf{x}-\mathbf{y})\delta_{\alpha\beta}, \tag{5.7}$$

one can show that spinor basis satisfies the following orthonormal relations [197],

$$\begin{aligned}&\mathcal{U}^{\dagger}_{k,\lambda}(t)\mathcal{U}_{k,\lambda'}(t) = \delta_{\lambda\lambda'}, \quad \mathcal{V}^{\dagger}_{k,\lambda}(t)\mathcal{V}_{k,\lambda'}(t) = \delta_{\lambda\lambda'},\\ &\mathcal{U}^{\dagger}_{k,\lambda}(t)\mathcal{V}_{k,\lambda'}(t) = 0,\end{aligned} \tag{5.8}$$

where,

$$\mathcal{U}_{k,\lambda}(\tau) = \begin{pmatrix} f_k(t)\zeta_\lambda(\mathbf{k}) \\ g_k(t)\boldsymbol{\sigma}\cdot\hat{k}\zeta_\lambda(\mathbf{k})\end{pmatrix} \; ; \; \mathcal{V}_{k,\lambda} = \begin{pmatrix} -g^*_k(t)\zeta_{-\lambda}(\mathbf{k}) \\ -f_k(t)\boldsymbol{\sigma}\cdot\hat{k}\zeta_{-\lambda}(\mathbf{k})\end{pmatrix}, \tag{5.9}$$

with the ζ_λ as the eigenstates of helicity operator, $\boldsymbol{\sigma}\cdot\mathbf{k}\xi_\lambda = \lambda k\xi_\lambda$. The antiparticle modes can be obtained utilizing the charge conjugation operator $\mathcal{V}_{k,\lambda} = \mathcal{U}^c_{k,\lambda} \equiv \mathrm{C}\,\bar{\mathcal{U}}^T_{k,\lambda} = \mathrm{i}\gamma^2\mathcal{U}^*_{k,\lambda}$ and $-\mathrm{i}\sigma_2\zeta^*_\lambda(\mathbf{k}) = \lambda\zeta_{-\lambda}(\mathbf{k})$. Using the normalization of the modes we derive the following relation between the time dependent function associated with the spinors as

$$|f_k(t)|^2 + |g_k(t)|^2 = 1. \tag{5.10}$$

Now to find out $\mathcal{U}_{k,\lambda}(t)$ and $\mathcal{V}_{k,\lambda}(t)$ we follow the approach of [197]. Substituting the mode decomposition in (5.3) we obtain

$$\begin{aligned}&\mathrm{i}\partial_t f_k(t) - \lambda k g_k(t) - m_\psi p^{1/6}(t) f_k(t) = 0,\\ &\mathrm{i}\partial_t g_k(t) - \lambda k f_k(t) + m_\psi p^{1/6}(t) g_k(t) = 0.\end{aligned} \tag{5.11}$$

We decouple the equation to obtain the e.o.m of the individual field as,

$$\begin{aligned}&\partial^2_t f_k(t) + \left[k^2 + m^2_\psi p^{\frac{1}{3}}(t) + \mathrm{i}m_\psi\partial_t\left(p^{1/6}(t)\right)\right] f_k(t) = 0,\\ &\partial^2_t g_k(t) + \left[k^2 + m^2_\psi p^{\frac{1}{3}}(t) - \mathrm{i}m_\psi\partial_t\left(p^{1/6}(t)\right)\right] g_k(t) = 0.\end{aligned} \tag{5.12}$$

To solve these differential equations numerically we consider the initial vacuum state as Bunch-Davies [82, 167], $f_k(t) \sim N_k e^{-\mathrm{i}\omega_k t}$, with $\omega_k(t) = \sqrt{k^2 + m^2_\psi p^{1/3}(t)}$ denoting the positive frequency mode, at some initial time $t = t_0$. One might consider this instant as the point when the fluctuation is turned on. The initial normalization can be fixed from (5.10) as $N_k = \sqrt{(\omega_k(t) + p^{1/6}(t)m_\psi)/2\omega_k(t)}$, that will provide for the required initial conditions, $f_k(t) \sim N_k e^{-\mathrm{i}\omega_k t}$ and $\partial_\tau f_k(t) \sim -\mathrm{i}N_k\omega_k e^{-\mathrm{i}\omega_k t}$. With this setup, we find out the solution of $f_k(t)$ from (5.12) numerically in Mathematica. This solution will be used to evaluate the observable quantities discussed in the following section.

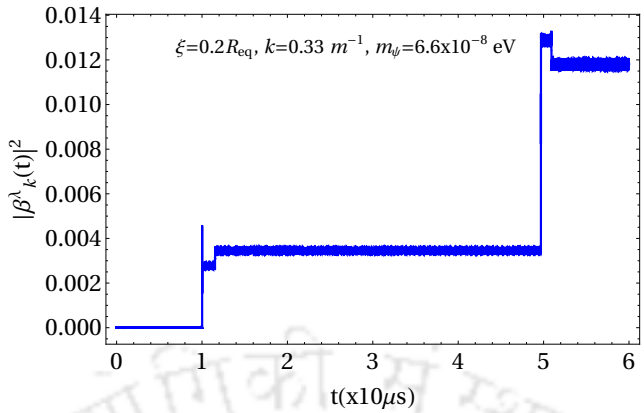

Figure 5.1: Spectral number density has been plotted with the conformal time for fixed, $k = 0.33m^{-1}$, tuning parameter, $\xi = 0.2R_{\rm eq}$, where $R_{\rm eq} = 4.5\mu m$ is the ambient radius of the bubble. Whereas the mass of the fermion considered to be, $m_\psi = 6.6 \times 10^{-8}$ eV.

5.3 Neutrino number spectrum

The Hamiltonian of the system can be written as [196, 199],

$$H = \sum_{\lambda=\pm1} \int \frac{d^3k}{(2\pi)^3} \Big[(\hat{b}^\dagger_{\mathbf{k},\lambda} \hat{b}_{\mathbf{k},\lambda} - \hat{d}_{-\mathbf{k},\lambda} \hat{d}^\dagger_{-\mathbf{k},\lambda}) E_k(t) + \hat{d}_{-\mathbf{k},\lambda} \hat{b}_{\mathbf{k},\lambda} F_k(t) + \hat{b}^\dagger_{\mathbf{k},\lambda} \hat{d}^\dagger_{-\mathbf{k},\lambda} F^*_k(t) \Big], \tag{5.13}$$

where, energy E_k and squeezing F_k functional [196] are,

$$\begin{aligned} E_k(t) &= \mathrm{Im}\{f_k(t)\partial_t f^*_k(t) + g_k(t)\partial_t g^*_k(t)\} = -2\lambda k \mathrm{Re}[f_k(t) g^*_k(t)] + m_\psi p^{1/6}(t)\{2|f_k(t)|^2 - 1\}, \\ F_k(t) &= -\mathrm{i}(-f_k(t)\partial_t g_k(t) + g_k(t)\partial_t f_k(t)). \end{aligned} \tag{5.14}$$

Introducing time dependent creation and annihilation operators

$$\begin{aligned} \hat{b}_{\mathbf{k},\lambda}(t) &= \alpha_k(t)\hat{b}_{\mathbf{k},\lambda} + \beta_k(t)\hat{d}^\dagger_{-\mathbf{k},\lambda'}, \\ \hat{d}^\dagger_{\mathbf{k},\lambda'}(t) &= -\beta^*_k(t)\hat{b}_{\mathbf{k},\lambda} + \alpha^*_k(t)\hat{d}^\dagger_{-\mathbf{k},\lambda'}, \end{aligned} \tag{5.15}$$

with the Bogoliubov coefficients, $\alpha_k(t), \beta_k(t)$c satisfying the following constraint,

$$|\alpha_k|^2 + |\beta_k|^2 = 1. \tag{5.16}$$

Diagonalization of the Hamiltonian (5.13) requires that the coefficient of $\hat{d}_{-\mathbf{k},\lambda}\hat{b}_{\mathbf{k},\lambda}$ to be zero [196],

$$2E_k(t)\beta^*_k(t)\alpha_k(t) + F_k(t)\alpha^2_k(t) - F^*_k(t)\beta^{*2}_k(t) = 0, \tag{5.17}$$

which leads to the following expression of the Bogoliubov coefficient,

$$|\beta^\lambda_k(t)|^2 = \frac{|F_k|^2(t)}{2\omega_k(t)(E_k(t) + \omega_k(t))} = \frac{\omega_k(t) - E_k(t)}{2\omega_k(t)}, \tag{5.18}$$

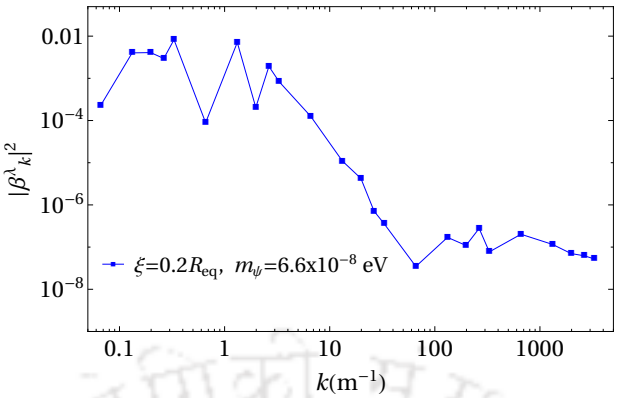

FIGURE 5.2: Behaviour of the Number spectrum of the fermion. Log scale is used in both of the axes.

where we have used $E_k^2(t) + F_k^2(t) = \omega_k^2(t)$. Finally, substituting the expression of $E_k(t)$ from (5.14) we obtain the expression for the occupation number density $|\beta_k^\lambda|^2$ as [179, 199],

$$|\beta_k^\lambda(t)|^2 = \frac{1}{2} + \frac{m_\psi p^{1/6} - 2i(f_k^* \partial_t f_k - f_k \partial_t f_k^*)}{2\omega_k(t)}, \tag{5.19}$$

We now analyze in detail the characteristics of the neutrino number spectrum $|\beta_k^\lambda(t)|^2$ in terms of tuning parameters ξ and neutrino mass, m_ψ. Using the solution of the Dirac equation (5.11) in to (5.19) we have plotted the time evolution of the neutrino number density $|\beta_k^\lambda(t)|^2$ in Fig.5.1 for a fixed wave number $k = 0.33m^{-1}$, also considering the mass of neutrino $m_\psi = 6.6 \times 10^{-8}$ eV. From the plot, it is clear that at the time when the bubble shrinks to its minimum radius say $t = 60\mu$s, the sudden jump in the neutrino number density occurs, and such a jump is repeated with the same time period as that of the oscillating bubble. Therefore, the parametric resonance, which is responsible for the photon flux as observed in the experiment [59, 61], also causes the production of flashes of neutrinos and can in principle be detected. We further plotted the number spectrum which shows a peak near around 1 m^{-1}. Under our adopted numerical method, we could get the spectrum in the range $(0, 10^5)$ m^{-1} of k, as shown in blue dotted points Fig.5.2. Further numerical investigation is needed to extend that range to a higher frequency. We should also mention that the magnitude of the produced number density is small compared to the maximum allowable value of $|\beta_k|^2 \sim 1$ (5.16). It will be interesting to consider explicit conformal breaking coupling as has been utilized for photon in the previous chapter and check whether this magnitude could be enhanced. We save this analysis as our future project. In the next section, we define neutrino energy flux that can also be experimentally measured. .

5.4 Neutrino Energy Flux

The expectation value of this Hamiltonian can be expressed in terms of neutrino number spectrum as [179],

$$\langle H \rangle = \sum_{\lambda=1,2} \int \frac{d^3k}{(2\pi)^3}\, \omega_k(t) |\beta_k^\lambda(t)|^2 \delta^3(0), \tag{5.20}$$

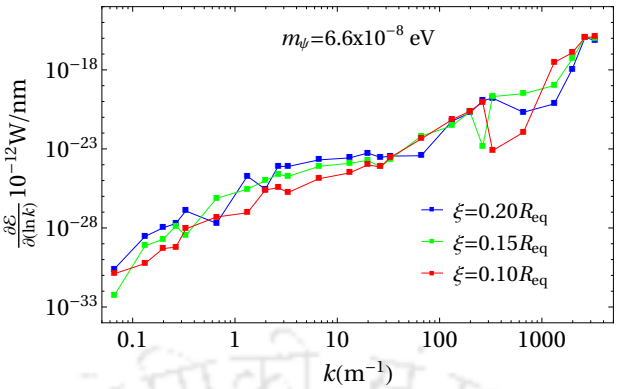

FIGURE 5.3: Neutrino energy flux per unit time has been plotted with the frequency, k for various values of the tuning parameter ξ.

where $\delta^3(0)$ = spatial volume [97]. This immediately leads to spectral energy density as,

$$\frac{\partial}{\partial \ln k}\left(\frac{\langle H\rangle}{\delta^3(0)}\right) = \sum_{\lambda=1,2} 4\pi k^3 \omega_k(t)|\beta_k^\lambda(t)|^2. \tag{5.21}$$

The dimension of the above quantity is simply energy per unit volume. Upon converting into the unit of Watt per nanometer which is convenient for the experimental measurement we have

$$\frac{\text{Flux}}{s\times \text{nm}} = \frac{\partial\mathcal{E}}{\partial \ln k}\times\frac{4\pi(0.2\mu\text{m})^2}{50\text{ps}}\left[\frac{\text{Watt}}{\text{nm}}\right], \tag{5.22}$$

where, in the definition, we have made use of the experimentally measured bubble radius $\sim 0.2\mu m$[178] at the moment of emission of the photon flux with pulse width $\sim$ 50ps [61], as neutrino emission will follow the same pattern as that of the photons. We numerically evaluate the above expression using (5.1), and plotted in Fig.5.3 for three different values of the parameter $\xi = (0.20, 0.15, 0.10)R_{\text{eq}}$, with the wave number k. Interestingly, one can see the increasing trend in the flux with the wave number k. As expected, from the coupling prescription with the background, increasing the value of ξ will lead to more production, which is clearly visible from Fig.5.3 in the low frequency range up to $k \sim 100m^{-1}$. However, in the high frequency range, generally, production being very less (see Fig.5.2) and frequency of the modes playing the dominant role, we find it hard to distinguish the effect of ξ. Now, recall that the proposed analog metric (1.120) is conformally flat, hence the neutrino mass plays the primary role in realising the parametric resonance as it is the mass term (5.3) which breaks the conformal invariance. Therefore, we have further plotted the energy flux in Fig.5.4 for three different values of neutrino mass, $m_\psi = (6.6\times10^{-10}, 6.6\times10^{-8}, 6.6\times10^{-6})$ eV. Initially, the energy spectrum increases in magnitude as we increase the mass, and then it saturates at around $m_\psi \sim 10^{-6}$ eV. Saturation is more explicit in the high frequency range as the frequency plays the dominant role in the effective potential of the equation of motion (5.12) at a higher frequency. The sudden jump of the bubble during moments of transition to the minimum radius poses a challenge in obtaining the numerical solution for heavier masses, which appears in the equation of motion (5.12) as a multiplying factor with the metric coefficients. Hence, a more advanced numerical method (such as the methods discussed in [175, 176]) suitable to handle stiff ordinary differential equations is required to present

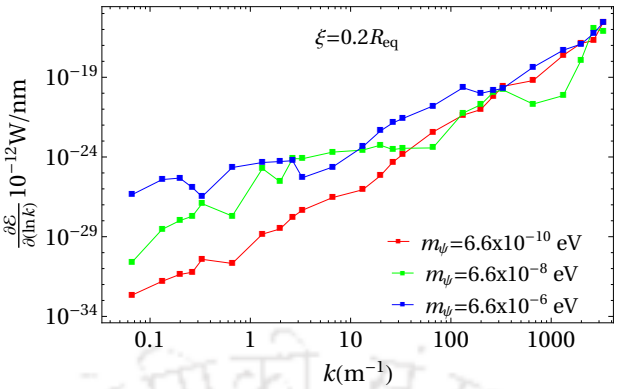

FIGURE 5.4: Neutrino energy flux per unit time has been plotted with the frequency, k for the different mass of the neutrino.

a better representation of the spectrum for heavier mass. Nevertheless, in the present analysis, we have mainly shown that the neutrino can be produced periodically via parametric amplification [200]. To our knowledge, this is the first case study of neutrino production in the context of analog fluid medium.

5.5 Summary And Discussion

In the time dependent background quantum particle production is an intriguing phenomena which is the subject of investigation for a long time [179, 193–201]. It has been successfully applied in the early universe cosmological scenario. It would indeed be interesting if such phenomena could be observed in real laboratory systems. Sonoluminescence is assumed to be one such phenomena where quantum photon production is believed to be one of the possible mechanisms. In the previous chapter, we studied this event and proposed a formalism in the framework of analog geometric model. We further emphasised that non-perturbative parametric resonance plays a central role in explaining such phenomena.

The geometric framework is universal in nature which motivates us to look into the possibility of neutrino production in such an analog model. Therefore, we proposed a minimal coupling prescription of the neutrino field with the analog geometry of the oscillating bubble. Along with the flashes of photons, the neutrino field is indeed observed to experience parametric amplification due to the oscillating bubble, and that produces flashes of neutrinos from the quantum vacuum. We have computed both the neutrino number density and energy density spectrum in the experimental unit. We have been able to obtain the flux in the low frequency region up to $\sim 10^5 \mathrm{m}^{-1}$. Interestingly the produced flux in terms of frequency (k) can be matched with the experimental results if it is observed. The smallness of the magnitude can be attributed to the fact that we have restricted our analysis to purely minimal interaction with the background acoustic metric. To enhance production, further exploration with more explicit conformal breaking coupling could be an interesting project for the future.

Conclusion and outlook 6

"They became acquainted with sorrow and loved sorrow; they thirsted for suffering, and said that truth could only be attained through suffering. Then science appeared."

—*Fyodor Dostoevsky, The Dream of a Ridiculous Man, and the Little Orphan*

In this thesis, we have presented our analysis broadly within the context of time-dependent systems. In the first scenario, our focus has been specifically directed towards the Schwarzschild black hole as it rings down during the last phase of the BH-BH or BH-NS merger. Considering scalar (2) and electromagnetic field (3) we have shown that these fields can extract energy from the ringing black holes. This excess energy turns up in the form of a negative absorption cross section of the ringing black holes. In the literature, this negative absorption cross section is attributed to the superradiant nature of the BHs. This suggests that during the course of its ringdown phase interacting fields can extract energy from the BHs and become amplified. The absorption cross section further oscillates quasi-periodically with time and encodes the decay time scale of the gravitational quasinormal modes of the black holes. GW induced time varying superradiance signal, in principle, should be easier to detect than the static one. For such a case, though, the challenge arises due to its very short time scale of oscillation.

Our primary goal has been to obtain a detectable signature of the ringdown phase. With this motivation, in the context of scalar superradiance we treated the scalar field as an axion. However, direct detection of axion is challenging. Therefore, we have exploited the natural interaction of axion with photon/fermions and calculated the observable such as rotation of the plane of polarization, and nucleon dipole moment which can in principle be measured in the laboratory located far away from the BHs.

Compared to the above, the direct signal of the superradiant electromagnetic field would be of greater importance, and we have analysed it in the subsequent chapter (3). BH-BH or BH-Neutron star mergers should have produced such transient superradiant EM signals. However, due to their

large mass $> M_\odot$ the wavelength of the superradiant signal would be very large of order 10 km, and observing such signal is far from any present day experimental limit. However, for PBHs such constraints can be ameliorated, and those can emit superradiant signals in the higher frequency range. We found within the existing experimental setup LOFAR may have the potential to detect such superradiant signals within its existing sensitivity limit for the PBHs mass $\sim 0.1 M_\odot$.

The key issue that remains to be understood is the role of the interaction surface r_{int} which plays an integral part in the evaluation of the absorption cross section. Given the fact that any external field should feel the ringing black hole space time up to spatial infinity, a probable approach to account for this effect would be to integrate the absorption cross section with respect to r_{int}. We find this procedure numerically challenging. Hence the future study should aim at simplifying this formalism and devise a strategy to integrate out the effect of the interaction surface from the framework. Given this issue, we should reiterate that the nature of the superradiant cross section makes it intuitively obvious that the aggregated effect may not vanish. This particular aspect makes our analysis very much significant.

An immediate extension to this analysis could be a generalization to the spinning black hole as it rings down, given the fact that usual rotating black holes already exhibit the superradiant cross section for bosonic fields. Other potential extensions may include the scattering of a GW wave [202–204] itself due to the ringing black hole and finding the observable signature in the current GW detectors, LIGO/Virgo/KAGRA. Another important direction could be to consider a binary black hole system [205] in the ringing phase.

In the context of a fluid system in the chapter.(4), we have taken up the interesting phenomena of Sonoluminescence due to an oscillating air bubble in water. We have attempted to propose a mechanism for the repeated light emission during each period of oscillation of the bubble, utilizing the effective acoustic metric. With a nonminimal coupling via the Ricci scalar of this metric, the electromagnetic field breaks the conformal symmetry of the action, thereby producing photon flux. We have obtained the number spectrum through our non-perturbative analysis which accounts for the resonant production of photons. We have also elaborately discussed the issue of divergence in the existing models based on the dynamical Casimir effect in our perturbative analysis (4.3) to further validate our formalism of non-perturbative production.

The universality of the nature of particle production in time dependent background has motivated us to put forward a proposal for a fermion in the chapter.(5) in a very similar manner to photon production. However, as we have seen, for fermion the conformal symmetry can be broken more simply by considering minimal coupling and talking about massive fermion. Following the same non-perturbative formalism we have deduced the number spectrum and power spectrum of the produced fermion of mass range $10^{-10} - 10^{-6}$eV. For this smallness of the mass, we have identified the fermion as a neutrino. Being inspired by the event of Sonoluminescence we have referred to this phenomena of producing neutrinos as Sononeutrinoescence. These findings could open up a window of opportunity to detect neutrinos in a laboratory-based setup. Of course, given the smallness of the produced spectrum, further investigation is required to increase the amount of production. One possible approach is to consider various conformal breaking coupling and check the magnitude of the produced flux.

Culminating the two contexts of dynamical systems that we have broadly discussed in the thesis, a possible future scenario is to investigate the scattering phenomena in the time dependent analog systems, that have characteristic similarities with the astrophysical systems[206–208]. This could be an interesting development on top of the already existing studies [55, 209–212] about the

superradiant enhancement of fluid fluctuations in the analogue background, as the case of the oscillating analog system have not been explored in detail.

I

Appendices

Appendix A

Metric perturbation

Here, we provide the explicit form of the ten independent basis tensors in terms of $\mathcal{G}^{\alpha\beta}_{\mu\nu} = (\delta^\alpha_\mu\delta^\beta_\nu + \delta^\beta_\mu\delta^\alpha_\nu)$ as,

$$
\begin{aligned}
&(a^{(0)}_{lm})_{\mu\nu} = \frac{1}{2}Y_{lm}\mathcal{G}^{tt}_{\mu\nu} \quad , \quad (a^{(1)}_{lm})_{\mu\nu} = \frac{\mathrm{i}}{\sqrt{2}}Y_{lm}\mathcal{G}^{tr}_{\mu\nu} \quad , \quad (a_{lm})_{\mu\nu} = \frac{1}{2}Y_{lm}\mathcal{G}^{rr}_{\mu\nu} \ , \\
&(b^{(0)}_{lm})_{\mu\nu} = \frac{\mathrm{i}r}{\sqrt{2l(l+1)}}(\partial_\theta Y_{lm}\mathcal{G}^{t\theta}_{\mu\nu} + \partial_\phi Y_{lm}\mathcal{G}^{t\phi}_{\mu\nu}) \quad , \quad (b_{lm})_{\mu\nu} = \frac{r}{\sqrt{2l(l+1)}}(\partial_\theta Y_{lm}\mathcal{G}^{r\theta}_{\mu\nu} + \partial_\phi Y_{lm}\mathcal{G}^{r\phi}_{\mu\nu}) \ , \\
&(c^{(0)}_{lm})_{\mu\nu} = \frac{r}{\sqrt{2l(l+1)}}\left(\frac{1}{s_\theta}\partial_\phi Y_{lm}\mathcal{G}^{t\theta}_{\mu\nu} - s_\theta\partial_\theta Y_{lm}\mathcal{G}^{t\phi}_{\mu\nu}\right) \ , \\
&(c_{lm})_{\mu\nu} = \frac{\mathrm{i}r}{\sqrt{2l(l+1)}}\left(\frac{1}{s_\theta}\partial_\phi Y_{lm}\mathcal{G}^{r\theta}_{\mu\nu} - s_\theta\partial_\theta Y_{lm}\mathcal{G}^{r\phi}_{\mu\nu}\right) \ , \\
&(d_{lm})_{\mu\nu} = \frac{-\mathrm{i}r^2}{\sqrt{2l(l+1)(l-1)(l+2)}}\left(-\frac{1}{2s_\theta}X_{lm}\mathcal{G}^{\theta\theta}_{\mu\nu} + s_\theta W_{lm}\mathcal{G}^{\theta\phi}_{\mu\nu} + \frac{s_\theta}{2}X_{lm}\mathcal{G}^{\phi\phi}_{\mu\nu}\right) \ , \\
&(g_{lm})_{\mu\nu} = \frac{r^2}{2\sqrt{2}}(Y_{lm}\mathcal{G}^{\theta\theta}_{\mu\nu} + s^2_\theta Y_{lm}\mathcal{G}^{\phi\phi}_{\mu\nu}) \ , \\
&(f_{lm})_{\mu\nu} = \frac{r^2}{\sqrt{2l(l+1)(l-1)(l+2)}}\left(\frac{1}{2}W_{lm}\mathcal{G}^{\theta\theta}_{\mu\nu} + X_{lm}\mathcal{G}^{\theta\phi}_{\mu\nu} - \frac{s^2_\theta}{2}W_{lm}\mathcal{G}^{\phi\phi}_{\mu\nu}\right) \ ,
\end{aligned}
\tag{A.1}
$$

where, $X_{lm} = 2\partial_\phi(\partial_\theta - \cot\theta)Y_{lm}$ and $W_{lm} = (\partial^2_\theta - \cot\theta\partial_\theta - (1/\sin^2\theta))Y_{lm}$.

The odd parity perturbation components under gauge transformation take the following form,

$$
\begin{aligned}
\mathbf{h}^{(o)}_{lm} = \frac{\mathrm{i}}{r}\sqrt{2l(l+1)}\Big[&\mathrm{i}\Big\{h^{(0)}_{lm}(t,r) - \frac{\partial\Lambda_{lm}}{\partial t}\Big\}\mathbf{c}^{(0)}_{lm}(\Omega) + \Big\{h^{(1)}_{lm}(t,r) - r^2\frac{\partial}{\partial r}\Big(\frac{\Lambda_{lm}}{r^2}\Big)\Big\}\mathbf{c}_{lm}(\Omega) \\
&- \frac{1}{2r}\sqrt{(l-1)(l+2)}(h^{(2)}_{lm}(t,r) + 2\Lambda_{lm}(t,r))\mathbf{d}_{lm}(\Omega)\Big]
\end{aligned}
\tag{A.2}
$$

where the radial parts of the non-zero components of odd parity perturbation (temporal part is governed by $e^{-\mathrm{i}\omega t}$) in the Regge-Wheeler gauge are given by,

$$
\begin{aligned}
h^{(1)}_{lm}(\omega,r) &= \frac{r^2}{r-2M}Z_{(\mathrm{o})}(\omega,r) \\
h^{(0)}_{lm}(\omega,r) &= \frac{\mathrm{i}}{\omega}\frac{d}{dr_*}\Big(rZ_{(\mathrm{o})}(\omega,r)\Big)
\end{aligned}
\tag{A.3}
$$

Expression of the even parity perturbation components under gauge transformation turns out as,

$$\begin{aligned}
\mathbf{h}^{(\mathrm{e})}_{lm} &= \Big(1-\frac{2M}{r}\Big)\Big\{H^{(0)}_{lm}(t,r) - 2\Big(1-\frac{2M}{r}\Big)^{-1}\Big(\frac{\partial \mathcal{M}_0}{\partial t} - \frac{M}{r^3}(r-2M)\mathcal{M}_1\Big)\Big\}\mathbf{a}^{(0)}_{lm} \\
&- \sqrt{2}\mathrm{i}\Big\{H^{(1)}_{lm}(t,r) - \Big(\frac{\partial \mathcal{M}_1}{\partial t} + \frac{\partial \mathcal{M}_0}{\partial r} - \frac{2M}{r(r-2M)}\mathcal{M}_0\Big)\Big\}\mathbf{a}^{(1)}_{lm} \\
&+ \Big(1-\frac{2M}{r}\Big)^{-1}\Big\{H^{(2)}_{lm}(t,r) - 2\Big(1-\frac{2M}{r}\Big)\Big(\frac{\partial \mathcal{M}_1}{\partial r} + \frac{M}{r(r-2M)}\mathcal{M}_1\Big)\Big\}\mathbf{a}_{lm} \\
&- \frac{\mathrm{i}}{r}\sqrt{2l(l+1)}\Big\{h^{(0)(e)}_{lm}(t,r) - \Big(\frac{\partial \mathcal{M}_2}{\partial t} + \mathcal{M}_0\Big)\Big\}\mathbf{b}^{(0)}_{lm} \\
&+ \frac{1}{r}\sqrt{2l(l+1)}\Big\{h^{(1)(e)}_{lm}(t,r) - \Big(\frac{\partial \mathcal{M}_2}{\partial r} - \frac{2}{r}\mathcal{M}_2 + \mathcal{M}_1\Big)\Big\}\mathbf{b}_{lm} \\
&+ \sqrt{\{l(l+1)(l-1)(l+2)/2\}}\Big\{G_{lm}(t,r) - \frac{2}{r^2}\mathcal{M}_2\Big\}\mathbf{f}_{lm} \\
&+ \Big[\sqrt{2}\Big\{K_{lm}(t,r) - \frac{2}{r^2}(r-2M)\mathcal{M}_1\Big\} - \frac{l(l+1)}{2}\Big\{G_{lm}(t,r) - \frac{2}{r^2}\mathcal{M}_2\Big\}\Big]\mathbf{g}_{lm}
\end{aligned} \tag{A.4}$$

where the radial parts of the non-zero even wave components (temporal part is governed by $e^{-\mathrm{i}\omega t}$) in the Regge-Wheeler gauge are given by,

$$\begin{aligned}
H^{(0)}_{lm}(\omega,r) &= \frac{\lambda r(r-2M) - \omega^2 r^4 + M(r-3M)}{(r-2M)(\lambda r+3M)}K_{lm}(\omega,r) + \frac{M(\lambda+1) - \omega^2 r^3}{\mathrm{i}\omega r(\lambda r+3M)}H^{(1)}_{lm}(\omega,r) \\
H^{(1)}_{lm}(\omega,r) &= -\mathrm{i}\omega\frac{\lambda r^2 - 3\lambda M r - 3M}{(r-2M)(\lambda r+3M)}Z_{(\mathrm{e})}(\omega,r) - \mathrm{i}\omega r\frac{dZ_{(\mathrm{e})}(\omega,r)}{dr} \\
K_{lm}(\omega,r) &= \frac{\lambda(\lambda+1)r^2 + 3\lambda M r + 6M^2}{r^2(\lambda r+3M)}Z_{(\mathrm{e})}(\omega,r) + \frac{r-2M}{r}\frac{dZ_{(\mathrm{e})}(\omega,r)}{dr}
\end{aligned} \tag{A.5}$$

Appendix B

Superradiance due to ringing BH

B.1 Expression of the source terms $\mathcal{P}_{lmc\gamma}$ and $\bar{\mathcal{P}}_{lmc\gamma}$

The source term in the Eq.(2.3) can be given as, $\mathcal{P}_{lmc\gamma}\xi^{c\gamma}(t,r) = \frac{1}{2}e^{-\mathrm{i}\omega t}P_{lm}(t,r)$, with $P_{lm}(t,r) = P^{(\mathrm{e})}_{lm}(t,r) + P^{(\mathrm{o})}_{lm}(t,r)$, where,

$$
\begin{aligned}
P^{(\mathrm{e})}_{lm}(t,r) &= f(r)\sum_{c\gamma}\Lambda^{(2,0)}_{c\gamma lm}\Big[f(r)^{-1}(\tilde{H}_{20}+\tilde{K}_{20})(\mathrm{i}\omega\partial_t\xi^{c\gamma}(t,r)-\partial_t^2\xi^{c\gamma}(t,r))\\
&+\frac{1}{r^2}\partial_r\{r^2f(r)(-\tilde{H}_{20}+\tilde{K}_{20})\partial_r\xi^{c\gamma}(t,r)\}-3f(r)^{-1}\tilde{G}_{20}(\mathrm{i}\omega\partial_t\xi^{c\gamma}(t,r)-\partial_t^2\xi^{c\gamma}(t,r))\\
&-3\frac{1}{r^2}\partial_r\{r^2f(r)\tilde{G}_{20}\partial_r\xi^{c\gamma}(t,r)\}-\mathrm{i}\omega\tilde{H}^{(1)}_{20}\partial_r\xi^{c\gamma}(t,r)+\tilde{H}^{(1)}_{20}\partial_t\partial_r\xi^{c\gamma}(t,r)\\
&+\frac{1}{r^2}\partial_r(r^2\tilde{H}^{(1)}_{20}\partial_t\xi^{c\gamma}(t,r))+6\frac{1}{r^2}f(r)\tilde{h}^{(1)(e)}_{20}\partial_r\xi^{c\gamma}(t,r)-\frac{c(c+1)}{r^2}\tilde{G}_{20}\xi^{c\gamma}(t,r)\Big]\\
&+f(r)\frac{1}{r^2}\Big[\sum_{c\gamma}2\gamma\Lambda^{(2,0)}_{c\gamma lm}+3\sqrt{\frac{2}{3}}\sum_{c\gamma}\sqrt{(c-\gamma)(c+\gamma+1)}\Lambda^{(2,-1)}_{c(\gamma+1)lm}\Big]\times\\
&\times\Big[\partial_r\{f(r)\tilde{h}^{(1)(e)}_{20}\xi^{c\gamma}(t,r)\}+f(r)\tilde{h}^{(1)(e)}_{20}\partial_r\xi^{c\gamma}_0(r)-\tilde{G}_{20}\xi^{c\gamma}(t,r)\Big]\\
&+f(r)\frac{1}{r^2}\sqrt{\frac{5}{4\pi}}\tilde{G}_{20}l(l+1)\xi^{lm}(t,r)-f(r)\frac{1}{r^2}m^2\tilde{G}_{20}\frac{3}{2}\sqrt{\frac{5}{\pi}}\xi^{lm}(t,r)\\
&+f(r)\frac{1}{r^2}\frac{m}{2}\sqrt{\frac{5}{\pi}}\Big[\partial_r\Big\{f(r)\tilde{h}^{(1)(e)}_{20}\xi^{lm}(t,r)\Big\}+f(r)\tilde{h}^{(1)(e)}_{20}\partial_r\xi^{lm}(t,r)-\tilde{G}_{20}\xi^{lm}(t,r)\Big],
\end{aligned}
\tag{B.1}
$$

$$
\begin{aligned}
P^{(\mathrm{o})}_{klm}(r) &= f(r)\frac{1}{r^2}\sum_{c\gamma}\mathrm{i}\gamma\sqrt{15}\Lambda^{(1,0)}_{c\gamma lm}\Big[\partial_r\{f(r)\tilde{h}^{(1)(\mathrm{o})}_{20}\xi^{c\gamma}(t,r)\}+f(r)\tilde{h}^{(1)(\mathrm{o})}_{20}\partial_r\xi^{c\gamma}(t,r)+\frac{1}{r^2}\tilde{h}^{(1)}_{20}\xi^{c\gamma}(t,r)\Big]\\
&+f(r)\frac{3}{2}\sqrt{\frac{5}{\pi}}\frac{1}{r^4}\tilde{h}^{(2)}_{20}\Big[\sqrt{\frac{\pi}{3}}\sum_{c\gamma}2\gamma\Lambda^{(1,0)}_{c\gamma lm}+2\sqrt{\frac{2\pi}{3}}\sum_{c\gamma}\Lambda^{(1,-1)}_{c(\gamma+1)lm}\sqrt{(c-\gamma)(c+\gamma+1)}\Big]\mathrm{i}\gamma\xi^{c\gamma}(t,r).
\end{aligned}
\tag{B.2}
$$

We have made use of Wigner-3j symbols as can be seen in the above equations, with the main definition given as

$$
Y^m_l(\theta,\phi)Y^{m'}_{l'}(\theta,\phi) = \sum_{c\gamma}\Lambda^{(l',m')}_{lmc\gamma}Y^{\gamma}_{c}(\theta,\phi) \tag{B.3}
$$

where,

$$\Lambda^{(l',m')}_{lmc\gamma} = (-1)^{\gamma}\sqrt{\frac{(2l'+1)(2l+1)}{4\pi}}\sqrt{2c+1}\begin{pmatrix} l & l' & c \\ m & m' & -\gamma \end{pmatrix}\begin{pmatrix} l & l' & c \\ 0 & 0 & 0 \end{pmatrix}.$$

For the non-zero value of the Wigner $3j$ coefficient $\begin{pmatrix} l & l' & c \\ m & m' & -\gamma \end{pmatrix}$, all the l values should satisfy the triangle law; the sum of any two l should be greater than equal to the third one and the sum of all the m values should be zero. Similarly, for the other source term in the Eq.(2.3), we will have associated operator $\bar{\mathcal{P}}_{lmc\gamma}$ which is the function of the complex conjugate of metric fluctuation, $h^*_{\mu\nu}$. For this case $\bar{\mathcal{P}}_{lmc\gamma}\xi^{c\gamma}(t,r) = \frac{1}{2}e^{i\omega^* t}\bar{P}_{lm}(t,r)$, where $\bar{P}_{lm}(t,r)$ can be obtained by replacing $\omega \to -\omega^*$ in the expression of $P_{lm}(t,r)$ and simultaneously taking the complex conjugate of the radial part of the fluctuation components.

B.2 Time varying rotation of the plane of polarization of photon

In this section we will study the conversion of axion to photon (vice-versa), specifically focussing on the axion background. However to start with we will consider a constant magnetic field along with the time dependent axion background. In the later part, we will only consider the axion part only, having additional effects in the final results. Taking the following action, where axion couples ($g_{\phi\gamma\gamma}$ is the coupling constant) with photon,

$$S = \int \sqrt{-g}d^4x[-\frac{1}{2}(\partial_\mu\phi\partial^\mu\phi + m^2_\phi\phi^2) - \frac{1}{4}F_{\mu\nu}F^{\mu\nu} - \frac{1}{4}g_{\phi\gamma\gamma}\phi F_{\mu\nu}\tilde{F}^{\mu\nu}] \tag{B.4}$$

we obtain the inhomogeneous Maxwell equation by varying the action with respect to A_μ as,

$$\partial_\mu F^{\mu\nu} + g_{\phi\gamma\gamma}\tilde{F}^{\mu\nu}\partial_\mu\phi = 0 \tag{B.5}$$

and inhomogeneous scalar equation by varying the action with respect to ϕ as,

$$\partial_\mu\partial^\mu\phi - m^2_\phi\phi - \frac{1}{4}g_{\phi\gamma\gamma}F_{\mu\nu}\tilde{F}^{\mu\nu} = 0 \tag{B.6}$$

Considering the radiation gauge, $\bar{\nabla}\cdot\bar{A} = 0, A_0 = 0$, both the scalar (B.6) and Maxwell equation (B.5) can be simplified as,

$$\begin{aligned} &\partial_t\bar{E} - \bar{\nabla}\times\bar{B} - g_{\phi\gamma\gamma}\bar{B}\partial_t\phi - g_{\phi\gamma\gamma}\bar{\nabla}\phi\times\bar{E} = 0 \\ &-\partial^2_t\phi + \nabla^2\phi - m^2_\phi\phi + g_{\phi\gamma\gamma}\bar{B}\cdot\partial_t\bar{A} = 0 \end{aligned} \tag{B.7}$$

Symmetry of the background-fields motivate us to consider the propagation direction of the axion and photon fluctuation along z, for simplification. So, expressing the scalar and em field as background with fluctuation,

$$\begin{aligned} \phi(t,z) &= \phi_0(t) + \tilde{\phi}(t,z) \\ \bar{B} &= \bar{B}_0 + \bar{\nabla}\times\bar{A}(t,z) \end{aligned} \tag{B.8}$$

we can derive the linearized equation governing the evolution of fluctuation as,

$$-\partial_t^2 \bar{A} + \nabla^2 \bar{A} - g_{\phi\gamma\gamma}[\bar{B}_0 \partial_t \tilde{\phi}(t,z) + \partial_t \phi_0(t) \bar{\nabla} \times \bar{A}] = 0 \tag{B.9}$$

and

$$-\partial_t^2 \tilde{\phi} + \nabla^2 \tilde{\phi} - m_\phi^2 \tilde{\phi} + g_{\phi\gamma\gamma} \bar{B}_0 \cdot \partial_t \bar{A} = 0 \tag{B.10}$$

Assuming the time scale of variation of the background field is much larger than the axion-photon wavelength. Also, we consider $\omega \sim \mathrm{k}$, so that we can write the fluctuation as plane waves like

$$\begin{aligned} \tilde{\phi}(t,z) &= \phi_\omega(t) e^{-\mathrm{i}\omega t} e^{-\mathrm{i}\omega z} \\ A(t,z) &= \mathrm{i} \begin{pmatrix} A_\omega^x(t) e^{-\mathrm{i}\omega t} \\ A_\omega^y(t) e^{-\mathrm{i}\omega t} \end{pmatrix} e^{-\mathrm{i}\omega z} \end{aligned} \tag{B.11}$$

We obtain the fluctuation equation of the Fourier modes of axion and photon, like the Schrodinger equation as,

$$\begin{aligned} \mathrm{i}\partial_t A_\omega^x(t) &= -\frac{1}{2} g_{\phi\gamma\gamma} B_0^x \phi_\omega(t) + \frac{\mathrm{i}}{2} g_{\phi\gamma\gamma} \dot{\phi}_0(t) A_\omega^y(t)] \\ \mathrm{i}\partial_t A_\omega^y(t) &= -\frac{1}{2} g_{\phi\gamma\gamma} B_0^y \phi_\omega(t) - \frac{\mathrm{i}}{2} g_{\phi\gamma\gamma} \dot{\phi}_0(t) A_\omega^x(t)] \\ \mathrm{i}\partial_t \phi_\omega(t) &= \frac{m_\phi^2}{2\omega} \phi_\omega(t) - \frac{1}{2} g_{\phi\gamma\gamma} B_0^x A_\omega^x(t) - \frac{1}{2} g_{\phi\gamma\gamma} B_0^x A_\omega^y(t) \end{aligned} \tag{B.12}$$

In matrix form these equations can be assembled as

$$\mathrm{i}\partial_t \begin{pmatrix} \phi_\omega(t) \\ A_\omega^x(t) \\ A_\omega^y(t) \end{pmatrix} = \begin{pmatrix} \Delta_m & \Delta_x & \Delta_y \\ \Delta_x & 0 & \Delta_\phi \\ \Delta_y & -\Delta_\phi & 0 \end{pmatrix} \begin{pmatrix} \phi_\omega(t) \\ A_\omega^x(t) \\ A_\omega^y(t) \end{pmatrix} \tag{B.13}$$

where $\Delta_m = \frac{m_\phi^2}{2\omega}$, $\Delta_i = -\frac{1}{2} g_{\phi\gamma\gamma} B_i (i \to x, y)$, $\Delta_\phi = \frac{\mathrm{i}}{2} g_{\phi\gamma\gamma} \dot{\phi}_0$. Considering $\Psi(t) = \{\phi_\omega(t), A_\omega^x(t), A_\omega^y(t)\}$, we rewrite the above equation

$$\mathrm{i}\partial_t \Psi = [H_0 + \tilde{H}(t)]\Psi \tag{B.14}$$

where ,

$$\tilde{H}(t) = \begin{pmatrix} 0 & \Delta_x & \Delta_y \\ \Delta_x & 0 & \Delta_\phi \\ \Delta_y & -\Delta_\phi & 0 \end{pmatrix} \tag{B.15}$$

In the following discussion we will work in interaction picture

$$\Psi_{int}(t) = \mathcal{U}^\dagger(t)\Psi(t), \quad H_{int} = \mathcal{U}^\dagger(t)\tilde{H}(t)\mathcal{U}(t), \quad \mathcal{U}(t) = e^{-\mathrm{i}\int^t H_0(t')dt'} \tag{B.16}$$

so that the equation (B.14) becomes

$$\begin{aligned}&\mathrm{i}\partial_t\Psi_{int}(t) = H_{int}\Psi_{int},\\ &\implies \Psi_{int}(t) = e^{-\mathrm{i}\int^t H_{int}(t')dt'}\Psi_{int}(0) \implies \Psi^{n+1}_{int}(t) = -\mathrm{i}\int^t H_{int}(t' \quad)dt'\Psi^n_{int}(t' \quad)\end{aligned} \tag{B.17}$$

Taking upto second order (considering the coupling $g_{\phi\gamma\gamma}$ very small) we get

$$\Psi_{int} = \Big(1 - \mathrm{i}\int_{t_0}^t H_{int}(t')dt' - \int_{t_0}^t H_{int}(t')dt'\int_{t_0}^{t'} H_{int}(t'')dt''\Big)\Psi(0) \tag{B.18}$$

After substituting this expression we get

$$\begin{aligned}A_x(t) &= A_x(0) - \mathrm{i}\Delta_x\tilde{\Delta}_m\phi^\omega(0) - \mathrm{i}\int^t \Delta_\phi dt' A^\omega_y(0) - \int^t dt'\Delta_\phi\int^{t'} dt''\tilde{\Delta}_m\Delta_x\phi^\omega(0)\\ &- \int^t dt'\Big(\Delta_x\tilde{\Delta}_m\int^{t'} dt''\Delta_x\tilde{\Delta}_m - \Delta_\phi\int^{t'} dt''\Delta_\phi\Big)A^\omega_x(0) - \int^t dt'\Delta_x\tilde{\Delta}_m\int^{t'} dt''\Delta_y\tilde{\Delta}_m A^\omega_y(0)\\ A_y(t) &= A_y(0) - \mathrm{i}\Delta_y\tilde{\Delta}_m\phi^\omega(0) + \mathrm{i}\int^t \tilde{\Delta}_\phi dt' A^\omega_x(0) + \int^t dt'\Delta_\phi\int^{t'} dt''\tilde{\Delta}_m\Delta_y\phi^\omega(0)\\ &- \int^t dt'\Big(\Delta_y\tilde{\Delta}_m\int^{t'} dt''\Delta_y\tilde{\Delta}_m - \Delta_\phi\int^{t'} dt''\Delta_\phi\Big)A^\omega_y(0) - \int^t dt'\Delta_y\tilde{\Delta}_m\int^{t'} dt''\Delta_x\tilde{\Delta}_m A^\omega_x(0)\end{aligned} \tag{B.19}$$

where, we have used $\Psi_{int}(0) = \Psi(0)$ and $\tilde{\Delta}_m = \int^t \Delta_m dt'$(B.13). Upto second order in the perturbative evaluation of stokes parameters we have found that the magnetic field background contributes separately with the axion background. We will consider the contribution coming solely from axion background. So, without magnetic field background. We have found the expression of Stokes parameters (considering $\Delta_x = 0 = \Delta_y$)

$$\begin{aligned}I(t) &= I(0)\Big\{1 + \tilde{\Delta}^*_\phi\tilde{\Delta}_\phi + \int^t dt'(\Delta_\phi\tilde{\Delta}_\phi + c.c)\Big\} + (\tilde{\Delta}_\phi + \tilde{\Delta}^*_\phi)V(0)\\ Q(t) &= Q(0)\Big\{1 - \tilde{\Delta}^*_\phi\tilde{\Delta}_\phi + \int^t dt'(\Delta_\phi\tilde{\Delta}_\phi + c.c)\Big\} - \mathrm{i}(\tilde{\Delta}_\phi - \tilde{\Delta}^*_\phi)U(0)\\ U(t) &= U(0)\Big\{1 - \tilde{\Delta}^*_\phi\tilde{\Delta}_\phi + \int^t dt'(\Delta_\phi\tilde{\Delta}_\phi + c.c)\Big\} + \mathrm{i}Q(0)(\tilde{\Delta}_\phi - \tilde{\Delta}^*_\phi)\\ V(t) &= V(0)\Big\{1 - \tilde{\Delta}^*_\phi\tilde{\Delta}_\phi + \int^t dt'(\Delta_\phi\tilde{\Delta}_\phi + c.c)\Big\} + I(0)(\tilde{\Delta}_\phi + \tilde{\Delta}^*_\phi)\\ Q(t) &\pm \mathrm{i}U(t) = \{1 \mp (\tilde{\Delta}_\phi - \tilde{\Delta}^*_\phi)\}\langle Q(0) \pm \mathrm{i}U(0)\rangle \sim e^{\mp\mathrm{i}\theta}\langle Q(0) \pm \mathrm{i}U(0)\rangle\end{aligned} \tag{B.20}$$

It can be checked from the above expressions of stokes parameters that, ϕ being real, there will be no conversion between axion and photon. But different helicity states will be affected and time dependence of the axion field would lead to distinguishable effects. The rotation (up to first order in the coupling constant) of the plane of linear polarization, for very small θ, can be identified as $\theta \sim (\tilde{\Delta}_\phi - \tilde{\Delta}^*_\phi)/\mathrm{i}$. And the interesting point is that because of the ringing oscillation we will see time varying rotation of the linear polarization.

B.3 Source terms in the nonhomogeneous differential equations of the EM field

In this section, we have presented the explicit expression of the source terms of the following set of equations, discussed (3.6) in the chapter.3,

$$\begin{aligned}\mathcal{L}_0\chi_1^{lm}+\mathcal{Q}^i_{lmc\gamma}(h)\chi_i^{c\gamma}+\bar{\mathcal{Q}}^i_{lmc\gamma}(h^*)\chi_i^{c\gamma}=0\\ \mathcal{L}_0\chi_2^{lm}+\mathcal{R}^i_{lmc\gamma}(h)\chi_i^{c\gamma}+\bar{\mathcal{R}}^i_{lmc\gamma}(h^*)\chi_i^{c\gamma}=0\end{aligned} \tag{B.21}$$

The expression for the source terms $\mathcal{Q}^i_{lmc\gamma}(h)\chi_i^{c\gamma}$ can be expressed as

$$\mathcal{Q}^i_{lmc\gamma}(h)\chi_i^{c\gamma}=\partial_r(E0)-\frac{1}{f(r)}\partial_t(E1) \tag{B.22}$$

where, E_0 and E_1 have the following structure:

$$\begin{aligned}
E0=\frac{e^{-i\omega t}}{2}\Bigg[&\Lambda^{(0,0)}_{c\gamma lm}\Big\{-f(r)c(c+1)\chi_1^{c\gamma}(t,r)(-2\tilde{h}_{20}^{(1)(e)}(2\sqrt{5}))+\frac{1}{r^2}\partial_t\chi_2^{c\gamma}(t,r)\tilde{h}_{20}^{(2)}(2\sqrt{5})c(c+1)\\
&-\chi_4^{c\gamma}(t,r)\tilde{G}_{20}c(c+1)2\sqrt{5}+\frac{1}{r^2}\partial_t\chi_2^{c\gamma}(t,r)\tilde{h}_{20}^{(2)}\frac{3}{2}\sqrt{\frac{5}{\pi}}4\gamma\frac{\pi}{3}\frac{1}{\sqrt{4\pi}}\Big\}\\
&+\Lambda^{(1,0)}_{c\gamma lm}(t,r)\Bigg\{\mathrm{i}\gamma\partial_t\chi_2^{c\gamma}(t,r)\Big(-2(\tilde{H}_{20}+\tilde{G}_{20})\sqrt{15}-2\tilde{G}_{20}\frac{3}{2}\sqrt{\frac{5}{\pi}}\Big(2\gamma\sqrt{\frac{\pi}{3}}\Big)\Big)\\
&-2f(r)\partial_t\chi_2^{c\gamma}(t,r)(-\mathrm{i}\gamma\partial_r\tilde{h}_{20}^{(1)(e)}\sqrt{15})-f(r)\Big(-c(c+1)\partial_r\chi_1^{c\gamma}(t,r)(2(\tilde{K}_{20}-3\tilde{G}_{20}))\\
&-2\partial_r\chi_4^{c\gamma}(t,r)(-\mathrm{i}\gamma\tilde{h}_{20}^{(1)(o)}\sqrt{15})-2\chi_4^{c\gamma}(t,r)(-\mathrm{i}\gamma\partial_r h_{20}^{(1)(o)}\sqrt{15})\\
&-2\mathrm{i}\gamma\tilde{H}_{20}^{(1)}\partial_r\chi_2^{c\gamma}(t,r)\sqrt{15}+c(c+1)\chi_1^{c\gamma}(t,r)2\tilde{h}_{20}^{(1)(o)}(-\mathrm{i}\gamma\sqrt{15})+2\partial_t\partial_r\chi_2^{c\gamma}(t,r)(-\tilde{h}_{20}^{(1)(e)}\sqrt{15})\Big)\\
&-\chi_4^{c\gamma}(t,r)\tilde{h}_{20}^{(2)}\Big(3\mathrm{i}\gamma\sqrt{15}+2\mathrm{i}\gamma 2\gamma\sqrt{\frac{\pi}{3}}\frac{3}{2}\sqrt{\frac{5}{\pi}}-\mathrm{i}\gamma\frac{3}{2}\sqrt{\frac{5}{\pi}}2\sqrt{\frac{\pi}{3}}\Big)\Bigg\}\\
&+\Lambda^{(2,0)}_{c\gamma lm}\Bigg\{-f(r)\Big(-c(c+1)\chi_1^{c\gamma}(t,r)\partial_r(2(\tilde{K}_{20}-3\tilde{G}_{20}))+c(c+1)\chi_1^{c\gamma}(t,r)4\tilde{h}_{20}^{(1)(e)}\\
&+2\chi_3^{c\gamma}(t,r)\tilde{H}_{20}^{(1)}c(c+1)\Big)-\chi_4^{c\gamma}(t,r)\Big(-2c(c+1)\tilde{H}_{20}-2\tilde{G}_{20}c(c+1)\Big)\\
&+\frac{1}{r^2}\partial_t\chi_2^{c\gamma}(t,r)\tilde{h}_{20}^{(2)}\Big(-2c(c+1)+\frac{3}{2}\sqrt{\frac{5}{\pi}}4\gamma\frac{\pi}{3}\frac{2}{\sqrt{20\pi}}\Big)\Bigg\}\\
&+\tilde{\Lambda}^{(2,0)}_{c\gamma lm}\Bigg\{f(r)\Big(2\partial_r\chi_4^{c\gamma}(t,r)\tilde{h}_{20}^{(1)(e)}+2\chi_4^{c\gamma}(t,r)\partial_r\tilde{h}_{20}^{(1)(e)}-c(c+1)\chi_1^{c\gamma}(t,r)2\tilde{h}_{20}^{(1)(o)}+2\chi_3^{c\gamma}(t,r)\tilde{H}_{20}^{(1)}\\
&+4\partial_t\partial_r\chi_2^{c\gamma}(t,r)\tilde{h}_{20}^{(1)(o)}+2\partial_t\chi_2^{c\gamma}(t,r)\partial_r\tilde{h}_{20}^{(1)(o)}\Big)-2\chi_4^{c\gamma}(t,r)(\tilde{H}_{20}+\tilde{G}_{20})+\frac{3}{r^2}\partial_t\chi_2^{c\gamma}(t,r)\tilde{h}_{20}^{(2)}\Bigg\}\\
&+\frac{1}{r^2}\partial_t\chi_2^{c\gamma}(t,r)\tilde{h}_{20}^{(2)}\Big\{\frac{3}{2}\sqrt{\frac{5}{\pi}}\Big(\frac{2}{3}\sqrt{2\pi}\sqrt{(c-\gamma)(c+\gamma+1)}\frac{1}{\sqrt{4\pi}}\Lambda^{(2,-1)}_{c\gamma+1lm}\Big)\Big\}+\frac{2}{r^2}\chi_4^{lm}(t,r)\tilde{G}_{20}m^2\frac{3}{2}\sqrt{\frac{5}{\pi}}\Bigg]
\end{aligned} \tag{B.23}$$

and,

$$
\begin{aligned}
E1 = \frac{e^{-\mathrm{i}\omega t}}{2}\Bigg[&\Lambda^{(0,0)}_{c\gamma lm}(t,r)\Big\{-\partial_r\chi_2^{c\gamma}(t,r)f(r)\frac{\tilde{h}^{(2)}_{20}}{r^2}\frac{3}{2}\sqrt{\frac{5}{\pi}}4(\gamma-c(c+1))\frac{\pi}{3}\frac{1}{\sqrt{4\pi}}\\
&+2\chi_2^{c\gamma}(t,r)\Big(-c(c+1)f(r)\frac{\tilde{h}^{(1)(\mathrm{o})}_{20}}{r^2}(\sqrt{5})+c(c+1)2\sqrt{\frac{\pi}{3}}f(r)\frac{\tilde{h}^{(1)(\mathrm{o})}_{20}}{r^2}\sqrt{15}(\frac{1}{\sqrt{4\pi}})\Big)\\
&+f(r)\tilde{G}_{20}\frac{3}{2}\sqrt{\frac{5}{\pi}}\Big(-\chi_3^{c\gamma}(t,r)c(c+1)4\frac{\pi}{3}\frac{1}{\sqrt{4\pi}}\Big)\Big\}+\Lambda^{(1,0)}_{c\gamma lm}\Big\{2\chi_4^{c\gamma}(t,r)\gamma\omega\tilde{h}^{(1)(\mathrm{o})}_{20}\sqrt{15}\\
&-\partial_r\chi_2^{c\gamma}(t,r)f(r)2\mathrm{i}\gamma(\tilde{H}_{20}-\tilde{G}_{20})\sqrt{15}+\partial_t\chi_4^{c\gamma}(t,r)\mathrm{i}\gamma\tilde{h}^{(1)(\mathrm{o})}_{20}\sqrt{15}-\partial_t\chi_2^{c\gamma}(t,r)(-2\tilde{H}^{(1)}_{20}\sqrt{15}\mathrm{i}\gamma\\
&+2\gamma\omega h^{(1)(\mathrm{e})}_{20}\sqrt{15})+\partial_t^2\chi_2^{c\gamma}(t,r)(-2\mathrm{i}\gamma\tilde{h}^{(1)(\mathrm{e})}_{20}\sqrt{15})+2\chi_2^{c\gamma}(t,r)(-c(c+1)\mathrm{i}\gamma f(r)h^{(1)(\mathrm{e})}_{20}\sqrt{15})\\
&+\chi_3^{c\gamma}(t,r)f(r)\mathrm{i}\gamma\frac{\tilde{h}^{(2)}_{20}}{r^2}2\sqrt{15}(1-\gamma)+f(r)\tilde{G}_{20}\frac{3}{2}\sqrt{\frac{5}{\pi}}2\mathrm{i}\gamma\partial_r\chi_2^{c\gamma}(t,r)2\gamma\sqrt{\frac{\pi}{3}}\Big\}\\
&+\Lambda^{(1,-1)}_{c\gamma+1lm}\Big(2\sqrt{\frac{2\pi}{3}}\sqrt{(c-\gamma)(c+\gamma+1)}\Big)\Big\{\mathrm{i}\gamma\chi_3^{c\gamma}(t,r)f(r)\frac{\tilde{h}^{(2)}_{20}}{r^2}+2\mathrm{i}\gamma f(r)\tilde{G}_{20}\partial_r\chi_2^{c\gamma}(t,r)\frac{3}{2}\sqrt{\frac{5}{\pi}}\Big\}\\
&+\Lambda^{(2,0)}_{c\gamma lm}\Big\{2\chi_4^{c\gamma}(t,r)\tilde{H}^{(1)}_{20}(-c(c+1))-\partial_r\chi_2^{c\gamma}(t,r)f(r)\frac{\tilde{h}^{(2)}_{20}}{r^2}\frac{3}{2}\sqrt{\frac{5}{\pi}}4(\gamma-c(c+1))\frac{\pi}{3}\frac{1}{\sqrt{4\pi}}\\
&+2\chi_2^{c\gamma}\Big(-c(c+1)f(r)\frac{\tilde{h}^{(1)(\mathrm{o})}_{20}}{r^2}(-4)+c(c+1)2\sqrt{\frac{\pi}{3}}f(r)\frac{\tilde{h}^{(1)(\mathrm{o})}_{20}}{r^2}\sqrt{15}(\frac{2}{\sqrt{20\pi}})\Big)\\
&+\chi_3^{c\gamma}(t,r)f(r)\Big(2\tilde{H}_{20}c(c+1)\Big)+2(\tilde{K}_{20}-3\tilde{G}_{20})\Big(\mathrm{i}\omega c(c+1)\chi_1^{c\gamma}(t,r)-c(c+1)\partial_t\chi_1^{c\gamma}(t,r)\Big)\\
&+f(r)\tilde{G}_{20}\frac{3}{2}\sqrt{\frac{5}{\pi}}\Big(-\chi_3^{c\gamma}(t,r)c(c+1)4\frac{\pi}{3}\frac{2}{\sqrt{20\pi}}\Big)\Big\}\\
&-\Lambda^{(2,-1)}_{c\gamma+1lm}\partial_r\chi_2^{c\gamma}(t,r)f(r)\frac{\tilde{h}^{(2)}_{20}}{r^2}\frac{3}{2}\sqrt{\frac{5}{\pi}}\Big(\frac{2}{3}\sqrt{2\pi}\sqrt{(c-\gamma)(c+\gamma+1)}\frac{1}{\sqrt{4\pi}}\Big)\\
&+\tilde{\Lambda}^{(2,0)}_{c\gamma lm}\Big\{2\chi_4^{c\gamma}(t,r)\tilde{H}^{(1)}_{20}+2\chi_4^{c\gamma}(t,r)\mathrm{i}\omega\tilde{h}^{(1)(\mathrm{e})}_{20}-2\partial_t\chi_4^{c\gamma}(t,r)\tilde{h}^{(1)(\mathrm{e})}_{20}-\partial_r\chi_2^{c\gamma}(t,r)3f(r)\frac{\tilde{h}^2_{20}}{r^2}\\
&-\partial_t\chi_2^{c\gamma}(t,r)\{-2\mathrm{i}\omega\tilde{h}^{(1)(\mathrm{o})}_{20}\}+\partial_t^2\chi_2^{c\gamma}(t,r)(-2\tilde{h}^{(1)(\mathrm{o})}_{20})+2\chi_2^{c\gamma}\Big(-c(c+1)f(r)\frac{\tilde{h}^{(1)(\mathrm{o})}_{20}}{r^2}\Big)\\
&+\chi_3^{c\gamma}(t,r)f(r)\Big(-2\tilde{H}_{20}+2\tilde{G}_{20}\Big)\Big\}\\
&+f(r)\tilde{G}_{20}\frac{3}{2}\sqrt{\frac{5}{\pi}}\chi_3^{lm}(t,r)(-2m^2+l(l+1))+\partial_r\chi_2^{lm}(t,r)f(r)\frac{\tilde{h}^{(2)}_{20}}{r^2}\frac{3}{2}\sqrt{\frac{5}{\pi}}\Big(2m^2-l(l+1)\Big)\Bigg]
\end{aligned}
\tag{B.24}
$$

Given the expression for $\mathcal{Q}^i_{lmc\gamma}(h)\chi_i^{c\gamma}$, one can derive the contribution $\bar{\mathcal{Q}}^i_{lmc\gamma}(h^*)\chi_i^{c\gamma}$ coming from the complex conjugate part of the background metric by simply taking the conjugate of every metric coefficients that appeared in the previous equation for (B.22). As a consequence, we also have a 1/2 factor in front of every source term. For the source terms in the equation (B.21)

governing χ_2^{lm}, we have,

$$\mathcal{R}^i_{lmc\gamma}(h)\chi_i^{c\gamma} = \frac{e^{-\mathrm{i}\omega t}}{2}\Bigg[\Lambda^{(0,0)}_{c\gamma lm}\Big\{\chi_3^{c\gamma}\Big(-\frac{2f(r)\tilde{h}^{(2)}_{20}}{r^3}+\frac{(\tilde{h}^{(2)}_{20}f'(r)+f(r)\partial_r\tilde{h}^{(2)}_{20})}{r^2}\Big)2\sqrt{5}\gamma(\gamma+1)$$
$$+\chi_3^{c\gamma}\frac{2f(r)\tilde{h}^{(1)(\mathrm{o})}_{20}}{r^2}2\gamma(\gamma+1)\sqrt{5}+\partial_r\chi_3^{c\gamma}\frac{f(r)\tilde{h}^{(2)}_{20}}{r^2}2\sqrt{5}\gamma(\gamma+1)+\chi_4^{lm}\frac{\mathrm{i}\omega}{r^2f(r)}\tilde{h}^{(2)}_{20}2\sqrt{5}\gamma(\gamma+1)$$
$$+\mathrm{i}\chi_4^{c\gamma}\frac{1}{r^2f(r)}\tilde{h}^{(2)}_{20}2\sqrt{5}\gamma(\gamma+1)-\frac{\gamma(\gamma+1)}{r^2}\Big(2\mathrm{i}\omega\chi_1^{c\gamma}(t,r)-\partial_t\chi_1^{c\gamma}(t,r)\Big)\tilde{h}^{(1)(\mathrm{o})}_{20}(\sqrt{10}-\sqrt{5})$$
$$-\chi_2^{c\gamma}(t,r)2\gamma(\gamma+1)\Big(\frac{2}{r^3}f(r)\tilde{h}^{(1)(\mathrm{e})}_{20}-\frac{1}{r^2}\partial_r\tilde{h}^{(1)(\mathrm{e})}_{20}-\frac{1}{r^2}\tilde{h}^{(1)(\mathrm{e})}_{20}f'(r)\Big)(\sqrt{10}-\sqrt{5})$$
$$+\chi_2^{c\gamma}(t,r)\gamma(\gamma+1)\frac{1}{r^2}2(\tilde{K}_{20}-3\tilde{G}_{20})(\sqrt{10}-\sqrt{5})+\partial_r\chi_2^{lm}(t,r)\Big(f'(r)l(l+1)2\tilde{G}_{20}\sqrt{5}$$
$$-f(r)\frac{1}{r^2}2\tilde{h}^{(1)(\mathrm{e})}_{20}2l(l+1)\sqrt{5}+f(r)\frac{1}{r^2}2l(l+1)\tilde{h}^{(1)(\mathrm{e})}_{20}(\sqrt{10}-\sqrt{5})-4i\omega\tilde{H}^1_{20}l(l+1)\sqrt{5}\Big)$$
$$+\partial_r^2\chi_2^{lm}(t,r)f(r)l(l+1)2\tilde{G}_{20}\sqrt{5}\Big\}$$
$$+\Lambda^{(1,0)}_{c\gamma lm}\Big\{2\gamma\omega\tilde{H}^{(1)}_{20}\sqrt{15}\chi_3^{c\gamma}(t,r)-6f(r)\mathrm{i}\gamma\sqrt{\frac{5}{3}}\partial_r\tilde{G}_{20}\chi_3^{c\gamma}(t,r)-f'(r)2\tilde{G}_{20}\sqrt{15}\mathrm{i}\gamma\chi_3^{c\gamma}(t,r)$$
$$-2(\tilde{H}_{20}f'(r)+f(r)\partial_r\tilde{H}_{20})\mathrm{i}\gamma\sqrt{15}\chi_3^{c\gamma}(t,r)+\frac{2f(r)\tilde{h}^{(1)(\mathrm{e})}_{20}}{r^2}(2+l(l+1))\sqrt{15}\mathrm{i}\gamma\chi_3^{c\gamma}(t,r)$$
$$-f(r)2(\tilde{G}_{20}-\tilde{H}_{20})\sqrt{15}\mathrm{i}\gamma\partial_r\chi_3^{c\gamma}(t,r)-\chi_4^{c\gamma}(t,r)2\mathrm{i}\gamma\sqrt{15}\partial_r\tilde{H}^{(1)}_{20}-2\chi_4^{c\gamma}(t,r)\sqrt{15}\frac{\gamma\omega}{f(r)}(\tilde{H}_{20}-\tilde{G}_{20})$$
$$+2\sqrt{15}\mathrm{i}m\tilde{H}^{(1)}_{20}\partial_r\chi_4^{lm}(t,r)+2G\sqrt{15}\mathrm{i}\gamma\partial_t\chi_4^{c\gamma}(t,r)+\frac{\gamma(\gamma+1)}{r^2}\Big(2i\omega\chi_1^{c\gamma}(t,r)-\partial_t\chi_1^{c\gamma}(t,r)\Big)\sqrt{15}\mathrm{i}\gamma\tilde{h}^{(1)(\mathrm{e})}_{20}$$
$$-\Big(\frac{2f(r)\tilde{h}^{(1)(\mathrm{e})}_{20}}{r^3}-\frac{(\tilde{h}^{(1)(\mathrm{e})}_{20}f'(r)+f(r)\partial_r\tilde{h}^{(1)(\mathrm{e})}_{20})}{r^2}\Big)\sqrt{15}\mathrm{i}\gamma\chi_2^{c\gamma}(t,r)$$
$$+\partial_r\chi_2^{c\gamma}(t,r)\Big(-\frac{2f(r)\tilde{h}^{(2)}_{20}}{r^3}+\frac{(\tilde{h}^{(2)}_{20}f'(r)+f(r)\partial_r\tilde{h}^{(2)}_{20})}{r^2}\Big)2\sqrt{15}\mathrm{i}\gamma$$
$$+2\partial_r\chi_2^{c\gamma}(t,r)f(r)\frac{1}{r^2}\tilde{h}^{(1)(o)}_{20}\Big((2+l(l+1))\sqrt{15}\mathrm{i}\gamma+\sqrt{15}l(l+1)\mathrm{i}\gamma\Big)$$
$$+\partial_r^2\chi_2^{c\gamma}(t,r)f(r)\frac{1}{r^2}\tilde{h}^{(2)}_{20}\sqrt{15}\mathrm{i}\gamma+\partial_t\chi_2^{c\gamma}(t,r)\mathrm{i}\omega\frac{\tilde{h}^{(2)}_{20}}{r^2f(r)}2\sqrt{15}\mathrm{i}\gamma-\partial_t^2\chi_2^{c\gamma}(t,r)\frac{1}{r^2f(r)}\tilde{h}^{(2)}_{20}2\sqrt{15}\mathrm{i}\gamma\Big\}$$
$$+\Lambda^{(2,0)}_{c\gamma lm}\Big\{-2\chi_3^{c\gamma}(t,r)\Big(-\frac{2f(r)\tilde{h}^{(2)}_{20}}{r^3}+\frac{(\tilde{h}^{(2)}_{20}f'(r)+f(r)\partial_r\tilde{h}^{(2)}_{20})}{r^2}\Big)\gamma(\gamma+1)$$
$$-8\chi_3^{c\gamma}(t,r)\frac{2f(r)\tilde{h}^{(1)(\mathrm{o})}_{20}}{r^2}l(l+1)-2\partial_r\chi_3^{c\gamma}(t,r)\frac{f(r)\tilde{h}^{(2)}_{20}}{r^2}\gamma(\gamma+1)-\chi_4^{\gamma}\frac{\mathrm{i}\omega}{r^2f(r)}\tilde{h}^{(2)}_{20}2\gamma(\gamma+1)$$
$$+\frac{2\mathrm{i}\gamma}{f(r)}\partial_t\chi_4^{c\gamma}(t,r)\Big(-\sqrt{15}\tilde{H}_{20}r^2+\frac{(\gamma+1)}{r^2}\tilde{h}^{(2)}_{20}\Big)-\frac{\gamma(\gamma+1)}{r^2}\Big(2i\omega\chi_1^{c\gamma}-\partial_t\chi_1^{c\gamma}\Big)\tilde{h}^{(1)(\mathrm{o})}_{20}(2\sqrt{2}+4)$$
$$+\chi_2^{c\gamma}\Big(-2\gamma(\gamma+1)\Big(\frac{2}{r^3}f(r)\tilde{h}^{(1)(\mathrm{e})}_{20}-\frac{f(r)}{r^2}\partial_r\tilde{h}^{(1)(\mathrm{e})}_{20}-\frac{1}{r^2}\tilde{h}^{(1)(\mathrm{e})}_{1}f'(r)\Big)(2\sqrt{2}+4)$$
$$+l(l+1)\frac{1}{r^2}2(\tilde{K}_{20}-3\tilde{G}_{20})(2\sqrt{2}+4)\Big)$$
$$+\partial_r\chi_2^{c\gamma}(t,r)\Big(-\gamma(\gamma+1)f'(r)\tilde{H}_{20}+\gamma(\gamma+1)2\tilde{G}_{20}+f(r)\frac{1}{r^2}2\gamma(\gamma+1)\tilde{h}^{(1)(\mathrm{e})}_{20}(2\sqrt{2}+12)$$
$$+2i\omega\tilde{H}^{(1)}_{20}8\gamma(\gamma+1)\Big)-\partial_r^2\chi_2^{c\gamma}(t,r)f(r)\gamma(\gamma+1)2\tilde{G}_{20}$$
$$-\partial_t\chi_2^{c\gamma}(t,r)\Big(-2\partial_r\tilde{H}^{(1)}_{20}\gamma(\gamma+1)-\mathrm{i}\omega\frac{1}{f(r)}2\gamma(\gamma+1)(\tilde{H}_{20}-\tilde{G}_{20})\Big)$$
$$+\partial_t^2\chi_2^{c\gamma}(t,r)\frac{1}{f(r)}\gamma(\gamma+1)2(\tilde{G}_{20}-\tilde{H}_{20})+4\partial_t\partial_r\chi_2^{c\gamma}(t,r)\tilde{H}^{(1)}_{20}\gamma(\gamma+1)\Big\}$$

$$
\begin{aligned}
&+\tilde{\Lambda}^{(2,0)}_{c\gamma lm}\Big\{2\chi_3^{c\gamma}(t,r)\Big(-\frac{2f(r)\tilde{h}^{(2)}_{20}}{r^3}+\frac{(\tilde{h}^{(2)}_{20}f'(r)+f(r)\partial_r\tilde{h}^{(2)}_{20})}{r^2}\Big)\\
&-\chi_3^{c\gamma}(t,r)\frac{2f(r)\tilde{h}^{(1)(\mathrm{o})}_{20}}{r^2}2\gamma(\gamma+1)(3+\gamma(\gamma+1))+2\partial_r\chi_3^{c\gamma}(t,r)\frac{f(r)\tilde{h}^{(2)}_{20}}{r^2}+2\chi_4^{c\gamma}(t,r)\frac{\mathrm{i}\omega}{r^2f(r)}\tilde{h}^{(2)}_{20}\\
&-2\partial_t\chi_4^{c\gamma}(t,r)\frac{1}{r^2f(r)}\tilde{h}^{(2)}_{20}+\Big(2i\omega\frac{\gamma(\gamma+1)}{r^2}\chi_1^{c\gamma}(t,r)-\frac{\gamma(\gamma+1)}{r^2}\partial_t\chi_1^{c\gamma}(t,r)\Big)\tilde{h}^{(1)(\mathrm{o})}_{20}\\
&+\chi_2^{c\gamma}(t,r)\Big(2\gamma(\gamma+1)\Big(\frac{2}{r^3}f(r)\tilde{h}^{(1)(e)}_{20}-\frac{1}{r^2}\partial_r\tilde{h}^{(1)(e)}_{20}-\frac{1}{r^2}\tilde{h}^{(1)(\mathrm{e})}_{20}f'(r)\Big)-\gamma(\gamma+1)\frac{1}{r^2}4(\tilde{K}_{20}-3\tilde{G}_{20})\\
&+\partial_r\chi_2^{c\gamma}(t,r)\Big(f'(r)\tilde{H}_{20}+f'(r)2G-f(r)\frac{1}{r^2}2\tilde{h}^{(1)(\mathrm{e})}_{20}(3+\gamma(\gamma+1))-f(r)\frac{1}{r^2}2l(l+1)\tilde{h}^{(1)(\mathrm{e})}_{20}\\
&-f(r)2\partial_r(\tilde{K}_{20}-3\tilde{G}_{20})-2i\omega\tilde{H}^1_{20}(3+\gamma(\gamma+1))\Big)+\partial_r^2\chi_2^{c\gamma}(t,r)\Big(f(r)2\tilde{G}_{20}+2f(r)\tilde{H}_{20}\Big)\\
&-\partial_t\chi_2^{c\gamma}(t,r)\Big(2\partial_r\tilde{H}^{(1)}_{20}+\frac{2\mathrm{i}\omega}{f(r)}(\tilde{H}_{20}-\tilde{G}_{20})\Big)+\partial_t^2\chi_2^{c\gamma}(t,r)\frac{2}{f(r)}(\tilde{H}_{20}-\tilde{G}_{20})-4\partial_t\partial_r\chi_2^{c\gamma}(t,r)\tilde{H}^{(1)}_{20}\Big\}\\
&+3\mathrm{i}S_{c\gamma lm}\sqrt{\frac{5}{\pi}}\gamma\Big\{\chi_3^{c\gamma}(t,r)\Big(-f'(r)\tilde{G}_{20}+\frac{2f(r)\tilde{h}^{(1)(\mathrm{e})}_{20}}{r^2}\Big)-\partial_r\chi_3^{c\gamma}(t,r)f(r)\tilde{G}_{20}\Big)+\partial_t\chi_4^{c\gamma}(t,r)\tilde{G}_{20}r^2\\
&+\partial_r\chi_2^{c\gamma}(t,r)\Big(\Big(-\frac{2f(r)\tilde{h}^{(2)}_{20}}{r^3}+\frac{(\tilde{h}^{(2)}_{20}f'(r)+f(r)\partial_r\tilde{h}^{(2)}_{20})}{r^2}\Big)+2f(r)\frac{1}{r^2}\tilde{h}^{(1)(\mathrm{o})}_{20}\Big)\\
&+\partial_r^2\chi_2^{c\gamma}(t,r)f(r)\frac{1}{r^2}\tilde{h}^{(2)}_{20}+\partial_t\chi_2^{c\gamma}(t,r)\mathrm{i}\omega\frac{\tilde{h}^{(2)}_{20}}{r^2f(r)}-\partial_t^2\chi_2^{c\gamma}(t,r)\frac{1}{r^2f(r)}\tilde{h}^{(2)}_{20}\Big\}\\
&+3\tilde{S}_{c\gamma lm}\sqrt{\frac{5}{\pi}}\Big\{-\chi_3^{c\gamma}(t,r)\frac{f(r)\tilde{h}^{(1)(\mathrm{o})}_{20}}{r^2}2\gamma(\gamma+1)+\partial_r\chi_2^{c\gamma}(t,r)\Big(-f(r)\frac{1}{r^2}\tilde{h}^{(1)(\mathrm{e})}_{20}-i\omega\tilde{H}^{(1)}_{20}\Big)\Big\}\\
&+\chi_3^{lm}(t,r)\Big(3m^2\sqrt{\frac{5}{\pi}}\Big)\Big\{\Big(\frac{2f(r)\tilde{h}^{(2)}_{20}}{r^3}\frac{(\tilde{h}^{(2)}_{20}f'(r)+f(r)\partial_r\tilde{h}^{(2)}_{20})}{r^2}\Big)+\frac{2f(r)\tilde{h}^{(1)(\mathrm{o})}_{20}}{r^2}2l(l+1)\Big\}\\
&+\partial_r\chi_3^{lm}(t,r)\Big\{\frac{f(r)\tilde{h}^{(2)}_{20}}{r^2}\Big(-3m^2\sqrt{\frac{5}{\pi}}\Big)\Big\}+\chi_4^{lm}(t,r)\Big\{\frac{\mathrm{i}\omega}{r^2f(r)}\tilde{h}^{(2)}_{20}\Big(-3m^2\sqrt{\frac{5}{\pi}}\Big)\Big\}\\
&+\partial_t\chi_4^{lm}(t,r)\Big\{-\frac{1}{r^2f(r)}\tilde{h}^{(2)}_{20}\Big(-3m^2\sqrt{\frac{5}{\pi}}\Big)\Big\}+\chi_2^{lm}(t,r)\Big\{-l^2(l+1)^2(\tilde{K}_{20}-3\tilde{G}_{20})\Big)\Big)\Big\}\\
&+\partial_r\chi_2^{lm}(t,r)\Big\{+2(f(r)\tilde{H}'_{20}-f(r)\Big(-2l(l+1)\partial_r(\tilde{K}_{20}-3\tilde{G}_{20})\Big)-f'(r)3m^2\tilde{G}_{20}\sqrt{\frac{5}{\pi}}\\
&+f(r)\frac{1}{r^2}2\tilde{h}^{(1)(\mathrm{e})}_{20}\Big(3m^2\sqrt{\frac{5}{\pi}}\Big)\\
&+2i\omega\tilde{H}^{(1)}_{20}\Big(3m^2\sqrt{\frac{5}{\pi}}\Big)\Big\}-\partial_r^2\chi_2^{lm}(t,r)\Big\{f(r)\Big(3m^2\tilde{G}_{20}\sqrt{\frac{5}{\pi}}\Big)\Big\}+\partial_t^2\chi_2^{lm}(t,r)\Big\{\frac{1}{f(r)}\Big(3m^2\tilde{G}_{20}\sqrt{\frac{5}{\pi}}\Big)\Big\}\Big]
\end{aligned}
\tag{B.25}
$$

Some mathematical quantities we have utilized in the above equation, constructed out of $\Lambda^{(l',m')}_{lmc\gamma}$, are,

$$\begin{aligned}
S_{lmc\gamma} &\equiv 2m\sqrt{\frac{\pi}{3}}\sum_{c\gamma}\Lambda^{(1,0)}_{lmc\gamma} + 2\sqrt{\frac{2\pi}{3}}\sqrt{(l-m)(l+m+1)}\Lambda^{(1,-1)}_{lm+1c\gamma} \\
\tilde{S}_{lmc\gamma} &\equiv \frac{m}{3}\sqrt{4\pi}\Lambda^{(0,0)}_{lmc\gamma} + \frac{2m}{3}\sqrt{\frac{4\pi}{5}}\Lambda^{(2,0)}_{lmc\gamma} + 4\sqrt{2}\frac{\pi}{3}\sqrt{(l-m)(l+m+1)}\frac{1}{\sqrt{4\pi}}\Lambda^{(2,-1)}_{lm+1c\gamma} \\
\tilde{\Lambda}^{(2,0)}_{lmc\gamma} &\equiv -\Big[2m\Lambda^{(2,0)}_{lmc\gamma} + m\sqrt{5}\Lambda^{(0,0)}_{lmc\gamma} + \sqrt{(l-m)(l+m+1)}3\sqrt{\frac{2}{3}}\Lambda^{(2,-1)}_{lm+1c\gamma}\Big]
\end{aligned} \tag{B.26}$$

Given the expression for $\mathcal{R}^i_{lmc\gamma}(h)\chi_i^{c\gamma}$ one can derive the contribution $\bar{\mathcal{R}}^i_{lmc\gamma}(h)\chi_i^{c\gamma}$ in the same way described for $\bar{\mathcal{Q}}^i_{lmc\gamma}(h)\chi_i^{c\gamma}$.

B.4 Evaluation of the normalization factors

In the following discussion, our main focus will be to calculate the incident energy density and to formulate the procedure to calculate the normalization factors. We start with a circularly polarized [120] ingoing plane EM wave, in u-coordinate, propagating along z-direction towards the black hole as,

$$\begin{aligned}
A_x(u,x) &= e^{-\mathrm{i}k(u+2z)} \\
A_y(u,x) &= \mathrm{i}e^{-\mathrm{i}k(u+2z)}.
\end{aligned} \tag{B.27}$$

The approach to finding out the normalization factor is to compare the incident plane wave with the asymptotic form of the field solution, which is obtained in spherical coordinates. We, therefore, need to transform the plane EM wave written in cartesian coordinate, $\mathbf{A} = A_x\hat{x} + A_y\hat{y}$, to spherical coordinate by using, $A'_\mu(x') = (\partial x^\nu/\partial x'^\mu)A_\nu(x)$ as,

$$\begin{aligned}
A'_u(u,\mathbf{r}) &= A_u(u,\mathbf{x}); \quad A'_r(u,\mathbf{r}) = \sin\theta e^{\mathrm{i}\phi}A_x(u,\bar{x}) \\
A'_\theta(u,\mathbf{r}) &= r\cos\theta e^{\mathrm{i}\phi}A_x(u,\bar{x}); \quad A'_\phi(u,\mathbf{r}) = ir\sin\theta e^{\mathrm{i}\phi}A_x(u,\bar{x}),
\end{aligned} \tag{B.28}$$

where, we have used $A_z = 0$ and $A_y = \mathrm{i}A_x$. Of course, $A_x(u,\bar{x})$ should be expressed in spherical coordinates using Rayleigh expansion of the spatial part of a plane wave propagating along the z-direction given by

$$e^{-\mathrm{i}kz} = e^{-\mathrm{i}kr\cos\theta} = \sum_{l=0}(2l+1)\mathrm{i}^l j_l(\mathrm{k}r)P^0_l(\cos\theta). \tag{B.29}$$

Taking the derivative with respect to θ on both sides of the above equation one can discover the following expression also

$$e^{-\mathrm{i}kz} = e^{-\mathrm{i}kr\cos\theta} = \sum_{l=0}(2l+1)\mathrm{i}^l\frac{j_l(\mathrm{k}r)}{\mathrm{i}\mathrm{k}r}\frac{\partial_\theta P^0_l(\cos\theta)}{\sin\theta}. \tag{B.30}$$

Where one needs to use the relation $P_l^1(\cos\theta) = -\partial_\theta P_l^0(\cos\theta)$. Finally, one obtains the components of plane EM waves for circularly polarized light in spherical coordinates as [124],

$$\begin{aligned}
A'_u(u,\mathbf{r}) &= \sum_{lm} A'^{lm}_u(u,r)Y_{lm}(\Omega) = 0\\
A'_r(u,\mathbf{r}) &= \sum_{lm} A'^{lm}_r(u,r)Y_{lm}(\Omega)\\
&= \sum_{lm}(-1)^{l+1}\delta_{m1}\sqrt{4\pi(2l+1)l(l+1)}\frac{e^{-\mathrm{ik}(u+2r_*)}}{2\mathrm{k}^2r^2}Y_{lm}(\Omega) + \textit{outgoing part}\\
A'_s(u,\bar{r}) &= -\sum_{lm}(-1)^{l+1}\delta_{m1}\sqrt{\frac{4\pi(2l+1)}{l(l+1)}}\left[\mathrm{i}\Psi_s^{lm}(\Omega) + \Phi_s^{lm}(\Omega)\right]\frac{e^{-\mathrm{ik}(u+2r_*)}}{2k} + \textit{outgoing part}
\end{aligned} \tag{B.31}$$

Note that the δ_{m1} factor in the above expressions comes due to $e^{i\phi}$ in the A'_u and A'_ϕ components of the gauge field (see Eq.B.28 and B.31). The above expansions could be checked following $j_l(\mathrm{kr}) + \mathrm{i}n_l(\mathrm{kr}) \sim \frac{(-\mathrm{i})^{l+1}e^{\mathrm{ikr}}}{\mathrm{kr}}$, $j_l(\mathrm{kr}) - \mathrm{i}n_l(\mathrm{kr}) \sim \frac{\mathrm{i}^{l+1}e^{-\mathrm{ikr}}}{\mathrm{kr}}$ for $r \to \infty$ or $\mathrm{kr} >> 1$, that implies $j_l(\mathrm{kr}) \sim i^{l+1}\frac{e^{-\mathrm{ikr}}}{2\mathrm{kr}} + (-i)^{l+1}\frac{e^{\mathrm{ikr}}}{2\mathrm{kr}}$. Gauge invariant variables for circularly polarized light in this new gauge become

$$\begin{aligned}
\sum_{lm}\tilde{\chi}_1^{klm}(u,r)Y^{lm}(\Omega) &= \sum_{lm}\frac{r^2}{l(l+1)}(\partial_u A'^{lm}_r - \partial_r A'^{lm}_u)\\
&= -\mathrm{i}\sum_{lm}(-1)^{l+1}\delta_{m1}\sqrt{\frac{4\pi(2l+1)}{l(l+1)}}\frac{e^{-\mathrm{ik}(u+2r_*)}}{2\mathrm{k}}Y_{lm}(\Omega) + \textit{out going}
\end{aligned} \tag{B.32}$$

Also in the expansion of $A'_s(u,\bar{r})$ (B.31) one can check that the term with $\Phi_s^{lm}(\Omega)$ does not transform, and we denote this as,

$$\sum_{lm}\tilde{\chi}_2^{klm}(u,r)\Phi_s^{lm}(\Omega) = -\sum_{lm}(-1)^{l+1}\delta_{m1}\sqrt{\frac{4\pi(2l+1)}{l(l+1)}}\frac{e^{-\mathrm{ik}(u+2r_*)}}{2\mathrm{k}}\Phi_s^{lm}(\Omega) + \textit{out going} \tag{B.33}$$

(recall the $\frac{r^2}{l(l+1)}$ factor in the definition of $\tilde{\chi}_1$ from the main chapter). With the above gauge invariant variables, one can deduce the normalization factors from the asymptotic form of these fields,

$$\begin{aligned}
\sum_{lm}\tilde{\chi}_1^{klm}(u,r)Y^{lm}(\Omega) &= \sum_{lm}\mathcal{N}_1^{klm}[\mathcal{I}_1(u)e^{-\mathrm{ik}(u+2r_*)} + \mathcal{R}_1(u)e^{-\mathrm{ik}u}]Y_{lm}(\Omega),\\
\sum_{lm}\tilde{\chi}_2^{klm}(u,r)\Phi_s^{lm}(\Omega) &= \sum_{lm}\mathcal{N}_2^{klm}[\mathcal{I}_2(u)e^{-\mathrm{ik}(u+2r_*)} + \mathcal{R}_2(u)e^{-\mathrm{ik}u}]\Phi_s^{lm}(\Omega).
\end{aligned} \tag{B.34}$$

Comparing with (B.32) we fix the normalization factor to be

$$\begin{aligned}
\mathcal{N}_1^{klm} &= -\mathrm{i}(-1)^{l+1}\delta_{m1}\sqrt{\frac{4\pi(2l+1)}{l(l+1)}}\frac{1}{2\mathrm{k}\mathcal{I}_1(u\to\infty)},\\
\mathcal{N}_2^{klm} &= (-1)^l\delta_{m1}\sqrt{\frac{4\pi(2l+1)}{l(l+1)}}\frac{1}{2\mathrm{k}\mathcal{I}_2(u\to\infty)}.
\end{aligned} \tag{B.35}$$

We proceed with this crude approximation, considering only the effect in the static limit $u \to \infty$ and time dependent effect in the energy density will come from the rest of the part of the solution. We follow the definition of the incident energy density discussed in the previous section,

$$\partial_u \mathcal{G}_{in} = \mathscr{T}^z{}_u = [\mathscr{T}_{uz} - \mathscr{T}_{uu}], \tag{B.36}$$

but we will transform this quantity to the spherical coordinate using,

$$\mathscr{T}'_{\mu\nu}(x') = (\partial x^\alpha/\partial x'^\mu)\left(\partial x^\beta/\partial x'^\nu\right)\mathscr{T}_{\alpha\beta}(x) \tag{B.37}$$

So, after simplification,

$$\partial_u \mathcal{G} = \left\{\frac{1}{2} g^{ss}(\partial_u A_s - \partial_s A_u)(\partial_r A_s^* - \partial_s A_r^*) + c.c.\right\} - g^{ss}(\partial_u A_s - \partial_s A_u)(\partial_u A_s^* - \partial_s A_u^*) \tag{B.38}$$

and as the incident plane wave is considered to be propagating along the z-direction we suitably choose, $\theta \to 0$, as per the requirement.

In the following discussion, we want to express the gauge invariant combinations taking only the ingoing part of (B.34),

$$\begin{aligned}
\partial_u A_s - \partial_s A_u &= \sum_{lm}\left[\left(\partial_r \tilde{\chi}_1^{lm} - \partial_u \tilde{\chi}_1^{lm}\right)\Psi_s^{lm}(\Omega) + \partial_u \tilde{\chi}_2^{lm}\Phi_s^{lm}(\Omega)\right] \\
&= \mathrm{i}\sum_{lm}(-1)^{l+1}\delta_{m1}\sqrt{\frac{4\pi(2l+1)}{l(l+1)}}\Big[\frac{\mathrm{i}}{\mathrm{k}}\frac{d}{du}\left(\frac{\mathcal{I}_2^{lm}(u)}{\mathcal{I}_2^{lm}(u\to\infty)}\right)\Phi_s^{lm} + \frac{\mathcal{I}_2^{lm}(u)}{\mathcal{I}_2^{lm}(u\to\infty)}\Phi_s^{lm} \\
&\qquad + \frac{\mathrm{i}}{\mathrm{k}}\frac{d}{du}\left(\frac{\mathcal{I}_1^{lm}(u)}{\mathcal{I}_1^{lm}(u\to\infty)}\right)\Psi_s^{lm} + \frac{\mathcal{I}_1^{lm}(u)}{\mathcal{I}_1^{lm}(u\to\infty)}\mathrm{i}\Psi_s^{lm}\Big]\frac{e^{-\mathrm{ik}(u+2r)}}{2} + \textit{outgoing part} \\
\partial_r A_s - \partial_s A_r &= \sum_{lm}\left[\partial_r \tilde{\chi}_1^{lm}\Psi_s + \partial_r \tilde{\chi}_2^{lm}\Phi_s\right] \\
&= 2\mathrm{i}\sum_{lm}(-1)^{l+1}\delta_{m1}\sqrt{\frac{4\pi(2l+1)}{l(l+1)}}\left[\frac{\mathcal{I}_2^{lm}(u)}{\mathcal{I}_2^{lm}(u\to\infty)}\Phi_s^{lm}(\Omega) + \frac{\mathcal{I}_1^{lm}(u)}{\mathcal{I}_1^{lm}(u\to\infty)}\mathrm{i}\Psi_s^{lm}(\Omega)\right]\frac{e^{-\mathrm{ik}(u+2r)}}{2} \\
&\qquad + \textit{outgoing part}
\end{aligned} \tag{B.39}$$

where we have used the equations governing the gauge invariant variables in (u, r) coordinate for asymptotic Schwarzschild space-time (One may look at Appendix.B.6) as our aim to calculate the absorption cross section at $r \to \infty$. We express the above invariant combinations in Cartesian Coordinates in the following way :

$$\begin{aligned}
&\partial_u A_s - \partial_s A_u \\
&= \frac{\sum_{lm}(-1)^{l+1}\delta_{m1}\sqrt{\frac{4\pi(2l+1)}{l(l+1)}}\left[\frac{\mathrm{i}}{\mathrm{k}}\frac{d}{du}\left(\frac{\mathcal{I}_2^{lm}(u)}{\mathcal{I}_2^{lm}(u\to\infty)}\right)\Phi_s^{lm} + \frac{\mathcal{I}_2^{lm}(u)}{\mathcal{I}_2^{lm}(u\to\infty)}\Phi_s^{lm}\right]}{\sum_{lm}(-1)^{l+1}\delta_{m1}\sqrt{\frac{4\pi(2l+1)}{l(l+1)}}[\Phi_s^{lm}(\Omega) + \mathrm{i}\Psi_s^{lm}(\Omega)]} \times(-\mathrm{ik}A'_s(u,\mathbf{r})) \\
&+ \frac{\sum_{lm}(-1)^{l+1}\delta_{m1}\sqrt{\frac{4\pi(2l+1)}{l(l+1)}}\left[\frac{\mathrm{i}}{\mathrm{k}}\frac{d}{du}\left(\frac{\mathcal{I}_1^{lm}(u)}{\mathcal{I}_1^{lm}(u\to\infty)}\right)\Psi_s^{lm} + \frac{\mathcal{I}_1^{lm}(u)}{\mathcal{I}_1^{lm}(u\to\infty)}\mathrm{i}\Psi_s^{lm}\right]}{\sum_{lm}(-1)^{l+1}\delta_{m1}\sqrt{\frac{4\pi(2l+1)}{l(l+1)}}[\Phi_s^{lm}(\Omega) + \mathrm{i}\Psi_s^{lm}(\Omega)]} \times(-\mathrm{ik}A'_s(u,\mathbf{r})) \\
&= \xi_{us}(k,u)(-\mathrm{ik}A'_s(u,\mathbf{r})),
\end{aligned} \tag{B.40}$$

and

$$\partial_r A_s - \partial_s A_r = \frac{\sum_{lm}(-1)^{l+1}\delta_{m1}\sqrt{\frac{4\pi(2l+1)}{l(l+1)}}\left[\frac{\mathcal{I}_2^{lm}(u)}{\mathcal{I}_2^{lm}(u\to\infty)}\Phi_s^{lm}(\Omega)+\frac{\mathcal{I}_1^{lm}(u)}{\mathcal{I}_1^{lm}(u\to\infty)}\mathrm{i}\Psi_s^{lm}(\Omega)\right]}{\sum_{lm}(-1)^{l+1}\delta_{m1}\sqrt{\frac{4\pi(2l+1)}{l(l+1)}}[\Phi_s^{lm}(\Omega)+\mathrm{i}\Psi_s^{lm}(\Omega)]}(-2\mathrm{ik}A_s'(u,\mathbf{r})) = \xi_{rs}(k,u)(-2\mathrm{ik}A_s'(u,\mathbf{r})). \tag{B.41}$$

Where, $\xi_{rs}(k,u)$ and $\xi_{rs}(k,u)$, are used to denote the terms involving the ratio of l-sum in the above equation and have to be evaluated numerically. Whereas, $A_s'(u,\mathbf{r}))$ is the spherical representation of the plane wave in flat space. Substituting the above combinations in the expression of incident energy density we arrive at,

$$\begin{aligned}\partial_u\mathcal{G} &= \Big\{\frac{1}{2}g^{ss}(\partial_u A_s-\partial_s A_u)(\partial_r A_s^*-\partial_s A_r^*)+c.c.\Big\}-g^{ss}(\partial_u A_s-\partial_s A_u)(\partial_u A_s^*-\partial_s A_u^*)\\ &= 2\Big\{\frac{\mathrm{k}^2}{2}g^{ss}\xi_{us}(k,u)\xi_{rs}^*(k,u)A_s'(u,\mathbf{r})A^{*\prime}{}_s(u,\mathbf{r})+c.c.\Big\}-\mathrm{k}^2 g^{ss}|\xi_{us}(k,u)|^2A_s'(u,\mathbf{r})A^{*\prime}{}_s(u,\mathbf{r}),\end{aligned} \tag{B.42}$$

As a consistency check, one may look for the case of static black hole limit, which corresponds to $u\to\infty$. In this limit the combinations (B.40) and (B.41) become

$$\begin{aligned}\partial_u A_s-\partial_s A_u &= -\mathrm{ik}A_s'(u,\mathbf{r}),\\ \partial_r A_s-\partial_s A_r &= -2\mathrm{ik}A_s'(u,\mathbf{r}).\end{aligned} \tag{B.43}$$

Now substituting these combinations in (B.42), we get the incident energy density as,

$$\partial_u\mathcal{G} = 2\mathrm{k}^2\cos^2\theta+2\mathrm{k}^2-\mathrm{k}^2\cos^2\theta-\mathrm{k}^2 = 2\mathrm{k}^2 \tag{B.44}$$

and as the incident plane wave is considered to be propagating along the z-direction we suitably choose, $\theta\to 0$. The above value of the incident energy density for a static black hole limit matches with the result obtained in the existing literature [124].

B.5 Gauge field equations in (t,r)-coordinate for static Schwarzschild space time

Substituting the field components (3.3) in the equation of motion (3.1) of the gauge field, for static Schwarzschild space time dictated by the metric $g_0^{\mu\nu}(t,r)$ we obtain the following set of equation,

$$\begin{aligned}&f(r)\frac{1}{l(l+1)}\partial_r(r^2(\partial_t d^{lm}-\partial_r b^{lm}))+(b^{lm}-\partial_t k^{lm})=0,\\ &\frac{r^2}{l(l+1)}\partial_t(\partial_t d^{lm}-\partial_r b^{lm})+f(r)(h^{lm}-\partial_r k^{lm})=0,\\ &f(r)\partial_r(f(r)\partial_r a^{lm})-\partial_t^2 a^{lm}-f(r)\frac{l(l+1)}{r^2}a^{lm}=0,\end{aligned} \tag{B.45}$$

which can be simplified and expressed in terms of the gauge invariant variables (3.5) as,

$$\begin{aligned} &f(r)\partial_r\chi_1^{lm} + \chi_4^{lm} = 0 \\ &\partial_t\chi_1^{lm} + f(r)\chi_3^{lm} = 0 \\ &f(r)\partial_r(f(r)\partial_r\chi_2^{lm}) - \partial_t^2\chi_2^{lm} - f(r)\frac{l(l+1)}{r^2}\chi_2^{lm} = 0 \end{aligned} \tag{B.46}$$

The first two of the above set of equations can be decoupled to obtain the governing equation of χ_1^{lm} as,

$$f(r)\partial_r(f(r)\partial_r\chi_1^{lm}) - \partial_t^2\chi_1^{lm} - f(r)\frac{l(l+1)}{r^2}\chi_1^{lm} = 0 \tag{B.47}$$

B.6 Gauge field equation in (u, r) coordinate for static Schwarzschild space time

In this section, we discuss the coordinate transformation from (t, r) to $(u(= t - r_*), r)$ and derive the expressions for EM field components and their invariant combinations. Consider the general definition of coordinate transformation for rank-1 tensor, from $x^\mu(t, r) \to x'^\mu(u, r)$, given as [7],

$$\tilde{A}_\mu(x') = \frac{\partial x^\nu}{\partial x'^\mu}A_\nu(x) \tag{B.48}$$

under which the components (3.3) of the EM wave transform as

$$\begin{aligned} \tilde{A}_u(u, r) &= \frac{\partial t}{\partial u}A_t(t, r) = A_t(t, r) = b^{lm}(t, r)Y_{lm}(\Omega) \\ \tilde{A}_r(u, \mathbf{r}) &= \frac{\partial t}{\partial r}A_t(t, \mathbf{r}) + \frac{\partial r}{\partial r}A_r(t, \mathbf{r}) = \frac{1}{f(r)}A_t(t, \mathbf{r}) + A_r(t, \mathbf{r}) = \Big(d^{lm}(t, r) + \frac{b^{lm}(t, r)}{f(r)}\Big)Y_{lm}(\Omega) \\ \tilde{A}_\theta(u, \mathbf{r}) &= A_\theta(t, \mathbf{r}) \\ \tilde{A}_\phi(u, \mathbf{r}) &= A_\phi(t, \mathbf{r}) \end{aligned} \tag{B.49}$$

One can see that only one of the components changes due to the coordinate transformation, that is, $\tilde{d}^{lm}(u, r) = d^{lm}(u + r^*, r) + b^{lm}(u + r^*, r)/f(r)$. Utilizing this we rewrite the components of the propagating EM wave as,

$$\begin{aligned} \tilde{A}_u(u, \bar{r}) &= b^{lm}(u, r)Y_{lm}(\Omega) \\ \tilde{A}_r(u, \bar{r}) &= \tilde{d}^{lm}(u, r)Y_{lm}(\Omega) \\ \tilde{A}_s(u, \bar{r}) &= k_{lm}(u, r)\Psi_s^{lm}(\Omega) + a_{lm\mathrm{k}}(u, r)\Phi_s^{lm}(\Omega). \end{aligned} \tag{B.50}$$

From the equation of motion, $\nabla_\mu F^{\mu\nu} = 0$, one gets the following coupled equation of the EM field propagating in Schwarzschild space time,

$$\begin{aligned} &\partial_r\tilde{\chi}_1^{lm} + \tilde{\chi}_3^{lm} = 0 \\ &\partial_u\tilde{\chi}_1^{lm} + f(r)\tilde{\chi}_3^{lm} - \tilde{\chi}_4^{lm} = 0, \end{aligned} \tag{B.51}$$

which can be further combined to obtain a decoupled equation of the following form

$$\partial_r(f(r)\partial_r\tilde{\chi}_1^{lm}) - 2\partial_u\partial_r\tilde{\chi}_1^{lm} - \frac{l(l+1)}{r^2}\tilde{\chi}_1^{lm} = 0. \tag{B.52}$$

Also, the equation governing $\tilde{\chi}_2^{lm}$ turns out to be,

$$\partial_r(f(r)\partial_r\tilde{\chi}_2^{lm}) - 2\partial_u\partial_r\tilde{\chi}_2^{lm} - \frac{l(l+1)}{r^2}\tilde{\chi}_2^{lm} = 0 \tag{B.53}$$

where the expression for transformed invariant variables are $\tilde{\chi}_1^{lm}(u,r) = \frac{r^2}{l(l+1)}(\partial_u\tilde{d}^{lm}(u,r) - \partial_r b^{lm}(u,r))$ and $\tilde{\chi}_2^{lm}(u,r) = \tilde{a}^{lm}(u,r) = a^{lm}(u+r_*,r)$. Other invariant variables can be computed from the above constrained equation (B.51).

Appendix C

Diagonalization of the effective acoustic metric

The off-diagonal fluctuation metric discussed in the text is given by

$$ds^2 = -f(t,r)dt^2 + 2g(t,r)drdt + p(t)\left(dr^2 + r^2 d\Omega^2\right). \tag{C.1}$$

Now we rewrite the above metric to make it suitable for diagonalization,

$$ds^2 = -f(t,r)dt^2 - \frac{g^2(t,r)}{p(t)}dt^2 + \left(\sqrt{p(t)}\,dr + \frac{g(t,r)}{\sqrt{p(t)}}\,dt\right)^2 + p(t)r^2 d\Omega^2. \tag{C.2}$$

Considering the following transformation in the radial direction (look at Chapter-7 of [7] for discussions on coordinate transformation to diagonalize a spherically symmetric metric),

$$\frac{d\bar{r}}{X(t,r)} = \sqrt{p(t)}\,dr + \frac{g(t,r)}{\sqrt{p(t)}}\,dt. \tag{C.3}$$

Where $X(t,r)$ some arbitrary function, will be found out in a moment. This transformation leads us to deduce the following relations:

$$\frac{\partial \bar{r}}{\partial r} = X(t,r)\sqrt{p(t)}, \frac{\partial \bar{r}}{\partial t} = X(t,r)\frac{g(t,r)}{\sqrt{p(t)}}. \tag{C.4}$$

Recall the metric coefficients $p(t)$ and $g(t,r)$ given in the main chapter as,

$$\begin{aligned} p(t) &= 1 + \frac{\xi^3}{R^3}, \\ g(r,t) &= -\frac{\dot{R}\xi^3}{R^4}r. \end{aligned} \tag{C.5}$$

Denoting, $\sigma(t) = \xi^3/(R^3)$, we have the following integral equations respectively,

$$\begin{aligned} \bar{r} &= \frac{r}{3}\int d\sigma \frac{X(t,r)}{\sqrt{1+\sigma}} + \gamma(r), \\ \bar{r} &= \sqrt{1+\sigma(t)}\int dr X(t,r) + \tilde{\gamma}(t). \end{aligned} \tag{C.6}$$

To simplify our task we proceed by considering $X(t,r) \equiv\sim X(\sigma(t))$, i.e. dependence of X only on time. This gives us the following equation for $\bar{r}$,

$$\bar{r} = \frac{r}{3}\int d\sigma \frac{\zeta(\sigma)}{\sqrt{1+\sigma}} = r\sqrt{1+\sigma}X(\sigma), \tag{C.7}$$

where, we have set $\gamma(r) = \tilde{\gamma}(t) = 0$. Differentiating the later two equations w.r.t σ gives us the following differential equation for X,

$$-\frac{1}{2}X = 3(1+\sigma)\dot{X}\sigma. \tag{C.8}$$

Integrating both sides of the above equation, we arrive at,

$$X(\sigma) = \frac{1}{(1+\sigma)^{1/6}}. \tag{C.9}$$

Now, we know the functional form of the arbitrary function we assumed. Substituting the function in (C.7) we finally obtain,

$$\bar{r} = r(1+\sigma)^{1/3} = rp^{1/3}. \tag{C.10}$$

This rescaling of the radial coordinate will help one to diagonalize the metric.

C.1 Discretization of second order ODE using Crank-Nicholson Method

Having stiffness in the differential equation, arising from the sudden collapse of the water bubble, we resort to using those numerical discretization methods, which provide for better stability. The crank-Nicholson method is a popular implicit method [172, 173], mostly used in the case of partial differential equations, such as the heat equation, to discretize the first order differentiation in the time part. Generically, one can consider the following model differential equation

$$P(x)\frac{d^2y}{dx^2} + Q(x)\frac{dy}{dx} + R(x)y = 0, \tag{C.11}$$

with the initial conditions given as, $y(x_0)$ and $y_1(x_0)$. Now, we decompose the above second order ODE into two first order ODE,

$$\frac{dy}{dx} = y_1, \quad \frac{dy_1}{dx} = -\frac{Q(x)y_1 + R(x)y}{P(x)}. \tag{C.12}$$

The crank-Nicholson method is attributed to the following discretization scheme,

$$\begin{aligned} y^{n+1} &= y^n + \frac{h}{2}\left(\frac{dy}{dx}\Big|_{x_n} + \frac{dy}{dx}\Big|_{x_n+h}\right), \\ &= y^n + \frac{h}{2}\left(y_1|_{x_n} + y_1|_{x_n+h}\right), \end{aligned} \tag{C.13}$$

which we can also apply to the second equation of (C.12) to obtain,

$$y_1^{n+1} = y_1^n + \frac{h}{2}\left(\frac{dy_1}{dx}\Big|_{x_n} + \frac{dy_1}{dx}\Big|_{x_n+h}\right). \tag{C.14}$$

Where $n \in \mathcal{Z}$, set of integers, and $y^n \equiv y(x_n)$, $y_1^n \equiv y_1(x_n)$. Using the explicit expressions for dy_1/dx from (C.12), we can rewrite the above equation as,

$$y_1^{n+1} = y_1^n - \frac{h}{2}\left(\frac{dy_1}{dx}\Big|_{x_n} + \frac{Q(x_n+h)y_1^{n+1} + R(x_n+h)y^{n+1}}{P(x_n+h)}\right). \tag{C.15}$$

Now substituting the discretization of y^{n+1} from (C.13) we obtain,

$$\begin{aligned} y_1^{n+1} &= y_1^n + \frac{h}{2}\left[\frac{dy_1}{dx}\Big|_{x_n} - \frac{Q(x_n+h)y_1^{n+1}}{P(x_n+h)} - \frac{R(x_n+h)}{P(x_n+h)}\left\{y^n + \frac{h}{2}\left(y_1\Big|_{x_n} + y_1\Big|_{x_n+h}\right)\right\}\right], \\ \implies y_1^{n+1} &= \frac{y_1^n\left\{1 - \left(\frac{h}{2}\right)^2 \frac{R(x_n+h)}{P(x_n+h)}\right\} + \frac{h}{2}\left\{\frac{dy_1}{dx}\Big|_{x_n} - \frac{R(x_n+h)}{P(x_n+h)}y_n\right\}}{\left[1 + \frac{h}{2}\frac{Q(x_n+h)}{P(x_n+h)} + \left(\frac{h}{2}\right)^2 \frac{R(x_n+h)}{P(x_n+h)}\right]}. \end{aligned} \tag{C.16}$$

In the second step of the above equation, we have rearranged the terms, such that all the known quantities stay on the right-hand side. The steps up to the evaluation of the solution proceed as follows: starting from the initial conditions $y(x_0)$ and $y_1(x_0)$, evaluate the $y_1(x_0+h)$ from the above equation, and substitute in (C.13), which will provide for the solution $y(x_0+h)$. Now repeat the iteration to generate the solution for the consecutive points.

C.2 Fitted polynomial for the number density

Having a promising trend (fig.5.2) in the number density of photons, evaluated through our formalism, with the experimental measurement, we are compelled to fit our results by utilizing the following polynomial,

$$\begin{aligned} y =& 93.6x - 105.5x^2 + 51.3x^3 - 12.6x^4 + 1.6x^5 - 0.08x^6 - 0.004x^7 + 0.0008x^8 \\ & - 5\times10^{-6}x^9 + 1.4\times10^{-6}x^{10} - 1.6\times10^{-8}x^{11}, \end{aligned} \tag{C.17}$$

where $x \equiv \ln k$ and $y \equiv \ln|\beta_k|^2$.

Bibliography

[1] B. P. Abbott *et al.* [LIGO Scientific and Virgo], Phys. Rev. Lett. **116**, no.6, 061102 (2016)

[2] A. Goldstein, *et al.* Astrophys. J. Lett. **848**, no.2, L14 (2017)

[3] S. Perlmutter *et al.* [Supernova Cosmology Project], Nature **391**, 51-54 (1998)

[4] R. Löfstedt, B. P. Barber, and S. J. Putterman Physics of Fluids A: Fluid Dynamics 5, 2911 (1993);

[5] B. P. Barber, R. Löfstedt, S. J. Putterman, K. W. Weninger Volume 281, Issue 2, March 1997, Pages 65-143

[6] D. Baumann, Cambridge University Press, 2022, ISBN 978-1-108-93709-2, 978-1-108-83807-8

[7] T. Padmanabhan, Cambridge University Press, 2014, ISBN 978-7-301-22787-9

[8] R. P. Kerr, Phys. Rev. Lett. **11**, 237-238 (1963)

[9] S. M. Carroll, Cambridge University Press, 2019, ISBN 978-0-8053-8732-2, 978-1-108-48839-6, 978-1-108-77555-7

[10] L. Rezzolla, ICTP Lect. Notes Ser. **14**, 255-316 (2003) [arXiv:gr-qc/0302025 [gr-qc]].

[11] T. Regge and J. A. Wheeler, Phys. Rev. 108, 1063 (1957). doi:10.1103/PhysRev.108.1063

[12] F. J. Zerilli, Phys. Rev. Lett. **24**, 737-738 (1970)

[13] L. A. Edelstein and C. V. Vishveshwara, Phys. Rev. D 1, 3514 (1970). doi:10.1103/PhysRevD.1.3514

[14] F. J. Zerilli, Phys. Rev. D 2, 2141 (1970).

[15] S. Chandrasekhar and S. L. Detweiler, Proc. Roy. Soc. Lond. A 344, 441 (1975).

[16] S. Chandrasekhar Proc. Roy. Soc. Lond. A 343, 289-298 (1975).

[17] R. Price, K.S. Thorne, Astrophysical Journal, vol. 155, p.163

[18] C. Molina, P. Pani, V. Cardoso and L. Gualtieri, Phys. Rev. D **81**, 124021 (2010)

[19] B. P. Abbott *et al.* [LIGO Scientific and Virgo], Phys. Rev. Lett. **116**, no.13, 131103 (2016)

[20] B. P. Abbott *et al.* [LIGO Scientific and Virgo], Phys. Rev. D **93**, no.12, 122003 (2016)

[21] B. P. Abbott *et al.* [LIGO Scientific and Virgo], Phys. Rev. Lett. **116**, no.24, 241102 (2016)

[22] B. P. Abbott *et al.* [LIGO Scientific and Virgo], Phys. Rev. Lett. **116**, no.24, 241103 (2016)

[23] B. P. Abbott *et al.* [LIGO Scientific and Virgo], Phys. Rev. Lett. **119**, no.14, 141101 (2017)

[24] B. P. Abbott *et al.* [LIGO Scientific and Virgo], Phys. Rev. Lett. **119**, no.16, 161101 (2017)

[25] R. Abbott *et al.* [LIGO Scientific and Virgo], Phys. Rev. D **102**, no.4, 043015 (2020)

[26] B. P. Abbott *et al.* [LIGO Scientific and Virgo], Phys. Rev. Lett. **118**, no.12, 121101 (2017) [erratum: Phys. Rev. Lett. **119**, no.2, 029901 (2017)]

[27] B. P. Abbott *et al.* [LIGO Scientific and Virgo], Astrophys. J. Lett. **892**, no.1, L3 (2020)

[28] R. Abbott *et al.* [LIGO Scientific and Virgo], Astrophys. J. Lett. **896**, no.2, L44 (2020)

[29] B. P. Abbott *et al.* [LIGO Scientific and Virgo], Astrophys. J. Lett. **851**, L35 (2017)

[30] R. Abbott *et al.* [LIGO Scientific, Virgo and KAGRA], PoS **ICRC2023**, 1579 (2023)

[31] R. Abbott *et al.* [KAGRA, VIRGO and LIGO Scientific], Astrophys. J. Suppl. **267**, no.2, 29 (2023)

[32] R. Abbott *et al.* [KAGRA, VIRGO and LIGO Scientific], PTEP **2022**, no.6, 063F01 (2022)

[33] https://www.ligo.org/science/Publication-O3bCatalog/

[34] W. G. Unruh, Phys. Rev. D **14**, 3251-3259 (1976)

[35] V. Cardoso and R. Vicente, Phys. Rev. D **100**, no.8, 084001 (2019)

[36] William J Thompson Am. J. Phys. 60, 378–379 (1992)

[37] S. R. Das, G. W. Gibbons and S. D. Mathur, Phys. Rev. Lett. **78**, 417-419 (1997)

[38] E. T. Newman, R. Couch, K. Chinnapared, A. Exton, A. Prakash and R. Torrence, J. Math. Phys. **6**, 918-919 (1965)

[39] S. L. Detweiler and J. R. Ipser, Astrophys. J. **185**, 675-683 (1973)

[40] D. R. Brill, P. L. Chrzanowski, C. Martin Pereira, E. D. Fackerell and J. R. Ipser, Phys. Rev. D **5**, 1913-1915 (1972)

[41] A. A. Starobinsky, Sov. Phys. JETP **37**, no.1, 28-32 (1973)

[42] C. L. Benone and L. C. B. Crispino, Phys. Rev. D **99**, no.4, 044009 (2019)

[43] S. W. Hawking, Commun. Math. Phys. **43**, 199-220 (1975) [erratum: Commun. Math. Phys. **46**, 206 (1976)]

[44] C. L. Benone, E. S. de Oliveira, S. R. Dolan and L. C. B. Crispino, Phys. Rev. D **89**, no.10, 104053 (2014)

[45] Y. B. Zel'Dovich, JETP Lett.14, 180 (1971).

[46] Y. B. Zel'Dovich, Sov. Phys. JETP 35, 1085 (1972).

[47] J. D. Bekenstein and M. Schiffer, Phys. Rev. D **58**, 064014 (1998)

[48] R. Brito, V. Cardoso and P. Pani, Lect. Notes Phys. **906**, pp.1-237 (2015) 2020, [arXiv:1501.06570 [gr-qc]].

[49] R. Vicente, V. Cardoso and J. C. Lopes, Phys. Rev. D **97**, no.8, 084032 (2018)

[50] M. Richartz, S. Weinfurtner, A. J. Penner and W. G. Unruh, Phys. Rev. D **80**, 124016 (2009)

[51] B. Demirkaya, T. Dereli and K. Güven, [arXiv:1806.02139 [cond-mat.other]].

[52] J. Steinhauer, M. Abuzarli, T. Aladjidi, T. Bienaimé, C. Piekarski, W. Liu, E. Giacobino, A. Bramati and Q. Glorieux, Nature Commun. **13**, 2890 (2022)

[53] H. S. Vieira, K. Destounis and K. D. Kokkotas, Phys. Rev. D **107**, no.10, 104038 (2023)

[54] V. Cardoso, A. Coutant, M. Richartz and S. Weinfurtner, Phys. Rev. Lett. **117**, no.27, 271101 (2016)

[55] T. Torres, S. Patrick, A. Coutant, M. Richartz, E. W. Tedford and S. Weinfurtner, Nature Phys. **13**, 833-836 (2017)

[56] S. Patrick, A. Coutant, M. Richartz and S. Weinfurtner, Phys. Rev. Lett. **121**, no.6, 061101 (2018)

[57] V. Frumkin, K. Papatryfonos and J. W. M. Bush, Phys. Rev. Lett. **130**, no.6, 064002 (2023)

[58] Sonoluminescence: A Discussion, J. Acoust. Soc. Am. 32, 1459–1462 (1960)

[59] D. F. Gaitan, L. A. Crum, C. C. Church, and R. A. Roy, J. Acoust. Soc. Am. 91, 3166–3183 (1992)

[60] B. Gompf, R. Günther, G. Nick, R. Pecha, and W. Eisenmenger Phys. Rev. Lett. 79, 1405

[61] R. Hiller, S. J. Putterman and B. P. Barber, Phys. Rev. Lett. **69**, 1182-1184 (1992)

[62] Lord Rayleigh, Philos. Mag. 34, 94 (1917);

[63] M. Plesset, J. Appl. Mech. 16, 277 (1949)

[64] M. P. Brenner, S. Hilgenfeldt and D. Lohse, Rev. Mod. Phys. **74**, 425-484 (2002)

[65] S. Hilgenfeldt, S. Grossmann, D. Lohse (1999). Nature. 398. 402-405. 10.1038/18842.

[66] R. P. Taleyarkhan et al., Evidence for Nuclear Emissions During Acoustic Cavitation.Science295,1868-1873(2002).

[67] D. Bishwajyoti, A. Serge, Physica D: Nonlinear Phenomena, Volume 216, Issue 1, p. 136-156.

[68] Hendrick BG Casimir, Proc. Kon. Ned. Akad. Wet. Vol.51, p.793 (1948)

[69] M. J. Sparnaay, Nature, Volume 180, Issue 4581, pp. 334-335 (1957).

[70] M. J. Sparnaay, Physica, Volume 24, Issue 6, p. 751-764.

[71] J. Schwinger, Proc. Nat. Acad. Sci. 89, 4091–4093 (1992).

[72] J. Schwinger, Proc. Nat. Acad. Sci. 89, 11118–11120 (1992).

[73] J. Schwinger, Proc. Nat. Acad. Sci. 90, 958–959 (1993).

[74] J. Schwinger, Proc. Nat. Acad. Sci. 90, 2105–2106 (1993).

[75] J. Schwinger, Proc. Nat. Acad. Sci. 90, 4505–4507 (1993).

[76] J. Schwinger, Proc. Nat. Acad. Sci. 90, 7285–7287 (1993).

[77] J. Schwinger, Proc. Nat. Acad. Sci. 91, 6473–6475 (1994).

[78] S. Liberati, F. Belgiorno, M. Visser and D. W. Sciama, J. Phys. A **33**, 2251-2272 (2000)

[79] M. Visser, S. Liberati, F. Belgiorno and D. W. Sciama, Phys. Rev. Lett. **83**, 678-681 (1999)

[80] S. Liberati, M. Visser, F. Belgiorno and D. Sciama, Phys. Rev. D **61**, 085023 (2000)

[81] S. Liberati, M. Visser, F. Belgiorno and D. Sciama, Phys. Rev. D **61**, 085024 (2000)

[82] N. D. Birrell and P. C. W. Davies, Cambridge Univ. Press, 1984,

[83] C. Eberlein, Phys. Rev. Lett. **76**, 3842-3845 (1996)

[84] C. Eberlein, Phys. Rev. A **53**, 2772-2787 (1996)

[85] I. H. Brevik, V. N. Marachevsky and K. A. Milton, Phys. Rev. Lett. **82**, 3948-3951 (1999)

[86] C. S. Unnikrishnan and S. Mukhopadhyay, Phys. Rev. Lett. **77**, 4690-4690 (1996)

[87] K. A. Milton and Y. J. Ng, Phys. Rev. E **55**, 4207-4216 (1997)

[88] K. A. Milton and Y. J. Ng, Phys. Rev. E **57**, 5504-5510 (1998)

[89] A. Lambrecht, M. T. Jaekel and S. Reynaud, Phys. Rev. Lett. **78**, 2267 (1997)

[90] W. G. Unruh, Phys. Rev. D **14**, 870 (1976)

[91] W. G. Unruh, Phys. Rev. Lett. **46**, 1351-1353 (1981)

[92] M. Visser, Class. Quant. Grav. **15**, 1767-1791 (1998)

[93] C. Barcelo, S. Liberati and M. Visser, Living Rev. Rel. **8**, 12 (2005)

[94] M. E. Peskin and D. V. Schroeder, Addison-Wesley, 1995, ISBN 978-0-201-50397-5

[95] F. Halzen and A. D. Martin, "QUARKS AND LEPTONS: AN INTRODUCTORY COURSE IN MODERN PARTICLE PHYSICS,"

[96] K. Goto and Y. Kazama, PTEP **2019**, no.2, 023B01 (2019)

[97] V. Mukhanov and S. Winitzki, Cambridge University Press, 2007, ISBN 978-0-521-86834-1, 978-1-139-78594-5

[98] L. H. Ford, [arXiv:gr-qc/9707062 [gr-qc]].

[99] L. Kofman, A. D. Linde and A. A. Starobinsky, Phys. Rev. D **56**, 3258-3295 (1997))

[100] R. Abbott *et al.* [LIGO Scientific, KAGRA and VIRGO], Astrophys. J. Lett. **915**, no.1, L5 (2021)

[101] T. Marrodán Undagoitia and L. Rauch, J. Phys. G **43**, no.1, 013001 (2016)

[102] R. K. Leane, [arXiv:2006.00513 [hep-ph]].

[103] P. W. Graham and S. Rajendran, Phys. Rev. D **88**, 035023 (2013)

[104] I. G. Irastorza, [arXiv:2109.07376 [hep-ph]].

[105] M. Schumann, J. Phys. G **46**, no.10, 103003 (2019) doi:10.1088/1361-6471/ab2ea5 [arXiv:1903.03026 [astro-ph.CO]].

[106] M. A. Fedderke, P. W. Graham and S. Rajendran, Phys. Rev. D **100**, no.1, 015040 (2019)

[107] I. Obata, T. Fujita and Y. Michimura, Phys. Rev. Lett. **121**, no.16, 161301 (2018)

[108] T. Fujita, R. Tazaki and K. Toma, Phys. Rev. Lett. **122**, no.19, 191101 (2019)

[109] G. G. Raffelt, Lect. Notes Phys. **741**, 51-71 (2008) doi:10.1007/978-3-540-73518-2_3 [arXiv:hep-ph/0611350 [hep-ph]].

[110] P. W. Graham and S. Rajendran, Phys. Rev. D **84**, 055013 (2011)

[111] D. Budker, P. W. Graham, M. Ledbetter, S. Rajendran and A. Sushkov, Phys. Rev. X **4**, no.2, 021030 (2014)

[112] K. Nagano, H. Nakatsuka, S. Morisaki, T. Fujita, Y. Michimura and I. Obata, Phys. Rev. D **104**, no.6, 062008 (2021)

[113] S. Chigusa, T. Moroi and K. Nakayama, Phys. Lett. B **803**, 135288 (2020)

[114] Y. Chen, X. Xue and V. Cardoso, [arXiv:2308.00741 [hep-ph]].

[115] R. Roy and U. A. Yajnik, Phys. Lett. B **803**, 135284 (2020)

[116] R. Roy, S. Vagnozzi and L. Visinelli, Phys. Rev. D **105**, no.8, 083002 (2022)

[117] Y. Chen, J. Shu, X. Xue, Q. Yuan and Y. Zhao, Phys. Rev. Lett. **124**, no.6, 061102 (2020)

[118] G. W. Yuan, Z. Q. Xia, C. Tang, Y. Zhao, Y. F. Cai, Y. Chen, J. Shu and Q. Yuan, JCAP **03**, 018 (2021)

[119] R G Barrera et al 1985 Eur. J. Phys. 6 287

[120] J. D. Jackson, Wiley, 1998, ISBN 978-0-471-30932-1

[121] https://reference.wolfram.com/language/ref/AccuracyGoal.html

[122] L. C. B. Crispino and E. S. Oliveira, Phys. Rev. D **78**, 024011 (2008)

[123] S. A. Teukolsky and W. H. Press, Astrophys. J. **193**, 443-461 (1974)

[124] L. C. B. Crispino, E. S. Oliveira, A. Higuchi and G. E. A. Matsas, Phys. Rev. D **75**, 104012 (2007)

[125] D. C. Dai and D. Stojkovic, Phys. Lett. B **843**, 138056 (2023)

[126] L. C. S. Leite, S. Dolan and L. Crispino, C.B., Phys. Rev. D **98**, no.2, 024046 (2018)

[127] A. A. Starobinskil and S. M. Churilov, Sov. Phys. JETP **65**, no.1, 1-5 (1974)

[128] L. C. S. Leite, S. R. Dolan and L. C. B. Crispino, Phys. Lett. B **774**, 130-134 (2017)

[129] M. P. van Haarlem, M. W. Wise, A. W. Gunst, G. Heald, J. P. McKean, J. W. T. Hessels, A. G. de Bruyn, R. Nijboer, J. Swinbank and R. Fallows, *et al.* Astron. Astrophys. **556**, A2 (2013)

[130] A. Corstanje, S. Buitink, J. E. Enriquez, H. Falcke, J. R. Hörandel, M. Krause, A. Nelles, J. P. Rachen, P. Schellart and O. Scholten, *et al.* Astron. Astrophys. **590**, A41 (2016)

[131] S. Chandrasekhar, The maximum mass of ideal white dwarfs, Astrophys. J. 74, 81 (1931).

[132] S. W. Hawking and W. Israel, "THREE HUNDRED YEARS OF GRAVITATION,"

[133] M. Riajul Haque, E. Kpatcha, D. Maity and Y. Mambrini, Phys. Rev. D **108**, no.6, 063523 (2023)

[134] I. Musco, Phys. Rev. D **100**, no.12, 123524 (2019)

[135] M. Calzà, J. G. Rosa and F. Serrano, [arXiv:2306.09430 [hep-ph]].

[136] N. P. Branco, R. Z. Ferreira and J. G. Rosa, JCAP **04**, 003 (2023)

[137] J. G. Rosa and T. W. Kephart, Phys. Rev. Lett. **120**, no.23, 231102 (2018)

[138] B. Carr, K. Dimopoulos, C. Owen and T. Tenkanen, Phys. Rev. D **97**, no.12, 123535 (2018)

[139] B. Carr, K. Kohri, Y. Sendouda and J. Yokoyama, Rept. Prog. Phys. **84**, no.11, 116902 (2021)

[140] A. Escrivà, F. Kuhnel and Y. Tada, [arXiv:2211.05767 [astro-ph.CO]].

[141] M. Sasaki, T. Suyama, T. Tanaka and S. Yokoyama, Class. Quant. Grav. **35**, no.6, 063001 (2018)

[142] B. Carr, S. Clesse, J. Garcia-Bellido, M. Hawkins and F. Kuhnel, [arXiv:2306.03903 [astro-ph.CO]].

[143] A. Kashlinsky, Y. Ali-Haimoud, S. Clesse, J. Garcia-Bellido, L. Wyrzykowski, A. Achucarro, L. Amendola, J. Annis, A. Arbey and R. G. Arendt, *et al.* [arXiv:1903.04424 [astro-ph.CO]].

[144] D. N. Page, Phys. Rev. D **13**, 198-206 (1976)

[145] I. Baldes, Q. Decant, D. C. Hooper and L. Lopez-Honorez, JCAP **08**, 045 (2020)

[146] Giant Metrewave Radio Telescope, NCRA-TIFR

[147] Gupta, Y., Ajithkumar, B., Kale, H.S., Nayak, S., Sabhapathy, S., Sureshkumar, S.,et al.: 2017, Current Science 113, 707.

[148] H. T. Intema, P. Jagannathan, K. P. Mooley and D. A. Frail, Astron. Astrophys. **598**, A78 (2017)

[149] A. Weltman, P. Bull, S. Camera, K. Kelley, H. Padmanabhan, J. Pritchard, A. Raccanelli, S. Riemer-Sørensen, L. Shao and S. Andrianomena, *et al.* Publ. Astron. Soc. Austral. **37**, e002 (2020)

[150] National Radio Astronomy Observatory

[151] S. Sanidas, S. Cooper, C. G. Bassa, J. W. T. Hessels, V. I. Kondratiev, D. Michilli, B. W. Stappers, C. M. Tan, J. van Leeuwen and L. Cerrigone, *et al.* Astron. Astrophys. **626**, A104 (2019)

[152] D. Michilli, J. W. T. Hessels, R. J. Lyon, C. M. Tan, C. Bassa, S. Cooper, V. I. Kondratiev, S. Sanidas, B. W. Stappers and J. van Leeuwen, Mon. Not. Roy. Astron. Soc. **480**, no.3, 3457-3467 (2018)

[153] D. Michilli, C. Bassa, S. Cooper, J. W. T. Hessels, V. I. Kondratiev, S. Sanidas, B. W. Stappers, C. M. Tan, J. van Leeuwen and I. Cognard, *et al.* Mon. Not. Roy. Astron. Soc. **491**, no.1, 725-739 (2020)

[154] C. M. Tan, C. G. Bassa, S. Cooper, J. W. T. Hessels, V. I. Kondratiev, D. Michilli, S. Sanidas, B. W. Stappers, J. van Leeuwen and J. Y. Donner, *et al.* Mon. Not. Roy. Astron. Soc. **492**, no.4, 5878-5896 (2020)

[155] W. Unruh, Phys. Rev. Lett. **31**, no.20, 1265-1267 (1973)

[156] D. C. Dai and D. Stojkovic, [arXiv:2309.13511 [gr-qc]].

[157] O. J. C. Dias, R. Masachs, O. Papadoulaki and P. Rodgers, JHEP **04**, 196 (2020)

[158] A. B. Balakin and J. P. S. Lemos, Class. Quant. Grav. **22**, 1867-1880 (2005)

[159] F. W. Hehl and Y. N. Obukhov, Lect. Notes Phys. **562**, 479 (2001)

[160] C. Codirla and H. Osborn, Annals Phys. **260**, 91-116 (1997)

[161] J. Côté, V. Faraoni and A. Giusti, Gen. Rel. Grav. **51**, no.9, 117 (2019)

[162] P. Adshead, J. T. Giblin, T. R. Scully and E. I. Sfakianakis, JCAP **10**, 039 (2016)

[163] A. Talebian, A. Nassiri-Rad and H. Firouzjahi, Phys. Rev. D **105**, no.2, 023528 (2022)

[164] S. Tripathy, D. Chowdhury, R. K. Jain and L. Sriramkumar, Phys. Rev. D **105**, no.6, 063519 (2022)

[165] S. Tripathy, D. Chowdhury, H. V. Ragavendra, R. K. Jain and L. Sriramkumar, Phys. Rev. D **107**, no.4, 043501 (2023)

[166] K. Bamba and J. Yokoyama, Phys. Rev. D **69**, 043507 (2004)

[167] B. Allen, Phys. Rev. D **32**, 3136 (1985)

[168] T. Kobayashi and M. S. Sloth, Phys. Rev. D **100**, no.2, 023524 (2019)

[169] M. R. Haque, D. Maity and S. Pal, Phys. Rev. D **103**, no.10, 103540 (2021)

[170] H. Press, B.P. Flannery, S.A. Teukolsky, and W.T. Vetterling. Numerical Recipes. Cambridge University Press, 1986.

[171] O. Koch, P. Kofler and E. B. Weinmüller, Applied Numerical Mathematics Volume 34, Issues 2–3, July 2000, Pages 231-252

[172] X. Antoine, W. Bao, C. Bess, Computer Physics Communications 184 (2013) 2621–2633

[173] P. Muruganandam, S. K. Adhikari, Comput. Phys. Commun. 180 (2009) 1888-1912

[174] K. D. Lozanov, [arXiv:1907.04402 [astro-ph.CO]].

[175] Elrod, C., Ma, Y., Althaus, K., & Rackauckas, C. (2022, September). In 2022 IEEE High Performance Extreme Computing Conference (HPEC) (pp. 1-9). IEEE.

[176] Hairer, Ernst, and Gerhard Wanner. “Stiff differential equations solved by Radau methods." Journal of Computational and Applied Mathematics 111.1-2 (1999): 93-111.

[177] Hairer, E., Wanner, G.: Solving Ordinary Differential Equations II. Stiff and Differential-Algebraic Problems, 2nd edn. Springer Series in Computational Mathematics, vol. 14. Springer, Berlin (1996)

[178] Carlos Camara, Seth Putterman, and Emil Kirilov, Phys. Rev. Lett. 92, 124301

[179] Y. Ema, K. Nakayama and Y. Tang, JHEP **07**, 060 (2019)

[180] Ablowitz, M., & Fokas, A. (2021). Introduction to Complex Variables and Applications (Cambridge Texts in Applied Mathematics). Cambridge: Cambridge University Press.

[181] E. W. Kolb, S. Ling, A. J. Long and R. A. Rosen, JHEP **05**, 181 (2023)

[182] J. S. Schwinger, Phys. Rev. **82**, 664-679 (1951)

[183] Y. B. Zeldovich and A. A. Starobinsky, Zh. Eksp. Teor. Fiz. **61**, 2161-2175 (1971)

[184] L. H. Ford, Phys. Rev. D **35**, 2955 (1987)

[185] D. Maity and S. Pal, Phys. Lett. B **835**, 137503 (2022)

[186] Giovanni Milione, et al., Phys. Rev. Lett. 107 (5) (2011) 053601.

[187] J. Martin and V. Vennin, Phys. Rev. D **93**, no.2, 023505 (2016)

[188] A. Chakraborty and D. Maity, [arXiv:2309.10116 [hep-th]].

[189] M. Sajjad Athar, S. W. Barwick, T. Brunner, J. Cao, M. Danilov, K. Inoue, T. Kajita, M. Kowalski, M. Lindner and K. R. Long, *et al.* Prog. Part. Nucl. Phys. **124**, 103947 (2022)

[190] Giunti, Carlo, and Chung W. Kim, Fundamentals of Neutrino Physics and Astrophysics (Oxford, 2007; online edn, Oxford Academic, 1 Jan. 2010)

[191] N. Palanque-Delabrouille, C. Yèche, J. Baur, C. Magneville, G. Rossi, J. Lesgourgues, A. Borde, E. Burtin, J. M. LeGoff and J. Rich, *et al.* JCAP **11**, 011 (2015)

[192] P. A. R. Ade *et al.* [Planck], Astron. Astrophys. **594**, A13 (2016)

[193] A. D. Dolgov and D. P. Kirilova, Sov. J. Nucl. Phys. **51**, 172-177 (1990) JINR-E2-89-321.

[194] P. Adshead and E. I. Sfakianakis, Phys. Rev. Lett. **116**, no.9, 091301 (2016)

[195] A. del Rio, J. Navarro-Salas and F. Torrenti, Phys. Rev. D **90**, no.8, 084017 (2014)

[196] P. Adshead and E. I. Sfakianakis, JCAP **11**, 021 (2015)

[197] N. Herring and D. Boyanovsky, Phys. Rev. D **101**, no.12, 123522 (2020)

[198] D. J. H. Chung, L. L. Everett, H. Yoo and P. Zhou, Phys. Lett. B **712**, 147-154 (2012)

[199] M. Peloso and L. Sorbo, JHEP **05**, 016 (2000)

[200] P. B. Greene and L. Kofman, Phys. Lett. B **448**, 6-12 (1999)

[201] P. B. Greene and L. Kofman, Phys. Rev. D **62**, 123516 (2000)

[202] W. E. East, F. M. Ramazanoğlu and F. Pretorius, Phys. Rev. D **89**, no.6, 061503 (2014)

[203] J. G. Rosa, Phys. Lett. B **749**, 226-230 (2015)

[204] J. G. Rosa, Phys. Rev. D **95**, no.6, 064017 (2017)

[205] L. K. Wong, Phys. Rev. D **100**, no.4, 044051 (2019)

[206] E. Berti, V. Cardoso and J. P. S. Lemos, Phys. Rev. D **70**, 124006 (2004)

[207] S. Basak and P. Majumdar, Class. Quant. Grav. **20**, 3907-3914 (2003)

[208] T. Torres, S. Patrick, M. Richartz and S. Weinfurtner, Class. Quant. Grav. **36**, no.19, 194002 (2019)

[209] M. Cromb, G. M. Gibson, E. Toninelli, J. M. Padgett, E. M. Wright and D. Faccio, Nature Phys. **16**, no.10, 1069-1073 (2020)

[210] M. J. Jacquet, L. Giacomelli, Q. Valnais, M. Joly, F. Claude, E. Giacobino, Q. Glorieux, I. Carusotto and A. Bramati, Phys. Rev. Lett. **130**, no.11, 111501 (2023)

[211] L. Giacomelli and I. Carusotto, Phys. Rev. A **103**, no.4, 043309 (2021)

[212] T. A. S. Cardoso and M. Richartz, Phys. Rev. A **106**, no.6, 063310 (2022)